Modulation of macrophage responses by the vaccine adjuvant alum

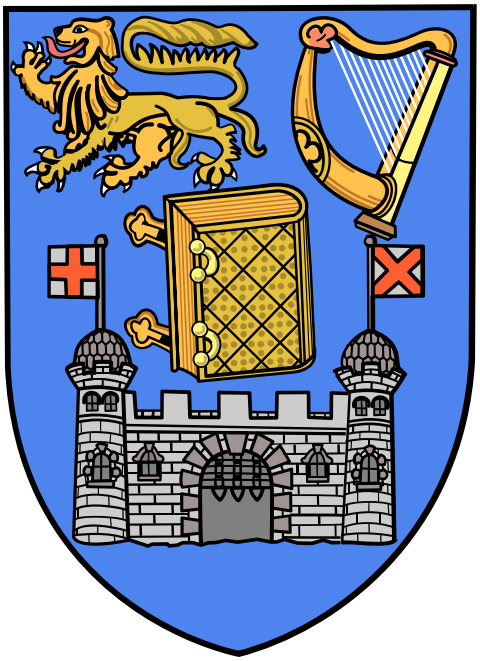

Thesis submitted to the University of Dublin for the

Degree of Doctor of Philosophy

by

Aoife Louise Gorman

School of Biochemistry and Immunology
Trinity Biomedical Sciences Institute
Trinity College Dublin
Ireland

April 2020

Declaration

I declare that this thesis has not been submitted as an exercise for a degree at this or any other university and it is entirely my own work. I agree to deposit this thesis in the University's open access institutional repository or allow the library to do so on my behalf, subject to Irish Copyright Legislation and Trinity College Library conditions of use and acknowledgement.

Aoife Louise Gorman

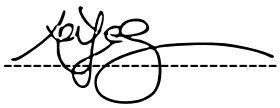

Abstract

Recent findings have challenged the classical view of innate versus adaptive immunity, suggesting that innate cells can retain some "memory" of past immunological insults. This "trained immunity" which allows for primed cellular responses to secondary infections is independent of T and B cells and is mediated by innate cells such as monocytes and macrophages. While it has been shown that certain live vaccines such as BCG can induce trained immunity, the training effects of non-living vaccines incorporating the widely used vaccine adjuvant alum have not been addressed. Alum has been predominantly used in several childhood vaccines due to effectiveness in promoting antibody responses and robust safety profile. However, the immunomodulatory effects of alum have not been fully elucidated. Using the *in vitro* model of training, alum was found to train innate cells to adopt a distinct morphology in addition to an increased capacity to proliferate through enhanced metabolic activity. The transcriptional profile of alum-trained macrophages was explored using the NanoString Inflammation panel one week after training *in vitro.* Alum globally downregulated pro-inflammatory gene expression while a small group of upregulated genes was identified which may shed light on the mechanisms underlying the establishment of these unconventional anti-inflammatory macrophages. One such gene, *Il1rn*, that encodes IL-1Ra, the natural inhibitor of the pro-inflammatory cytokine IL1-β, was significantly increased in response to alum alone. Interestingly, secretion of this anti-inflammatory cytokine was hindered by pre-treatment with rapamycin. Furthermore, the metabolic profile of macrophages stimulated with alum was reversed by rapamycin. These data suggest that stimulating macrophages with alum may favour a pro-resolution phenotype via activation of mammalian target of rapamycin (mTOR), altering cellular metabolism and proliferative capacity.

Publications

*Ewa Oleszycka, 1*Sean McCluskey, [1]Fiona A. Sharp, Natalia Munoz-Wolf., [2]Emily Hams, [1]**Aoife L. Gorman**, [2]Padraic G. Fallon, [1,3]**Ed C. Lavelle**. (2018). The vaccine adjuvant alum inhibits Th1 cellular responses via IL-10. *The European Journal of Immunology*. doi: 10.1002/eji.201747150. selected for the "In this issue" section of EJI.

Harte, C., **Gorman,A.L.,** McCluskey, S., Carty,M., Bowie, A.G., Scott, C.J. Meade, K.G. and **Lavelle, E.C.** (2017). Alum Activates the Bovine NLRP3 Inflammasome. *Frontiers in Immunology*. https://doi.org/10.3389/fimmu.2017.01494

Abbreviations

4E-BP1	Eukaryotic translation initiation factor 4E-binding protein 1
Alum	Aluminium hydroxide
APC	Antigen presenting cell
ARE	Antioxidant response element
ATP	Adenosine triphosphate
BCG	Bacille Calmette Guerin
BMDC	Bone marrow-derived dendritic cells
BMDM	Bone marrow-derived macrophages
BSA	Bovine serum albumin
Ccl	Chemokine (C-C motif) ligand
CD11b	Cluster of differentiation 11b
CD14	Cluster of differentiation 14
CD3	Cluster of differentiation 3
CD45	Cluster of differentiation 45
Csf1	Colony stimulating factor 1
CSV	Comma-separated values
DAMP	Danger associated molecular patterns
DC	Dendritic cell
DMEM	Dulbecco's modified eagle's medium
DNA	Deoxyribonucleic acid
DTP/DTaP/Tdap	Diphtheria-tetanus-pertussis (acellular)
EDTA	Ethylenediaminetetraacetic acid
ELISA	Enzyme-linked immunosorbent assay
EtOH	Ethanol
FACS	Fluorescence-activated cell sorting
FMO	Fluorescence minus one
FOV	Field of view
FSC-A	Forward scatter area
FSC-H	Forward scatter height

FSC-W	Forward scatter width
HBV	Hepatitis B virus
Hib	Haemophilius influenzae b
HK *E.coli*	Heat-killed *Escherichia coli*
HLA-DR	Human leukocyte antigen- antigen D related
HPV	Human papillomavirus
HRP	Horseradish peroxidase
HSCs	Hematopoietic stem cells
I.P.	Intraperitoneally
ICAM-1	Intercellular adhesion molecule 1
IFN-γ	Interferon gamma
IL-10	Interleukin 10
IL-1α/β	Interleukin 1 alpha/beta
Il1rn/IL-1Ra	Interleukin 1 receptor antagonist
IPV	Inactivated polio vaccine
ITAM	Immunoreceptor signalling motif
Keap-1	Kelch-like ECH-associated protein 1
LFA-1	Lymphocyte function-associated antigen 1 (
LPS	Lipopolysaccharide
M-CSF	Macrophage colony stimulating factor
Maff	Transcription factor MafF
Mafk	Transcription factor MafK
MAPK	Mitogen-activated protein kinase
MPLA	Monophosphoryllipid A
MSU	Monosodium urate
mTOR	Mammalian target of rapamycin
MV	Measles vaccine
NaCl	Sodium chloride
Nfe2l2	Nuclear Factor, Erythroid 2 Like 2
NFkB	Nuclear factor kappa-light-chain-enhancer of activated B cells
NH4Cl	Ammonium chloride

NLR	Nucleotide-binding oligomerization domain-like receptors
NLRP3	NACHT, LRR and PYD domains-containing protein 3
NOD2	Nucleotide-binding oligomerization domain-containing protein 2
OD	Optical density
ODN	Oligodeoxynucleotides
OPD	O-phenylenediamine dihydrochloride
OPV	Oral polio vaccine
PAMP	Pathogen associated molecular pattern
PBMC	Peripheral blood mononuclear cell
PBS	Phosphate buffered saline
PFA	Paraformaldehyde
PI3K	Phosphatidylinositol-4,5-bisphosphate 3-kinase
PMA	Phorbol 12-myristate 13-acetate
Poly (I)(C)	Polyinosinic-polycytidylic acid
PRR	Pathogen recognition receptor
PVP	Polyvinylpyrrolidone
RBCs	Red blood cells
RNA	Ribonucleic acid
ROS	Reactive oxygen species
RPMI	Roswell Park Memorial Institute medium
RT	Room temperature
S6K1	Ribosomal protein S6 kinase beta-1
SSC-A	Side scatter area
Syk	Spleen tyrosine kinase
TB	Tuberculosis
Th1	T helper 1 cell
Th2	T helper 2 cell
TLR	Toll like receptor
TMB	Tetramethylbenzidine
TNF-α	Tumour necrosis factor alpha
WHO	World Health Organisation

Acknowledgments

I would like to thank my supervisor Professor Ed Lavelle, for giving me the opportunity to work in the Lavelle lab and for trusting me with this project. I am so grateful for your advice and support over the last four years. Like most, my PhD had a rocky patch and you were so understanding and said all the things I needed to hear at the time. You have helped me get back the confidence I lost for a while and I will forever be thankful for that.

I am extremely privileged to have received a Government of Ireland Postgraduate Scholarship to carry out this work and I would like to thank the Irish Research Council for affording me this opportunity.

I am deeply grateful to Professor Steve Gordon and Dr John Browne at UCD School of Veterinary Medicine for all their help and encouragement with the NanoString experiments. Dr Gavin McManus for his help with the microscopy work, Barry Moran for his help with the flow cytometry and all the staff in TBSI.

The lab wouldn't be the same without all of its members, past and present. I would like to thank the previous members; Dulce, Ciaran, Craig, Seán, Filipa, Stephanie and Aqel. I would especially like to thank Katie and Hannah for your kind and caring support when times were tough. The current lab members- Natalia, Mimmi, Ross, Alex and Roisin. I feel truly blessed to be a part of such an incredible bunch of people and I want to thank you all, especially for making this final year so fun and exciting.

Joanna and Shauna…I can't believe the three musketeers are no longer in the same country let alone the same building!
Joanna, you were such an amazing undergraduate student and taught me more than I think I taught you! All your help and support, big or small, has made the last couple of years so much better than I ever thought it could be. You brought the lab to a crazy, weird and hilarious place and I love you for it.

Shauna, you don't know how much I appreciate literally everything you've done over the last year. Whether it's helping me with my thesis or just being a phone call away, you're an absolute gem and the lab won't be the same without you.

I am extremely grateful for the unwavering support, reassurance and encouragement my family have given me during this project and throughout my life. My parents, Bronwyn and Derek, you are the most incredible couple I've ever known and I'm so lucky to be your daughter. Thank you for all you do. Thank you for knowing exactly what to do all those times I doubted myself…you know me better than I know myself.

I'm so thankful to my brother Cian for all the random chats on my way to the bus. I'm so proud of everything you have achieved, especially as a fellow science graduate. Thanks for always making me laugh.

I'm extremely fortunate to have two very special ladies in my life, my Nanny Josie and my Nana Margaret. Thanks for all the prayers Nanny, I'm sure St Martha is fed up of hearing about me! Nana, you've been there from the very start of my Trinity journey, so it's only fitting that I'm back in Hampton Square for the final chapter.

A special acknowledgment to my fairy god-mother and partner in crime, Giselle. You are the most selfless person I know. I'm so grateful for everything you do.

I would like to thank Mary and Kevin for all their kindness and support not only during my PhD, but over the last 8 years.

Last, but by no means least, Aaron, you are literally the cement that holds me together. I could not have imagined a more thoughtful, supportive, kind and caring person to have by my side on this rollercoaster. I can't wait to see where the next adventure will take us.

Table of Contents

Declaration of authorship		I
Abstract		II
Publications		III
Abbreviations		IV
Acknowledgements		VII
Table of contents		IX
Chapter 1	**Introduction**	1
1.1.1	The History of Vaccination	1
1.1.2	Adjuvants	2
1.1.3	Alum	3
1.1.4	The Non-Specific Effects of Vaccines	5
1.1.5	Innate Immune Training	6
1.1.6	Innate Training of Hematopoietic Stem Cells	8
1.1.7	Pathogen Recognition Receptors	10
1.1.8	Toll-Like Receptors	10
1.1.9	Tolerance	11
1.1.10	Monocytes	13
1.1.11	Macrophages	13
1.1.12	Immunometabolism	15
1.1.13	Glycolysis	15
1.1.14	Oxidative Phosphorylation	15
1.1.15	mTOR	18
1.1.16	mTOR Complexes 1 and 2	18
1.1.17	mTOR Signalling	20
1.1.18	Role of mTOR in Immune Cells	22
1.1.19	Inflammation, Resolution and Repair	23
1.2	Hypothesis	24
1.3	Aims and Objectives	25
Chapter 2	**Materials and Methods**	26
2.1	Materials	26
2.1.1	General cell culture materials	26
2.1.2	Flow Cytometry	28
2.1.3	Enzyme-linked Immunosorbent Assay	29
2.1.4	RNA Isolation	30

2.1.5	Real-time PCR	30
2.1.6	Western Blot	32
2.1.7	NanoString	33
2.1.8	Seahorse Extracellular Flux	33
2.1.9	BCG Infection Assay	34
2.1.10	Confocal Microscopy	34
2.2	Methods	35
2.2.1	Ethics	35
2.2.2	Mice	35
2.2.3	Cell Culture	35
2.2.4	Cell Counting	35
2.2.5	Culture of L929 cells for M-CSF-conditioned media	36
2.2.6	PBMC and Monocyte Isolation	36
2.2.7	Bone Marrow Derived Macrophages	38
2.2.8	*In Vitro* Training of Adherent Human Monocytes or BMDMs	39
2.2.9	*In Vivo* Innate Training	40
2.2.10	Flow Cytometry	40
2.2.11	Enzyme-linked Immunosorbent Assay	40
2.2.12	Real-time PCR	41
2.2.13	Western Blot	42
2.2.14	NanoString nCounter System	43
2.2.15	Seahorse Extracellular Flux	45
2.2.16	BCG Infection Assay	47
2.2.17	Confocal Microscopy	48
2.2.18	Phase Contrast Microscopy	48
2.2.19	Statistical Analysis	49
Chapter 3	**Alum trains human monocytes and murine BMDMs**	50
3.1	Introduction	50
3.2	Aims	51
3.3	Hypothesis	52
3.4	Results	53
3.4.1	Human PBMC density centrifugation through two Percoll gradients (51% and 42%) and sedimentation through autologous plasma yields a highly purified and viable monocyte population	53
3.4.2	Alum trains human monocytes to produce more IL-10 and TNF-α upon secondary stimulation with LPS	56

3.4.3	Alum-trained murine BMDMs are primed for enhanced secretion of IL-10	59
3.4.4	Alum-training alters the morphology of murine BMDMs	61
3.4.6	Macrophage membrane integrity is maintained following stimulation with alum	67
3.4.7	Bone marrow cells isolated from *in vivo* trained mice display increased proliferative capacity	70
3.4.8	Alum-training strongly enhances secretion of the anti-inflammatory cytokines IL-10 and IL-1Ra following infection with BCG	73
3.4.9	Alum-training appears to globally down-regulate pro-inflammatory gene transcription in macrophages	75
3.5	Chapter 3 Discussion	81
Chapter 4	**Alum induces metabolic re-wiring and anti-inflammatory cytokine secretion through mTOR**	88
4.1	Introduction	88
4.2	Hypothesis	89
4.3	Aims	90
4.4	Results	91
4.4.1	Alum induces potent and sustained IL-1Ra secretion by macrophages	91
4.4.2	Macrophages display enhanced metabolic activity 7 days after training with alum	93
4.4.3	IL-1Ra secretion by alum-stimulated BMDMs is reduced by inhibition of the PI3K/mTOR pathway.	96
4.4.4	Rapamycin reduces alum-induced IL-1Ra secretion by BMDMs after 24 h and 7 days	99
4.4.5	Sustained secretion of IL-1Ra over time in response to alum is reduced by rapamycin	101
4.4.6	Secretion of IL-1Ra by human monocytes is enhanced by training with alum and this effect is reversed by rapamycin	103
4.4.7	The enhanced metabolic activity of alum-stimulated BMDMs is inhibited by rapamycin	105
4.4.8	Alum-dependent survival of BMDMs is markedly reduced by rapamycin	110
4.4.9	Alum rapidly induces mTORC1 activation in BMDMs	112

4.4.10	Alum upregulates expression of *Myc* and *Bcl2* in an mTOR dependent manner	114
4.5	Chapter 4 Discussion	116
Chapter 5	**General Discussion**	122
Bibliography	Bibliography	127
Supplementary	NanoString Gene List	143
	Alum induces ROS in BMDMs after 1 h	150

Chapter 1 Introduction

Protection of the host from invading pathogens is a fundamental response required by all organisms[1]. To this end, the immune system comprises a multifaceted framework of defensive barriers, specialized effector cells and an intricate network of cytokines and signalling pathways that have co-evolved alongside the pathogens that attempt to invade the host.

Classically, vertebrate immunity has been segregated into the innate and adaptive systems. This dichotomy identifies the adaptive system as a highly specific form of defence that possesses the ability to generate immunological memory of past infections. Conversely, the innate system, which is the primary line of defence during infection has been considered to be less specific and unable to remember previous immunological insults[2].

1.1.1 The History of Vaccination

As early as the 15th century, attempts were made to prevent deadly diseases such as smallpox through the method of variolation, by mimicking natural infection to generate protective immune responses. This method sought to transfer infection[3] by removing a piece of infected skin from the donor and transferring this to a fresh piece of scratched skin on susceptible individuals who contracted a mild form of the disease but were then rendered immune[4]. In 1718 Lady Mary Wortley Montague, a popular aristocrat and wife of the British ambassador to Turkey advocated for the uptake of variolation in British society, which was common practise in Turkey at the time, by having her own children variolated[5]. Although successful, variolation was found to cause significant and often fatal reactions thereby prompting this growing trend to be fine-tuned by vaccine pioneer Edward Jenner. An eight-year-old boy called James Phipps was vaccinated in 1798 by Jenner who injected the boy with matter derived from the cowpox lesions of a milkmaid, Sarah Nelms. Two months later Phipps was inoculated with fresh smallpox and when no disease developed Jenner concluded that he was completely protected[6].

The field of vaccination was further developed at the end of the 19th century with the observation by Louis Pasteur that pathogens could be attenuated by exposure to environmental factors such as high temperatures, oxygen and certain chemicals allowing him to produce vaccines against anthrax and rabies[7].

The attenuated BCG vaccine was subsequently developed by Calmette and Guerin by passaging *Mycobacterium bovis* (*MTb*) in artificial media at the beginning of the 20th century[8] followed shortly after by the development of the yellow fever vaccine by Max Theiler[9]. These developments firmly established the field of live, attenuated vaccines.

Traditionally vaccines were developed in this manner and although they have been administered to billions of people and elicit strong cellular and humoral immunity conferring protection (sometimes for several decades) there have been safety issues associated with some killed whole cell and live attenuated vaccines[10]. As such, subunit vaccines were developed in which only the microbial component, or antigen, necessary to induce appropriate protective immunity is administered (with an adjuvant), thereby improving the safety of the vaccine[11].The ideal vaccine is one that is safe, potent and confers long-term protection against infection. While subunit antigens are selected with these objectives in mind, in most cases immunogenicity is low compared to killed and live attenuated vaccines. This limitation has prompted the incorporation of adjuvants into subunit vaccines[12].

1.1.2 Adjuvants

Originating from the Latin "adjuvare" meaning to help or to aid, adjuvants can include mineral salts, synthetic particulates and oil-in-water emulsions in addition to components such as microbial products/toxins that are recognised by innate cell receptors[13]. These vital components are intended to potentiate the immune response to the antigen. Exerting their effects on innate cells, adjuvants prompt activation of and antigen uptake by dendritic cells, which serve as a bridge between innate and adaptive immunity and orchestrate antigen specific responses through T and B cells[14].

The term adjuvant was first proposed by Ramon in the early 1920s[15] followed by the first incorporation of an adjuvant into a vaccine in 1926[16]. Alexander Glenny noticed that diphtheria toxoid precipitated with aluminium potassium sulfate, or alum, significantly enhanced antibody production compared to toxoid alone when injected into guinea pigs[17]. Alum is the most widely used vaccine adjuvant and due to its effectiveness in promoting neutralising antibodies and robust safety profile is found in several childhood vaccines against hepatitis A, hepatitis B, diphtheria-tetanus-pertussis (DTaP, Tdap), *Haemophilus*

*influenza*e type b (Hib), human papillomavirus (HPV) and pneumococcal infection[16]. Other licenced vaccine adjuvants that are included in licensed vaccines include monophosphoryl lipid A (MPLA) incorporated into the HPV vaccine Cervarix, MF59 (an oil-in-water emulsion found in the flu vaccine Fluad), and AS03, another oil-in-water emulsion approved as a component of the H5N1 pre-pandemic vaccine Prepandrix[18].

1.1.3 Alum

Although used globally as a vaccine adjuvant since the early part of the 20th century, the mechanism by which alum induces its adjuvanticity has not been fully elucidated[18]. One of the most frequently referenced mechanisms of alum adjuvanticity is the antigen depot effect. It was postulated that alum enhanced antibody responses by functioning as an antigen "depot" when it was observed that the adjuvant formed nodules at the site of injection[18] enhancing immune responses by allowing prolonged antigen release[19]. This was widely accepted and scarcely challenged until further research into the "depot theory" concluded that formation of nodules at the site of injection is dispensable for the adjuvanticity of alum. Brewer *et al* observed that surgical excision of the alum "depot" two hours after vaccination did not affect antigen-specific IgG1 levels ruling out the requirement of depot formation as a mechanism of alum's adjuvant activity[20]. However, the model used was injection of antigen into the ear of mice, so it is possible that the importance of the antigen depot depends on the route of vaccination.

Signalling through PRRs has been suggested as an essential pathway for microbial PAMP based adjuvants such as CpG and MPL[21]. Unlike these pattern-associated molecular pattern (PAMP)-based adjuvants, alum does not signal through toll-like receptors. In addition to PAMPs, NOD-like receptors (NLRs) can also sense endogenous danger signals upon cellular damage[22]. Accordingly, a role for the NLRP3 inflammasome has also been proposed as a mechanism for alum's adjuvant activity[23]. Re *et al* showed that IL-1β and IL-18 release is induced in LPS-primed human and murine DCs by alum in a caspase-1-dependent manner[24]. Moreover several groups have also shown that some of alum's immunostimulatory activity *in vivo* could be attributed to uric acid release by the adjuvant[25]. This suggests an indirect mechanism for the NLRP3 inflammasome activation which is known to be activated by monosodium urate crystals[26]. However while caspase-1-

dependent IL-1β production is observed in APCs treated with alum, only IgE antibody production required the NLRP3 inflammasome[27]. These observations led many researchers to believe that with respect to alum's ability to drive humoral responses, NLRP3 is likely to be a dispensable component of alum's adjuvanticity[28]. Intriguingly, the crystalline properties of alum have been found to be crucial for its adjuvanticity as the predominant effect of crystal uptake by innate cells is the induction of necrotic cell death[29]. This has led to the theory that this necrotic cell death due to rupturing of plasma membranes by alum is pro-inflammatory in nature. It is also possible that some cells do not die following uptake of alum, but survive contact with the adjuvant and in fact possess increased APC activity thereby enhancing antibody production[27].

Further investigation into the crystalline properties of alum by Shi *et al* led to the observation that alum can bind to plasma membrane lipids on DCs independent of inflammasome activity or membrane proteins. This interaction leads to lipid sorting, an event that activates abortive phagocytosis and subsequent antigen uptake. Once these DCs have been activated they demonstrate high affinity for CD4 T cells via intercellular adhesion molecule-1 (ICAM-1) and lymphocyte function-associated antigen-1 (LFA-1) without the requirement for further association with alum[30]. Importantly, the manner in which alum interacts with DCs also occurs during MSU crystal-DC plasma membrane interaction via the aggregation of immunoreceptor signalling motif (ITAM)-containing receptors followed by spleen tyrosine kinase (Syk) and phosphatidylinositol 3-kinase (PI3K) mediated phagocytosis[31].

Although several mechanisms have been proposed, their roles in alum's adjuvanticity remain contentious. Several variables including vaccination route, immunization schedule and adjuvant dose may have contributed to the conflicting reports[32]. Nonetheless alum continues to be the most widely used adjuvant incorporated in currently licensed and routinely used human[15] and veterinary vaccines[33].

1.1.4 The Non-Specific Effects of Vaccines

An optimal vaccine would induce immune memory to facilitate a long lived adaptive immune response against a specific pathogen. However, an old idea has recently re-emerged which proposes that vaccines may also induce non-specific effects, independent of the specific target pathogen[34]. The BCG vaccine, which has been used since 1921 as the only vaccine against TB[35], has also become the main intravesical treatment for early stage non-muscle invasive bladder cancer[36]. It has recently been found to have other beneficial non-specific effects.

During the past few decades epidemiological studies have suggested that the BCG vaccine protects against non-mycobacterial infections as well as asthma[37]. Interestingly, when the BCG vaccine schedule was first established in Sweden in the 1940's, records show that general mortality was almost 3-fold lower among children who had received the vaccine. This decreased mortality could not be explained by TB prevention as the main protection was seen in infants that were not at high risk for developing this mycobacterial disease[38].

Trials carried out in the USA and the UK during the 1940-50s have recently been re-examined and demonstrate that when TB prevention was not the main outcome, those vaccinated with BCG showed a 25% reduction in non-TB and non-accidental deaths[39].

BCG is not the first vaccine claimed to induce beneficial non-specific effects. When Vaccinia was first administered to humans in the 19th century it became apparent that not only did it induce immunological protection from smallpox, recipients were also protected against a wide range of infectious diseases such as measles, syphilis and streptococcus-causing scarlet fever[39].

The non-specific effects of vaccines were investigated in a number of randomized trials carried out in Guinea-Bissau and Senegal, where disease burden is high and lower respiratory tract infections and diarrheal diseases are endemic[40].

The DTP vaccine, which successfully and specifically protects infants against three deadly diseases (diphtheria, tetanus and pertussis), actually increased mortality rates in female recipients[41]. Moreover, this unexplained increase in mortality for female neonates was found to be linked to the DTP vaccine being administered last during the infant immunisation scheme. This prompted further investigation into the non-specific effects of vaccines and several randomised control trials found that both MV and BCG were shown

to confer a non-specific, beneficial protective immunity thereby reducing all-cause mortality. Again, this non-specific effect was more prevalent in female recipients.

In relation to childhood survival in countries with a high incidence of diarrheal and respiratory tract infections it has been proposed that the most important outcome of live vaccines such as MV and BCG might actually be the non-specific protection more so than the specific prevention of acute measles infection[38] or TB, as children do not die of tuberculosis in the neonatal period[42]. In addition to this finding, the majority of the epidemiological data points toward a pattern whereby the type of vaccine may be an important factor for the non-specific effects of immunisation on childhood mortality and survival which are particularly apparent in females. It has been proposed that the beneficial non-specific effects are associated with live vaccines such as BCG, MV, OPV and Vaccinia, whereas the inactivated, alum-adjuvanted vaccines DTP, IPV and HBV are linked to an increased susceptibility, especially in females, to infection unrelated to the diseases these inactivated vaccines specifically protect infants from[38].

1.1.5 Innate Immune Training

However, without mechanistic insights it has been difficult to prove these epidemiological observations for the non-specific effects of vaccines, both beneficial and adverse. Thankfully, recent *in vitro* data and animal studies from several research groups have emerged that yield possible mechanistic evidence to back up decades of epidemiological data[39].

Following on from the plethora of epidemiological data on the non-specific effects of vaccines, a series of pioneering experiments were carried out by Netea *et al* in 2012 with a view to uncovering the immune mechanisms underlying these phenomena. Monocytes were isolated from healthy volunteers directly before and two weeks after vaccination with BCG and re-stimulated *ex vivo* with a range of unrelated bacterial and fungal pathogens. An increased induction of IFN-γ, TNF-α and IL-1β was observed in these monocytes and surprisingly this response endured for 3 months post vaccination[43]. Netea's group also showed that a single dose of the cell wall component of *C. albicans*, β-glucan, protected mice against *Staphylococcus aureus* challenge by inducing epigenetic rewiring and functional reprogramming of monocytes leading to enhanced cytokine production *in vitro*[44].

The epigenetic rewiring in these monocytes was found to be dependent on β-glucan signalling through the PRR, dectin-1, primarily resulting in modifications to histone trimethylation at H3K4[45].

This phenomenon which has been named "trained immunity" challenges the classical view of innate versus adaptive immunity, suggesting that innate cells can retain memory of past immunological insults[46]. Indeed, plants and invertebrates, although lacking an adaptive immune system are capable of establishing immunity against pathogenic reinfection[43]. Trained immunity is achieved through epigenetic alterations in DNA that modify the transcriptional potential of cells by regulating gene expression, subsequently rewiring intracellular signalling and metabolic pathways[47]. This rewiring allows for a long-term pro-inflammatory response that can be measured by increased cytokine production upon re-infection with unrelated pathogens. Additionally, the training effects observed following BCG administration were found to be dependent on NOD2 signalling[43], autophagy[48] and changes in histone methylation[45] which is suggested to account for some of the non-specific effects associated with this live vaccine in epidemiological observation studies.

Several important characteristics distinguish classical immunological memory from trained immunity and are outlined in Figure 1.1.1. Innate immune memory challenges the classical view of innate versus adaptive immunity, suggesting that innate cells can retain memory of past immunologic insults without somatic hypermutation or V(D)J recombination. The main cells that play a role in these phenomena are those of the myeloid lineage which include monocytes and macrophages. The specificity of innate immune cell recognition during infection involves pathogen recognition receptors encoded in the germline of myeloid cells. The increased responsiveness to secondary challenge that occurs during trained immunity is mediated by changes in metabolism, transcription factor expression and epigenetic reprogramming.

1.1.6 Innate Training of Hematopoietic Stem Cells

The longevity of innate immune training has been explored in several studies investigating the transference of innate memory via hematopoietic stem cells (HSCs). For example, HSCs and progenitor cells tolerized by TLR2 ligands give rise to macrophages with a similarly tolerant phenotype characterised by reduced production of inflammatory cytokines in response to inflammatory signals[49]. Another group investigating the effects of UV radiation on immunosuppression found that DC progenitors in the bone marrow of mice became functionally reprogrammed during radiation exposure via epigenetic rewiring and this effect was inherited by their differentiated progeny[50]. BCG itself was found to transcriptionally modify HSCs following direct exposure to the bone marrow via i.v. vaccination. This modification lead to cell expansion and a preference for enhanced myelopoiesis rather than lymphopoiesis. Macrophages stemming from these BCG-trained HSCs were epigenetically rewired for enhanced protection against pathogenic *Mtb* infection[51]. Several studies have also suggested the innate training potential of the microbiome leading to long term reprogramming of bone marrow progenitors. These include commensal-derived signals that modulate myelopoiesis[52], bacterial metabolites such as short chain fatty acids modulating DC differentiation through DC precursors[53] and finally commensal microbes that regulate neutrophil function via direct Nod1 recognition in the bone marrow[54].

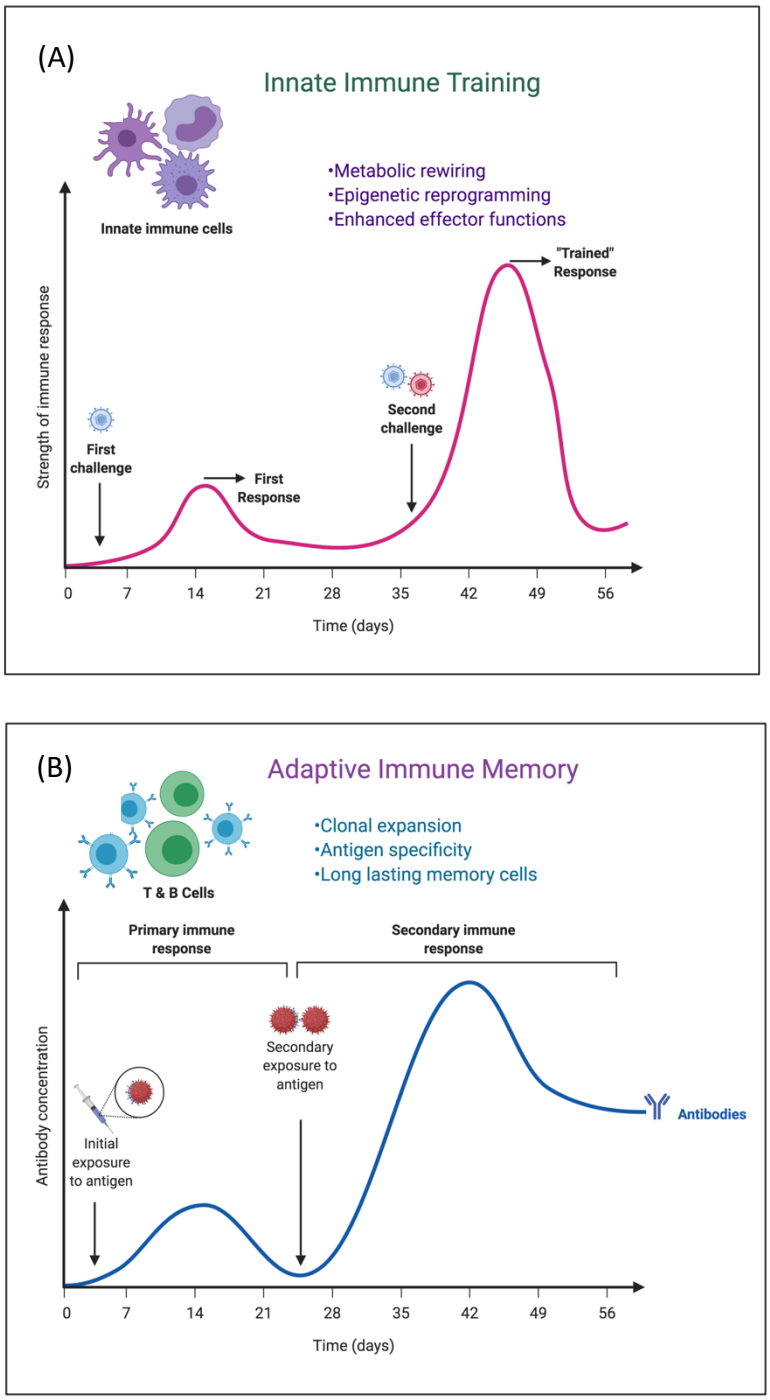

Figure 1.1.1 Innate Immune Training versus Adaptive Immune Memory. (A) Trained immunity is characterised by an initial challenge resulting in metabolic rewiring and epigenetic reprogramming giving enhanced effector functions upon restimulation with a second challenge. Innate training is dependent upon monocytes and macrophages and differs from classical adaptive immune memory (B) which involves clonal expansion, antigen specificity and memory B and T lymphocytes, which confers high specificity and, very often, long-term, pathogen-specific protection (up to decades).

1.1.7 Pathogen Recognition Receptors (PRRs)

The concept of innate memory is not a new one, with a vast body of literature describing the effect of innate "priming" in higher vertebrates both *in vitro* and *in vivo* when previously stimulated monocytes or macrophages adopt an altered responsiveness to an unrelated, secondary challenge[55]. In response to infection or damage to tissues the innate immune system is the main source of acute inflammation and in turn is responsible for activating adaptive immunity[56]. Whilst innate cells such as neutrophils, monocytes, macrophages and dendritic cells are crucial components of this system, other cells such as fibroblasts, epithelial and endothelial cells also serve to protect the host through innate immunity[57]. The way in which innate cells sense and respond to pathogens is through germline-encoded pattern recognition receptors (PRRs) by recognition of conserved microbial molecules called pattern-associated molecular patterns (PAMPs)[58]. Furthermore, endogenous molecules released from dying cells called damage-associated molecular patterns (DAMPs) similarly alert the innate system through PRRs[59]. There are four families of PRR which include transmembrane spanning proteins like Toll-like receptors (TLRs) and C-type lectin receptors (CLRs), and cytoplasmic members: Retinoic acid-inducible gene (RIG)-I-like receptors (RLRs) and NOD-like receptors (NLRs)[58]. The engagement of PRRs by various PAMPs or DAMPs upregulates specific gene expression pathways involved in the inflammatory response following infection or tissue damage[60].

1.1.8 Toll-Like Receptors

The TLRs were the first of the PRRs to be identified with 10 family members (TLR1-TLR10) in humans and 12 (TLR1-TLR9, TLR11-TLR13) in mice[61]. TLRs are transmembrane proteins that can localise to the cell surface or to intracellular compartments including the endoplasmic reticulum (ER), lysosomes or endolysosomes[62]. TLRs are comprised of a leucine-rich repeat (LRR) ectodomain which allows recognition of specific ligands, a transmembrane domain, and a cytoplasmic Toll/IL-1 receptor (TIR) domain that activates downstream signal transduction pathways[61]. PAMPs and DAMPs are recognised by specific TLRs through the ectodomain as a homo- or heterodimer in addition to interaction with a co-receptor or accessory molecule[63]. Adaptor molecules such as MyD88 and TRIF are recruited to TIR domains following TLR activation and initiate highly conserved signalling

pathways that activate several downstream molecules such as NF-κB[64], interferon regulatory factors (IRFs)[65] or mitogen-activated protein (MAP) kinases[66]. Different PAMPs/DAMPs can activate different TLRs leading to a specific transcriptional outcome. Depending on the particular PRR interaction in response to infection or damage these proteins can induce the expression of genes encoding pro-inflammatory cytokines, chemokines, type I interferons (IFNs) and antimicrobial proteins as well as regulatory proteins that have evolved to control excessive inflammation such as anti-inflammatory cytokines and proteins involved in the wound healing process[67].

Another way in which excessive inflammation is controlled is through negative regulation of TLR signalling ensuring that prolonged exposure to TLR ligands does not cause tissue damage[68].

1.1.9 Tolerance

TLR activation can be regulated by a process called tolerance that has been described in several cell types including monocytes, macrophages and dendritic cells. During this process, repeated or prolonged exposure of TLRs to their ligands induces a tolerant cellular state characterised by altered responsiveness of that cell to subsequent stimuli[58]. Tolerance can be induced by several members of the TLR family, however the TLR4 ligand lipopolysaccharide (LPS) is the best characterised and is also known as endotoxin tolerance[69]. Generally LPS tolerance results in a global alteration to the transcriptional profile of the cell characterised by the expression of anti-inflammatory and pro-resolution mediators (IL-10, TGF-β) as well as a downregulation of pro-inflammatory cytokines including TNF-α[70]. Furthermore, inhibitory molecules that downregulate important components of the TLR-4-dependent pathway are upregulated during tolerance as an additional layer of regulation of inflammation[71]. The mechanism by which exposure to a TLR ligand such as LPS reduces the inflammatory response to different TLR ligands is known as cross-tolerance[72]. Importantly the occurrence of endotoxin tolerance has been reported in several clinical settings including sepsis, trauma and pancreatitis highlighting its significance as an often fatal medical complication[73].

Tolerance studies carried out *in vitro* in mouse macrophages and human monocytes reported a global downregulation of inflammatory cytokines and chemokines such as TNF-

α, IL-6, IL-12, CCL3, CCL4 and CXCL10 upon re-stimulation with LPS[74]. Conversely, transcriptional analysis of upregulated genes include anti-inflammatory cytokines such as IL-10, TGFβ[75] and IL-Ra[76]. IL-10[77] and IL-1 receptor antagonist (IL-1Ra)[78] are important cytokines responsible for limiting inflammation. Figure 1.1.2 outlines IL-1Ra exerting its anti-inflammatory effects by competitively engaging the IL-1R, the receptor for pro-inflammatory IL-1 family members, without downstream pathway activation[79]. Gene expression studies have demonstrated global transcriptional rewiring in tolerised cells rather than simply a downregulation of LPS-induced gene expression that was previously suggested for the refractory state of these cells. As such, endotoxin tolerance was originally not considered as a branch of innate memory/training, however it has become increasingly apparent that this phenomenon involves complex modifications to innate cells following exposure to pathogens[69]. Indeed, macrophages have been found to selectively rewire certain histone proteins to modify gene expression patterns thereby adapting to prolonged exposure to pathogens[55].

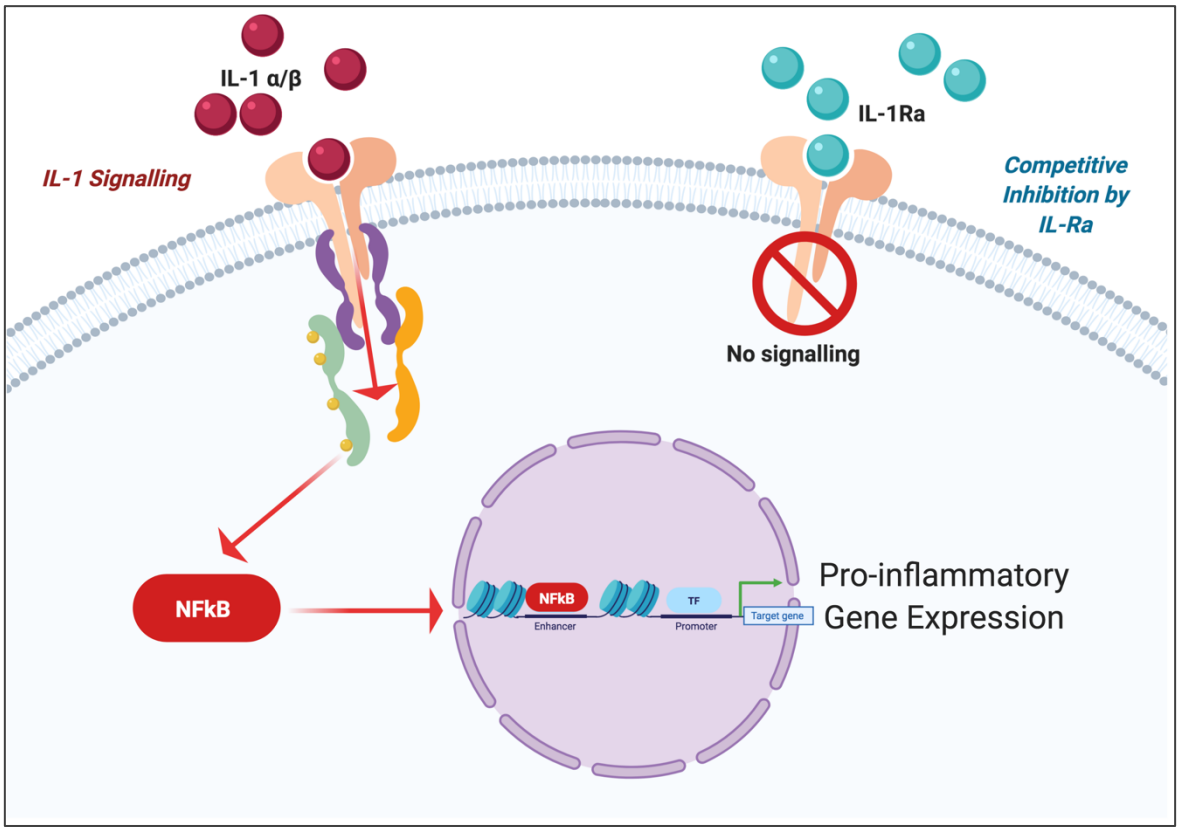

Figure 1.1.2 IL-1Ra competitive inhibition of IL-1 Signalling. IL-1Ra antagonises IL-1 signalling through competitive ligation of IL-1 receptors without engaging downstream signalling pathways. Following successful ligation of IL-1 family members such as IL-1α or IL-1-β downstream pathway activation converges on transcription factors such as NFkB followed by subsequent transcription of pro-inflammatory genes

1.1.10 Monocytes

Metchnikoff first described the phagocytic ability of blood derived cells in the late 19th Century. We now know these crucial members of the innate immune system as monocytes, two different subsets of which have been identified based on distinct chemokine receptor expression and migration patterns. In humans the two main subsets include CD14^{+}CD16^{-} and CD14^{+}CD16^{+} cells while in mice the subsets consist of Gr-1^{hi} and Gr-1^{low} cells[80]. Circulating monocytes have a short half-life, (classical Ly6C^{hi} monocytes 20h and non-classical Ly6C^{lo} monocytes 2.2d[81]) eventually undergoing death by apoptosis. They are subsequently replenished by new monocyte progenitors of the bone marrow. During disease, through inhibition of apoptotic pathways, monocytes can survive and enter tissues from the blood where they differentiate into macrophages and/or dendritic cells[82].

1.1.11 Macrophages

Unlike monocytes, macrophages possess a long lifespan ranging from months to years[83] and are capable of self-renewal[84]. These phagocytic cells are present in all tissues and carry out integral functions both at steady state and following infection or tissue damage. Macrophages can develop from circulating monocyte pre-cursors that enter the tissues, originating from bone marrow haematopoietic stem cells. However, resident macrophages also exist that develop in specific tissues during embryonic development and persist during the lifetime of the individual through the ability to self-renew[85]. Macrophages are extremely adaptable cells that are capable of alternating from one phenotype to another depending on the specific environmental cues that they encounter. The majority of studies characterising macrophage phenotypes have been carried out in primary cells stimulated *in vitro* using polarising ligands. Dichotomous categorization of macrophages into M1, or classical macrophages, and M2, or alternatively activated macrophages, has recently become a topic for debate due to the difficulty in classifying subtypes of a cell that is known for its plasticity and adaptability. Instead, macrophage polarization can be thought of as a hypothetical continuum, with M1 and M2 dichotomies bookending an uninterrupted series of macrophage polarization states. The conventional macrophage dichotomy suggests the establishment of distinct states depending on the local cytokine milieu to drive uncommitted macrophages (M0) to be polarised to M1, if stimulated with IFN-γ/LPS, or M2,

if exposed to IL-4/IL-13[86]. This functional separation has also extended to the metabolic phenotype of these highly plastic cells whereby M1 cells are associated with increased glycolysis to provide pyruvate for the trichloroacetic acid (TCA) cycle whilst increasing the ratio of NADH to NAD^+ thereby indirectly generating ATP[87] for rapid microbicidal and pro-inflammatory responses[88]. Conversely, M2 cells are more frequently associated with enhanced mitochondrial oxidative phosphorylation and, importantly, a fully intact TCA cycle, unlike their pro-inflammatory counterparts[89]. While it is true that the two extremes of macrophage polarisation states require distinct metabolic profiles to fuel specific functions depending on the context in which they become activated, it is a gross oversimplification of their biological complexity and plasticity.

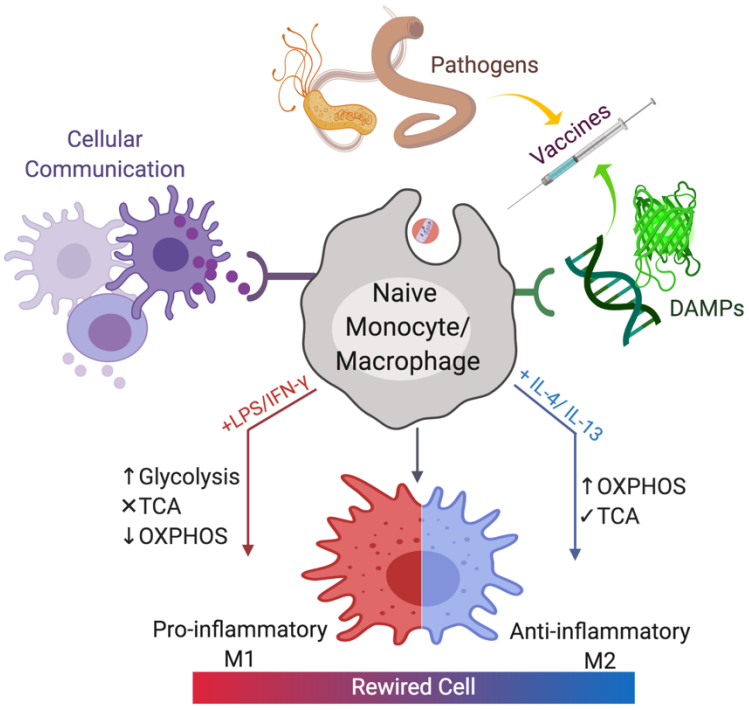

Figure 1.1.3 Macrophage polarity *in vitro* and *in vivo*. Naïve innate cells such as monocytes and macrophages are highly adaptable cells that can encounter a wide range of potentially polarising stimuli including pathogens, PAMPs and DAMPs, vaccines which can incorporate these as well as communication from other cells. In vitro, macrophages can be polarised into M1 or M2 cells through stimulation with LPS/IFN-g or IL-4/13, respectively. Macrophage polarisation results in metabolic rewiring and epigenetic remodelling and can be thought of as a type of innate training. M1 macrophages are highly pro-inflammatory effector cells and prefer to utilise glycolysis and downregulate OXPHOS. M2 macrophages are important regulators of inflammation and have essential roles in resolution and repair. They establish these healing properties by altering their metabolism towards enhanced OXPHOS and a fully intact TCA cycle, unlike their M1 counterparts.

1.1.12 Immunometabolism

Immune cell metabolism has been extensively researched over the years, particularly the role of immune cells in chronic metabolic diseases such as atherosclerosis, obesity and diabetes[90]. Several pathways involved in nutrient- and pathogen-sensing systems have co-evolved and are conserved across several phyla[91]. For this reason, inflammation and metabolism are intrinsically linked and the field of immunometabolism has emerged as one of the key molecular intersections in health and disease. Depending on their particular function at any given time, immune cells utilise metabolic pathways in order to generate biosynthetic intermediates to fuel the specific energy requirements needed for cell growth, proliferation or the rapid production of inflammatory mediators[92]. Although different metabolic pathways result in diverse end products, they are intrinsically linked by their shared fuel inputs and the biosynthetic products they generate which can act as precursors for alternative pathways[87].

1.1.13 Glycolysis

The way in which cells take up and process extracellular glucose is termed the glycolytic metabolic pathway, or glycolysis, to generate pyruvate, as well as other metabolic intermediates which can then feed into other pathways[93]. The glycolytic generation of cellular ATP is relatively inefficient compared to other pathways as only two ATP molecules are made for every glucose molecule processed during glycolysis. Importantly, one of the other by-products in glycolysis is the conversion of NAD+ to NADH. This metabolic flux is sustained by the reduction of pyruvate to lactate thereby maintaining NAD+ levels, a key intermediate used by several enzymes for biosynthesis pathways supporting anabolic growth. Additionally, glycolysis also provides intermediates for the synthesis of nucleotides, amino acids and fatty acids[87]. The phosphatidylinositol 3-kinase (PI3K) and mitogen-activated protein kinase (MAPK) pathways utilise glycolysis during cellular growth, particularly in rapidly proliferating cells[94].

1.1.14 Oxidative Phosphorylation

As well as increasing the ratio of NADH to NAD+, glycolysis provides pyruvate that feeds into the trichloroacetic acid (TCA) cycle, also known as the citric acid or Kreb's cycle. The

TCA cycle is located in the mitochondrial matrix in most quiescent cells and coupled with oxidative phosphorylation is an effective and efficient method for generating ATP for cellular longevity[95]. The pyruvate generated during glycolysis, or free fatty acids, are converted to acetyl coenzyme A (acetyl-CoA) that enters the TCA cycle by aldol condensation with oxaloacetate to form citrate[96]. Another vital fuel source for the TCA cycle is glutamate which is converted into the intermediate α-ketoglutarate[97]. At the end of the TCA the two major products formed are NADH and FADH2, which are the key sources of electrons for the electron transport chain (ETC) fuelling oxidative phosphorylation and, consequently, ATP production. The mammalian mitochondrial electron transport chain encompasses Complexes I-IV, and electron transporters ubiquinone and cytochrome c. Electron flow within the ETC is coupled to the generation of a proton gradient across the inner membrane, the energy from which can be used by ATP synthase (Complex V) to produce ATP[98]. The glycolytic, TCA and ETC integrated pathways are outlined in Figure 1.1.4.

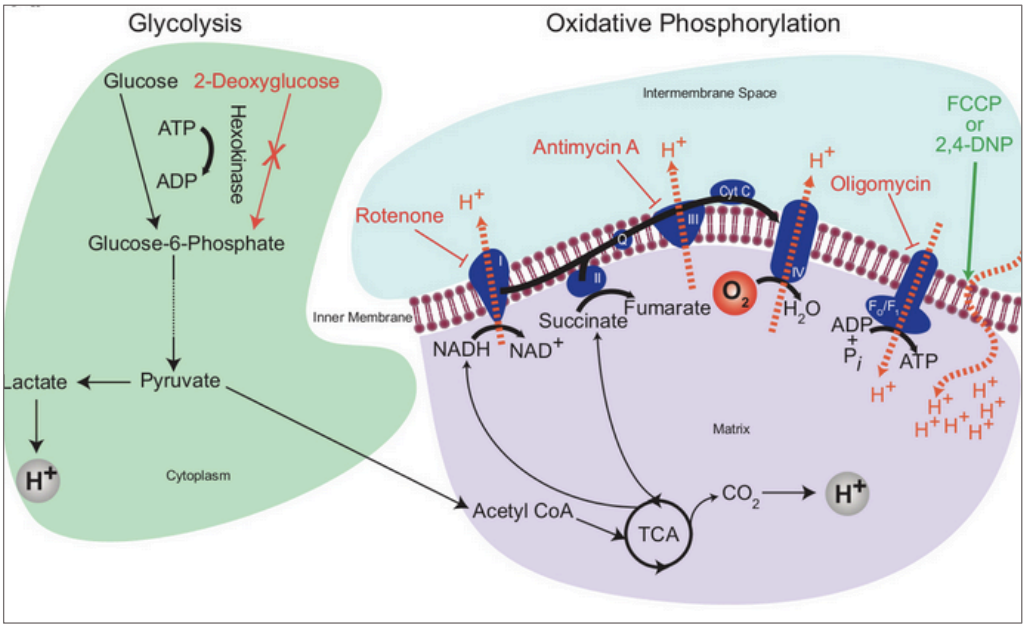

Figure 1.1.4 The Glycolytic and Oxidative Phosphorylation Pathways. Glucose is taken up by the cell and converted to glucose-6-phosphate which is then converted to pyruvate. Pyruvate can then feed into the TCA cycle where it is converted to acetyl CoA. Pyruvate can also be reduced to lactate thereby maintaining NAD+ levels. The mitochondrial electron transport chain (ETC) comprises complexes I-IV, as well as electron transporters ubiquinone and cytochrome c. Complex I establishes the hydrogen ion gradient by pumping four hydrogen ions across the membrane from the matrix into the intermembrane space and can be inhibited by Rotenone. Complex II receives $FADH_2$, which bypasses complex I, and delivers electrons directly to the electron transport chain. Ubiquinone (Q) accepts the electrons from both complex I and complex II and delivers them to complex III. Complex III (inhibited by Antimycin A) pumps protons through the membrane and passes its electrons to cytochrome c for transport to the fourth complex of proteins and enzymes. Complex IV reduces oxygen; the reduced oxygen then picks up two hydrogen ions from the surrounding medium to make water. This electron flow is coupled with the generation of a proton gradient across the inner membrane and the energy accumulated in the proton gradient is used by complex V (ATP synthase) to produce ATP. Complex V can be inhibited by Oligomycin.

1.1.15 mTOR

In addition to its role in protecting the host from pathogenic insults the innate immune system is responsible for maintaining tissue homeostasis by rapidly responding to the presence of pathogens or tissue damage[99]. In order to do this innate cells must possess molecular machinery capable of gauging the metabolic potential of the cell within its environment[100]. The mammalian target of rapamycin (mTOR) is an evolutionarily conserved serine/threonine kinase present in two protein complexes (mTORC1 and mTORC2) that is capable of controlling and orchestrating appropriate effector responses of immune cells[101]. As its name suggests, this 289-kDa protein kinase is a target of the immunosuppressant rapamycin[102]. Rapamycin is a macrolide antibiotic composed of a macrocyclic lactone of different sized rings exerting their effects by binding to bacterial 50S ribosomal subunits thereby impeding protein synthesis. This antibiotic which also possesses potent immunosuppressive properties was first isolated from Streptomyces *hygroscopicus* on Rapa Nui or Easter Island[103]. Its effects on inhibition of cell growth were found to act on a serine-threonine kinase that later became known as mammalian (or mechanistic) target of rapamycin (mTOR). Early experiments in yeast demonstrated that two TOR molecules were expressed: TOR1 and TOR2[104]. It was later discovered in mammals that only one TOR homolog exists which results in two distinct complexes, possessing different functions. mTORC1 is involved in regulating cell growth, metabolism and proliferation while mTORC2 governs cell survival and cytoskeleton organisation[105].

1.1.16 mTOR Complexes 1 and 2

The mTOR complex 1 (mTORC1) of these two functionally distinct complexes contains mTOR, the Rapamycin-sensitive adaptor protein of mTOR (Raptor) and mLST8 (mammalian lethal with Sec13 protein 8 or GbL)[106]. Raptor importantly controls the kinase activity of mTORC1 by enhancing substrate recruitment through engagement with the TOR signalling (TOS) motif on several of mTORC1 substrates such as 4E-BP1 and p70S6K[107]. mTORC1 additionally contains two inhibitory components: PRAS40 (proline-rich Akt substrate of 40 kDa) and DEPTOR (DEP domain containing mTOR interacting protein)[108]. mTORC2, on the other hand, possesses the Rapamycin-insensitive analog of mTOR (Rictor), as well as mTOR

itself, mLST8 and DEPTOR. Unlike mTORC1, mTORC2 also contains regulatory subunits mSin1 and Protor1/2[109].

Rapamycin itself does not directly inhibit the kinase activity of mTOR but binds to the immunophilin FKBP12 (FK506-binding protein of 12 kDa) which is coupled to mTOR FKBP-rapamycin-binding domain (FRB). This results in the inhibition of mTOR function by preventing its binding of the accessory protein Raptor which is required for the phosphorylation of mTOR's downstream targets[110]. Rapamycin's inhibitory effects are only effective on mTORC1 as the FRB protein (although present on both complexes) is only exposed on mTORC1, but is blocked by Rictor on mTORC2[109].

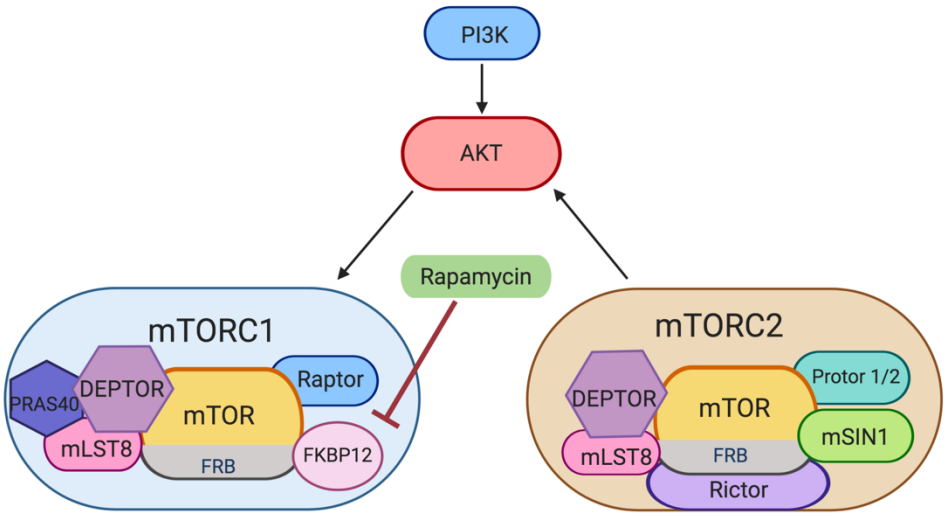

Figure 1.1.5 mTOR Complexes 1 and 2. The two mTOR complexes each contains the mTOR protein itself (including FRB and FKBP12), DEPTOR, mLST8 and PRAS40. mTORC1 contains the Rapamycin-sensitive adaptor protein of mTOR (Raptor). mTORC2, on the other hand, possesses the Rapamycin-insensitive analog of mTOR (Rictor) as well as regulatory subunits mSin1 and Protor1/2. mTORC1 can be activated through the PI3K/Akt pathway while activated mTORC2 can itself activate Akt.

In comparison to mTORC2, the upstream and downstream pathways of mTORC1 have been extensively characterised. This complex mediates cellular signalling from both intracellular and extracellular stimuli to coordinate downstream processes. The energy status of cells, as well as cellular stressors, including hypoxia, are involved in the activation of mTORC1[105]. Several extracellular signals including TLR ligands, cytokines and growth factors are also involved in the activation of this network and upon activation are capable of regulating a myriad of cellular anabolic processes including protein synthesis to aid cell growth[111]. For example, following stimulation with LPS, macrophages and dendritic cells significantly increase cellular protein synthesis which is dependent on activation of the phosphatidylinositol 3- kinase (PI3K)- mTORC1 pathway[112].

1.1.17 mTOR Signalling

As mentioned growth factors are also involved in the activation of this pathway, namely through engagement with receptor tyrosine kinases (RTKs) inducing their autophosphorylation on tyrosine residues[113]. These phosphotyrosine residues allow recruitment of PI3K to the cell membrane, catalysing the production of phosphatidylinositol-3,4,5-triphosphate (PIP3) by phosphorylating phosphatidylinositol-4,5-bisphosphate (PIP2)[114]. PIP3 can then recruit the signalling proteins with pleckstrin homology (PH) domains such as protein serine/threonine kinase-3'-phosphoinositide-dependent kinase 1 (PDK1) and Akt to the membrane[115]. Once Akt becomes activated it phosphorylates several downstream substrates involved in regulating cell survival, growth, proliferation and metabolism, importantly, the regulation of mTOR[109]. The tuberous sclerosis complex 1 (TSC1 or hamartin) and TSC2 or tuberin, become inactivated by Akt-dependent phosphorylation of TSC2, specifically, disrupting its interaction with TSC1[116]. The TSC1/2 complex functions as a GTPase-activating protein thereby inhibiting the activity of the GTP-binding protein Ras homology enriched in brain (Rheb)[117]. Once the TSC complex is disrupted, the now activated form of Rheb can directly bind mTORC1 activating its kinase activity[117]. Mitogen-activated protein kinases (MAPK) also inhibit TSC2 to activate mTORC1[118].

The manner by which activated mTORC1 exerts its downstream effects, such as increased protein synthesis, is through regulation of cap-dependent and cap-independent translation

of mRNAs by phosphorylating eIF4E-binding protein 1 (4E-BP1) and 4E-BP2, inhibitors of the eukaryotic translation initiation factor 4E (eIF4E)[119].

Other phosphorylation targets of mTORC1 include the ribosomal protein S6 kinase 1 (S6K1) and S6K2[120] which further relay this signalling pathway through phosphorylation and activation of S6 to induce protein translation, regulating cell size and motility[121].

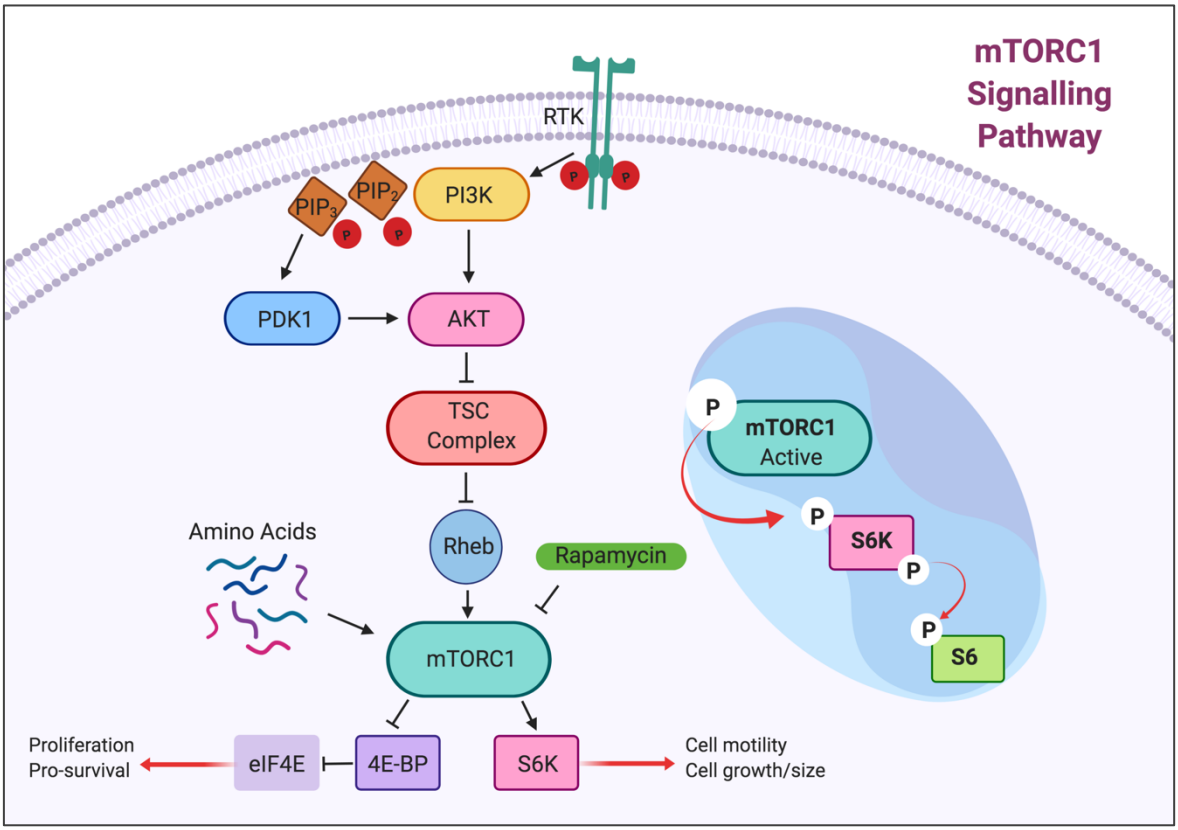

Figure 1.1.6 mTORC Signalling Pathway. Activation of the mTORC1 pathway can be triggered by engagement of receptor tyrosine kinases (RTKs) inducing recruitment of PI3K to the cell membrane. This then catalyses the production of phosphatidylinositol-3,4,5-triphosphate (PIP3) by phosphorylating phosphatidylinositol-4,5-bisphosphate (PIP2). PIP3 recruits the signalling proteins with pleckstrin homology (PH) domains such as protein serine/threonine kinase-3'-phosphoinositide-dependent kinase 1 (PDK1) and Akt to the membrane. The tuberous sclerosis complex 1 (TSC1 or hamartin) and TSC2 or tuberin, become inactivated by Akt-dependent phosphorylation of TSC2 and disrupt its interaction with TSC1 which functions as a GTPase-activating protein thereby inhibiting the activity of the GTP-binding protein Ras homology enriched in brain (Rheb). Once the TSC complex is disrupted, the now activated form of Rheb can directly bind mTORC1 activating its kinase activity on downstream targets 4EBP and S6K leading to proliferation, prosurvival, cell growth and motility. Amino acids can also directly activate mTOR.

1.1.18 Role of mTOR in Immune Cells

Several studies have demonstrated the functional regulation of a broad range of immune cells by mTOR. These include adaptive T and B cells as well as natural killer cells, dendritic cells, macrophages, and other innate cells such as neutrophils and mast cells[122].

A role for mTOR activation in the lineage differentiation of CD4 T cells has been extensively characterised[123]. When mTOR is deleted CD4 T cells lose the ability to differentiate into Th1, Th2 and Th17 following exposure to the corresponding stimui[124]. mTORs involvement in memory CD8 T cell differentiation has also been demonstrated. The administration of rapamycin in a lymphocytic choriomeningitis virus infection model increases the quantity of memory CD 8 T cells. Furthermore the quality of virus-specific CD8 T cells was enhanced following rapamycin treatment in this infection model[125].

B cells have been less well characterised in this field, however some early studies showed that when mTOR was inhibited by rapamycin, B cell proliferation, plasma cell differentiation and germinal centre responses were affected, thus attenuating the generation of high-affinity antibodies [126].

As previously mentioned innate immune cells rely on metabolic pathways to allow for appropriate functional adaptations during stress or infection[127]. This includes changes to morphology, migration to distal tissues and the rapid production of cytokines and chemokines, for example during the acute infection stage[128]. Similarly, when a microbial insult has been appropriately dealt with induction of the resolution phase is key to prevent potential damage to tissues. Many of the metabolic processes governing the restoration to homeostasis by innate cells during infection and inflammation are heavily regulated by the mTORC1-mTORC2 network[122]. In DCs and neutrophils mTORC1 is activated by growth factors such as granulocyte/macrophage colony-stimulating factor (GM-CSF) and FMS-related tyrosine kinase 3 ligand (FLT3L)[129,130]. In monocytes, macrophages and DCs TLR ligands activate mTORC1 and mTORC2[131]. Cytokines such as IL-4 and IL-15 can also induce activation of these complexes in macrophages[131] and NK cells[132], respectively.

In many ways, the highly plastic nature of innate cells relies on their ability to actively control metabolism in order to rapidly adapt their effector functions. This capacity for adaptation is strongly dependent on the availability of nutrients within the cellular environment[133]. For example activated mTORC1 directs cells towards anabolic metabolism

through hypoxia-inducible factor 1α (HIF1α), sterol regulatory element-binding proteins (SREBPs), Myc[134] and peroxisome proliferator-activated receptor-g (PPARg)[135]. Through these mediators mTOR activation supports the energy demands for synthesizing nucleic acids, proteins and lipids and does so via the processes of glycolysis and oxidative phosphorylation[136].

1.1.19 Inflammation, Resolution and Repair

Inflammation is a vital response by the immune system to any stimulus that presents a threat to tissue homeostasis. During the inflammatory response the main goal is to defuse the infectious agent that poses a threat and importantly to limit tissue damage[137]. Granulocytes such as neutrophils, eosinophils and basophils are rapidly recruited to the site of inflammation during the acute phase of inflammation[138]. Other immune cells near the site of infection or injury, including resident macrophages, become activated by DAMPs and pro-inflammatory mediators and further exacerbate the inflammatory response by recruiting leukocytes via chemokine release[99].

In addition to their role in acute inflammation in response to potentially infectious threats, monocytes and macrophages play vital roles in the resolution of this response and subsequent repair mechanisms associated with wound healing[139]. During the onset of repair, the macrophage population within damaged tissue switches to a more anti-inflammatory, M2-like phenotype to enhance healing through enhanced secretion of IL-10 and IL-1Ra[139]. Unsurprisingly, the metabolic demands of anti-inflammatory, pro-resolution macrophages are distinct from those more inflammatory anti-microbial M1-like subtypes.

1.2 Hypothesis

Alum is the most widely used vaccine adjuvant and successfully drives effective humoral immunity in several vaccines, safely conferring long term protection by preventing certain infectious diseases[140]. However, the mechanism through which alum exerts its adjuvant effects, although extensively investigated, has yet to be fully elucidated. We have shown that alum promotes the production of IL-10 that suppresses Th1 responses. The absence of IL-10 signalling does not compromise alum-induced cell infiltration to the site of injection but enhances antigen-specific Th1 responses after vaccination. Importantly innate cells such as macrophages and dendritic cells are key sources of IL-10 expression at the site of injection [141]. The non-specific effects of vaccines has been investigated by epidemiologists for several decades, particularly the beneficial effects of live vaccines such as BCG[142]. In regions where disease burden is high, neonates receiving live vaccines such as MV and BCG show enhanced survival with a reduced incidence of respiratory tract infections, diarrheal disease and neonatal sepsis[143]. The underlying mechanism for this epidemiological phenomenon has been proposed as innate immune training, whereby cells of the innate immune system can be primed to confer protection against re-infection[45] through epigenetic remodelling and metabolic rewiring. The production of a potent anti-inflammatory cytokine, IL-10, coupled with the established safety profile of this adjuvant, prompted the hypothesis that alum can train monocytes and macrophages to adopt an anti-inflammatory profile with enhanced capacity for resolution of inflammation and healing through altered metabolism.

1.3 Aims and Objectives

- Generate a robust innate training protocol in monocytes and macrophages
- Establish the innate training potential of the vaccine adjuvant alum
- Investigate the anti-inflammatory properties of alum-trained monocytes and macrophages
- Characterise the transcriptional profile of alum-trained macrophages
- Analyse the initial and long-term metabolic profile of alum-trained macrophages
- Investigate the potential metabolic pathways involved in alum-stimulated macrophages

Chapter 2 Materials and Methods

2.1 Materials

2.1.1 General cell culture materials

All materials were purchased from Sigma-Aldrich unless otherwise stated

Complete RPMI 1640 Medium (cRPMI)

Roswell Park Memorial Institute (RPMI) 1640 medium (Biosera) was supplemented with 10% (v/v) heat-inactivated (56˚C for 30 mins) filter sterilised foetal calf serum (FCS; Biosera), 50 U/mL penicillin (Gibco), 50 µg/mL streptomycin (Gibco) and 2 mM L-Glutamine (Gibco).

Complete DMEM Culture Medium (cDMEM)

Dulbecco's Modified Eagle Medium (DMEM; Biosera) was supplemented with 10% (v/v) heat-inactivated (56˚C for 30 mins) filter sterilised foetal calf serum (FCS; Biosera), 50U/mL penicillin (Gibco), 50 µg/mL streptomycin (Gibco) and 2mM L-Glutamine (Gibco).

0.88% ammonium chloride (NH_4Cl)

8.8 g of ammonium chloride was dissolved in 1 L of endotoxin-free water (Baxter) and filter sterilised using a 0.22 µm syringe-driven filter (Millipore).

Phosphate Buffered Saline

1X and 10X Endotoxin-free Phosphate Buffered Saline (PBS) (Biosciences)

Cell counting

Viable cells were counted by trypan blue (Sigma) exclusion using KOVA Glasstic cell counter slides with grids (Hycor Biomedical Inc.).

0.25% Trypsin-EDTA solution

2.5 g porcine trypsin and 0.2 g EDTA•4Na/L sterile-filtered in Hanks' Balanced Salt Solution (Sigma).

Ficoll Paque Gradient

23.5 mL Ficoll Paque Stock (GE Healthcare, UK) + 1.5 mL 1X PBS (thoroughly mixed) and divided into 2 X 50 mL falcon tubes

Percoll gradients

Percoll (Sigma-Aldrich)

51% Percoll gradient: 5 mL Percoll mixed with 4.75 mL PBS/EDTA/Plasma

42% Percoll gradient: 4 mL Percoll mixed with 5.5 mL PBS/EDTA/Plasma

1mM EDTA in PBS

1 mL 0.5M added to 500 mL 1X PBS

Table 2.1 Cell culture treatments

Cell culture treatment	Target/function	Supplier
Alum (Alhydrogel)	Various	Brenntag
LPS from Escherichia coli, Serotype R515	TLR4	Enzo Life Sciences
Zymosan	TLR2	Sigma
R848	TLR7/8	Invivogen
Poly (I)(C)	TLR3	Invivogen
β-Glucan from *S.Cerevisiae*	Dectin-1	Sigma
Pam3CSK4	TLR1/2	Invivogen
CpG	TLR9	Oligos
Heat-Killed *Mtb*	Various	Chondrex
PMA (Phorbol myristate acetate)	NFκB	Fisher Scientific
Ionomycin	Ca^{2+}	Fisher Scientific

Table 2.2 Inhibitors

Inhibitor	Target/function	Supplier
Rapamycin	mTORC1	Fisher
ZSTK474	Class I PI3K isoforms	Cell Signalling
Rotenone	Complex I ETC	Sigma
Oligomycin	ATP synthase	Sigma
Fluoro-Carbonyl Cyanide Phenylhdrazone (FCCP)	Dissipates mitochondrial membrane potential	Sigma
Antimycin A	Complex III ETC	Sigma
2-Deoxy-D-glucose (2-DG)	Glucose analog that inhibits glycolysis via hexokinase	Sigma

2.1.2 Flow Cytometry

Table 2.3 Flow Cytometry

Buffer Solutions	Composition
FACS Buffer	1X PBS was supplemented with 0.1% sodium azide and 2% heat-inactivated and filter sterilised FCS
4% Paraformaldehyde (PFA)	40g PFA in 1 L sodium phosphate buffer (13.4 g Na_2HPO_4, 6.9 g NaH_2PO_4, 1L dH2O). Heated for 30-45 min at 60˚C to dissolve and adjust to pH 7
Fixation Buffer	2% PFA in PBS
Fixation Diluent, Fixation Reagent, Permeabilisation Diluent, Permeabilisation Reagent	eBioscience™ Foxp3 /Transcription Factor Staining Buffer Set

Table 2.4 FACS antibodies

Marker	Fluorochrome	Clone	Supplier
hCD45	APC-H7	2D1	BD Bioscience
hCD11b	PE	VIM12	Invitrogen
hCD14	FITC	HCD14	BioLegend
hHLA-DR	BV786	G46-6	BD Bioscience
mCD11b	PECy7	M1/70	BD Bioscience
mF480	PerCP-Cy5.5	BM8	eBioscience
mGr1	APC-Cy7	RB6-8C5	BD Bioscience
mMHCII	APC	M5/114	eBioscience
PI	n/a	n/a	Sigma

2.1.3 Enzyme-linked Immunosorbent Assay (ELISA)

Table 2.5 ELISA buffers and solutions

Buffer and solutions	Composition
10X PBS (10L)	800g NaCl, 20g KCl, 116g Na_2HPO_4, 24g KH_2PO_4 was dissolved in 10L distilled H_20 and brought to pH 7.4
Phosphate citrate buffer	10.19g anhydrous citric acid and 14.6g Na_2HPO_4 was dissolved in 1L distilled H2O and brought to pH 5.5
Wash buffer	0.05% (v/v Tween 20 (Sigma) in 1X PBS
1% BSA	1% (w/v) Bovine Serum Albumin (Fisher Scientific) was dissolved in 1X PBS
Streptavidin HRP	HRP conjugated streptavidin diluted in 1 % BSA
Substrate	Mouse- 0-Phenylenediamine dihydrochloride (OPD; Sigma) Human- Tetramethyl benzidine (TMB; Millipore)
Stop solution	1M H_2SO_4

Table 2.6 ELISA antibodies

Antibody	Supplier	Capture Ab conc. (in PBS)	Blocking Solution	Top working Standard	Detection Ab conc.
IL-10 (Mouse)	Biolegend	1/200	1% BSA	2000 pg/mL	1/200
TNF-α (Mouse)	R&D Systems	1/120	1% BSA	2000 pg/mL	0.05 μg/mL
IL-1Ra (Mouse)	R&D Systems	1/180	1% BSA	10000 pg/mL	1/120
TNF-α (Human)	R&D Systems	1/120	1% BSA	1000 pg/mL	1/60
IL-1Ra (Human)	R&D Systems	1/120	1% BSA	2000 pg/mL	1/60
IL-10 (Human)	R&D Systems	1/120	1% BSA	2000 pg/mL	1/60

2.1.4 RNA isolation

High Pure RNA Isolation Kit (Roche, IN 46250-0414, USA) and Rneasy Plus Mini Kit (Qiagen) were used per manufacturer's instructions.

2.1.5 Real-time PCR

Table 2.7 cDNA Synthesis (Reverse Transcription)

Reagent	Concentration	Supplier
dNTPs	2.5 mM/NTP	Promega
Reverse Transcriptase buffer	-	Promega
Random primers 5' -NNNNNN-3'/ Random Hexamers	1 μg/μL	MWG Biotech
Ribonuclease Inhibitor (RNaseOUT)	40 U/μL	Invitrogen
M-MLV Reverse Transcriptase	200 U/μL	Promega

Table 2.8 Real-time PCR reagents

Reagent	Volume/Sample	Supplier
Kapa SYBR® Fast qPCR	5 μL	Kapa Biosystems
Nuclease-free H_20	1 μL	Roche
Forward Primer	0.5 μL	Invitrogen
Reverse Primer	0.5 μL	Invitrogen
cDNA Template	3 μL	-

Table 2.9 Primer Sequences

Gene Name	Primer Sequence 5'-3'
Bcl2 FP	TGAGTACCTGAACCGGCATCT
Bcl2 RP	GCATCCCAGCCTCCGTTAT
Myc FP	CAGCGACTCTGAAGAAGAGCA
Myc RP	GACCTCTTGGCAGGGGTTTG
Actb FP	TCCAGCCTTTCTTGGGT
Actb RP	GCACTGTGTTGGCATAGAGGTC

2.1.6 Western Blot

Table 2.10 Western Blot SDS PAGE

Buffer and solutions	Composition
10X SDS Running Buffer	144 g Glycine, 30 g Tris Base and 10 g SDS. Made up to a final volume of 1 L with dH_20
1X Transfer Buffer	2.25 g Tris Base, 10.5 g Glycine, 1 g SDS and 200 mL Methanol. Made up to final volume of 1 L with dH_20
Cell lysis buffer	Ripa Buffer (Sigma) with Phosphatase inhibitor cocktail 3 (Sigma) and Protease inhibitor cocktail (Sigma)
SDS-Loading Buffer (Laemmli 2X)	3.028 g Tris.Cl pH 6.8, 4 g SDS, 20 mL Glycerol, 100 mg Bromophenol Blue, 5% dithiothreitol (DTT) was added directly before use
10X TBST (Tris-buffered saline containing Tween-20)	80 g NaCl, 2 g KCl, 20 g Tris Base and 10 mL Tween-20. Made up to a final volume of 1 L with dH_20 and adjusted to pH 7.4
Blocking Buffer	1X TBST with 5% non-fat milk
Wash Buffer	1X TBST
Ladder	PageRuler Pre-stained ladder (10-180kDa: Thermo Scientific)

Table 2.11 SDS Gel

Resolving Gel Ingredients	**12%**	**Stacking Gel Ingredients**	
H_2O	6.6 mL	**H_2O**	5.5 mL
Acrylamide	8 mL	**Acrylamide**	1.3 mL
1.5M Tris pH 8.8	5 mL	**1M Tris pH 6.8**	1 mL
10% SDS	200 µL	**10% SDS**	80 µL
10% APS (add last)	200 µL	**10% APS (add last)**	80 µL
TEMED(add last)	8 µL	**TEMED(add last)**	8 µL

Table 2.12 Western Blot Antibodies (Diluted in 5% Milk in TBST)

Antibody	Source (Cat No.)	Dilution	Secondary Ab
Phospho-S6 kinase Thr389	Cell Signalling (9205S)	1:2500	α-Rabbit
Phospho-S6 S235/236	Cell Signalling (4858T)	1:2500	α-Rabbit
S6 ribosomal protein	Santa Cruz (sc-74459)	1:500	α-Mouse
β-Actin	Sigma (A2228)	1:500	α-Mouse

2.1.7 NanoString

nCounter® MAX Analysis System (School of Veterinary Medicine, UCD)

nCounter® Mouse Inflammation v2 Panel (CodeSet): Gene expression codeset profiling 254 genes; 248 inflammation-related mouse genes + 6 internal reference controls (12 reactions X 2 panels = 24 reactions total)

nCounter Cartridge: Consumables for nCounter MAX Analysis System (12 samples/cartridge)

2.1.8 Seahorse Extracellular Flux

96-well XF cell culture microplates, Seahorse XF media, base media and calibration buffer were purchased from Agilent technologies

2.1.9 BCG Infection Assay (School of Veterinary Medicine, UCD)

Table 2.13 BCG Buffers and Solutions

Buffer Solutions	Composition
Middlebrook 7H11 Agar (20 mL per petri dish)	10.5g 7H11 powder (company) + 450 mL distilled water + 2.5 mL glycerol (company) was dissolved and autoclaved and allowed to cool. 50 mL of 10X OADC enrichment was finally added
10X OADC	50 g BSA + 8.5 g NaCl + 20 g glucose made up to 1 L Baxter water and sterilised using SteriCup
0.05% Tween	Diluted in dH2O
RLT buffer	Qiagen RLT buffer + 1% 2-betamercaptoethanol
4% PFA	Diluted as before in PBS

2.1.10 Confocal Microscopy

Live cell imaging

Active mitochondria stain: Red-orange Tetramethylrhodamine, Methyl Ester, Perchlorate (TMRM) (Thermofisher Scientific)

Nuclear stain: Propidium Iodide (PI) (Sigma)

2.2 Methods

2.2.1 Ethics Statement

Human blood samples were collected from anonymous healthy blood donors from the Irish Blood Transfusion service (IBTS) under license number (BI-AG-300919) issued from the School of Biochemistry and Immunology Research Ethics Committee, Trinity College Dublin in accordance with the Declaration of Helsinki.

2.2.2 Mice

C57BL/6 mice aged 8-12 weeks were bred in Trinity Biomedical Sciences institute (TBSI) Comparative medicines Unit. Animals were maintained according to the regulations of the European Union and the Health Products Regulatory Authority (HPRA). All animal studies were approved by Trinity College Dublin Animal Research Ethics Committee (Ethical approval number 091210) and were performed under the appropriate licence. For *in vivo* studies, procedures were carried out under licence number AE191364/P079.

2.2.3 Cell Culture

Cells were cultured at 37˚C with atmospheric conditions of 95% humidity and 5% CO_2

2.2.4 Cell Counting

Cell counts were determined by trypan blue exclusion. A cell suspension sample was stained with trypan blue in the appropriate counting dilution and 10 μL of this cell/trypan mixture was loaded onto a KOVA Glasstic cell counter slide with grids (Hycor Biomedical Inc.) and viewed under a light microscope. The final cell count in cells/mL was ascertained using the formula:

$$\textit{Number of cells/mL} = \textit{cell number} \times 10^4 \textit{ cells/mL} \times \textit{dilution factor}$$

2.2.5 Culture of L929 cells for production of M-CSF-conditioned medium

A frozen vial of L929 cells was rapidly thawed in the water bath at 37˚C and added to 9 mL of pre-warmed cDMEM. The cells were centrifuged at 300 x g for 5 mins to rinse off any DMSO present in preservation media by discarding supernatant. The cell pellets were disrupted and re-suspended in 10 mL of cDMEM (w/o antibiotic) and transferred to a T75 flask containing pre-warmed cDMEM. Cells were left in the CO_2 incubator and checked daily until 90% confluency was established. At this point the medium was discarded and the cells washed with pre-warmed PBS without Ca^{2+}/Mg^{2+}. Cells were then incubated at 37˚C with 5mL of trypsin-EDTA solution for 5mins and pipetted up and down carefully to detach cells. 20 mL of cDMEM was added and the cells centrifuged for 5 min at 400g. The supernatants were discarded, the cells re-suspended in 25 mL of cDMEM and counted. Where appropriate, new stocks were stored by re-suspending 1-2 X 10^6 cells in 1 mL 10%DMSO/90%FBS and frozen immediately at -80 using a "Mr Frosty" freezing container. The rest of the cells were set up to generate cultures for M-CSF production by seeding cells at 0.5X10^6/mL and setting up cultures in T175 flasks and removing supernatants one week later. Depending on batch-to-batch variation of L929-conditioned media, 10-25% was used to differentiate BMDMs.

2.2.6 PBMC and Monocyte Isolation

Isolation of Non-Activated Monocytes from Human Buffy Coats

The isolation process included three steps. Firstly, mononuclear cells were separated from erythrocytes and polymorphonuclear leukocytes with a Ficoll gradient. Next, platelets were removed by sedimentation through autologous plasma. The final step was the separation of monocytes from lymphocytes with a Percoll gradient.

Separation of erythrocytes and polynuclear leukocytes

Buffy coats were diluted 1:1 with 1X PBS in 50 mL tubes and slowly layered onto Ficoll Paque without the two solutions mixing by holding two 50 mL tubes horizontally. The Ficoll Paque/blood gradient was then centrifuged at 400 x g (1359 rpm) for 30 mins at room temperature (RT).

Collection of autologous plasma and interface cells:

After centrifugation, plasma was collected from the supernatants and set aside in a 50 mL tube leaving approximately 5 mL plasma above the interface of the cells. Cells at the interface were carefully collected using a Pasteur pipette and transferred into a 50 mL tube containing 5 mL of 1 mM EDTA in 1X PBS. The collected cells were then topped up with a further 30 mL of 1 mM EDTA, centrifuged at 250 x g (1050 rpm) for 10 mins and the supernatants aspirated. The collected plasma was centrifuged at 2800 x g (3500 rpm) for 10 mins to pellet any remaining cell debris and 1 mL of the supernatant plasma was added to 25 mL of 1 mM EDTA for later preparation of Percoll gradient. The remaining plasma was divided into 50 mL tubes for subsequent platelet removal.

Platelet Removal:

1 mL of collected plasma was added to 3 mL of 1 mM EDTA, which was then used to dissolve the cell pellet by slowly pipetting with a 5 mL pipette. 6 mL of 1 mM EDTA was added and this cell/plasma/EDTA mixture was then gently layered onto plasma that was collected earlier and centrifuged for 10 mins at 150 x g (800 rpm) to separate platelets from mononuclear cells. The supernatant containing platelets were discarded leaving 2 mL of plasma with each cell pellet.

Cell Separation by Percoll Gradient

4 mL of 51% Percoll was added to a 15 mL tube followed by 4 mL of 42% Percoll. The mononuclear cell pellets were dissolved in 3 mL 1 mM EDTA by careful pipetting and the cells mixtures were layered onto the Percoll gradients and centrifuged at 650 x g (1700rpm) for 30 mins.

Washing and Plating

The supernatants were aspirated just above the white band of cells at intersection between 51% and 42% Percoll gradients. The cells were collected using a Pasteur pipette and added to a 50 mL falcon containing 2 mL of retained plasma and topped up with 1 mM EDTA, mixed by inversion and centrifuged at 250 x g (1050 rpm) for 10 mins. The supernatants were discarded and 3 mL of RPMI was used to dissolve the pellet carefully and finally made

up to 10 mL with RPMI and counted. Cells were seeded at 0.5 X 10^6 cells/well and allowed to adhere for 1 hr followed by washing with 1X PBS to remove non-adherent cells.

2.2.7 Bone Marrow Derived Macrophages (BMDMs)

Bone marrow-derived macrophages (BMDMs) were generated from C57BL/6 mice. Mice were euthanized using CO_2 and death confirmed by cervical dislocation. The femurs and tibiae were removed, cleaned of muscle tissue with a sterile gauze and separated. Bones were washed in petri dishes containing 70% EtOH for 5 seconds and then cDMEM. A 10 mL syringe was filled and attached to a 27G needle. The tips of the femur and tibia bone were minimally cut and kept in a sterile petri dish with fresh cDMEM. The bone marrow was flushed out into a petri dish by inserting the 27G needle and injecting cDMEM. Cell clumps were disrupted by repeat pipetting with a 19G needle. The cells were transferred to 50 mL falcon tubes and spun down at 1200 rpm for 5 mins. The supernatant was removed and 1 mL of 0.88 % NH_4Cl red blood cell lysis solution was added. After two mins, the reaction was stopped with 25 mL of cDMEM. The cell mixture was centrifuged at 1200 rpm for 5 mins. The supernatant was removed. The cell pellet was re-suspended in 10 mL cDMEM. Cell numbers were counted using trypan blue dye exclusion. The volume was adjusted to give 1x10^6 cells/mL in cDMEM with 10%-25% L929-conditioned medium containing M-CSF depending on the particular batch used. Next, 20 mL of cell suspension was transferred to large non-TC treated petri dishes. On day three, 20 mL of cDMEM containing 10%-25% L929 was added to large non-TC treated petri dishes. On day 5, the petri dish culture media was removed using a pipette and 10 mL of cold 1 mM EDTA in PBS was added. The petri dishes were placed on ice. After 10-15 mins the PBS was vigorously pipetted to remove cells. Cells were then transferred into 50 mL falcon tubes and spun at 1200 rpm for 5 mins. The supernatants were discarded and cells were re-suspended in cDMEM supplemented with half the concentration of L929-conditioned medium used to differentiate BMDMs and made up to a final concentration of 1x10^6 cells/mL. Cells were incubated overnight and trained/stimulated the next day.

2.2.8 *In Vitro* Training of Adherent Human Monocytes or BMDMs

On day 0, adherent monocytes or BMDMs were trained by incubating for 24 hrs at 37˚C, 5% CO_2 with either alum (10 μg/mL) or medium: cRPMI (monocytes), cDMEM (BMDMs). On day 1, the supernatants were removed from the wells and the remaining stimuli were washed with warm PBS and fresh cRPMI or cDMEM was added to the wells and then left for 6 days, changing the media on the 3rd day. After 6 days, the trained monocytes/BMDMs were re-stimulated with a range of TLR agonists. Depending on final read-out, cells were re-stimulated by incubating at 37˚C, 5% CO_2 for specific time-points on day 7. Either supernatants or cell lysates were collected and downstream assays carried out.

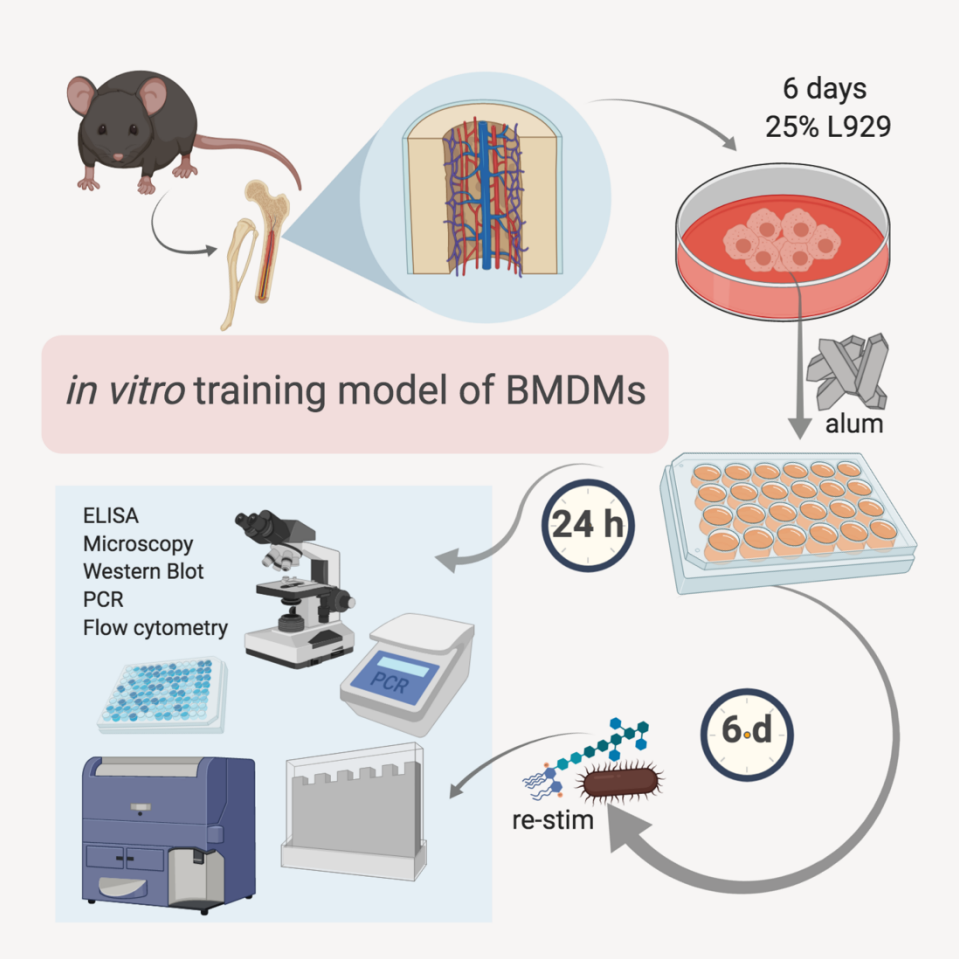

Figure 2.2.1 Outline of *in vitro* training model of macrophages and downstream experiments. Bone marrow cells are isolated from tibia and femur of mice and differentiated for 6 days in 10-25% L929-conditioned media. On day 6 of differentiation, BMDMs are plated and exposed to training stimuli (alum) for 24 h followed by a washout. The trained BMDMs are then rested for 6 days and re-stimulated with TLR agonists or infected with BCG (depending on the particular experimental question). Supernatants can be taken for ELISA, or cells lysed for Western Blot or q-PCR/NanoString. Alternatively cells are imaged by phase contrast/fluorescent microscopy.

2.2.9 *In Vivo* Innate Training

C57BL/6 mice were injected intraperitoneally (I.P.) with PBS or 1 mg of alum 3 or 7 days prior to euthanisation. Mice were euthanised by CO_2 and death confirmed by cervical dislocation. The femurs and tibias were taken and BMDMs set up as previously outlined.

2.2.10 Flow cytometry

Fluorochrome compensation was established using anti-rat and anti-hamster Ig k chain negative control compensation beads (BD Pharmingen), or cells, were stained with a single antibody. Auto-fluorescence thresholds were established by staining samples with fluorescence-minus-one (FMO) control stains in which the fluorochrome of interest was omitted. This allowed for the distinction between autofluorescent cells from cells expressing low levels of individual surface markers. Debris was excluded from analysis by identifying true cell populations from side scatter-area (SSC-A) versus forward scatter-area (FSC-A) plots. Single cells were found by analysing FSC-width (W)/height (H) versus FSC-A. Samples were acquired using Diva software and analysed using FlowJo (Treestar, Oregon).

2.2.11 Enzyme-linked immunosorbent assay (ELISA)

Measuring cytokine secretion

Cytokine concentrations from cell culture supernatants were measured using commercially available ELISA kits from R&D Systems and Biolegend. All antibodies and recombinant cytokine standard concentrations, buffers and diluents and incubation times for the different ELISA kit components are listed in Table 2.6.

ELISA protocol for the quantification of cytokine secretion

High binding plates (Greiner Bio One) were coated with capture antibody in PBS or sodium carbonate buffer, depending on the cytokine of interest (50 μL/well) and incubated overnight at 4˚C or RT. After washing with PBS-Tween (wash buffer), the plates were incubated for 1 or 2 hrs (depending on kit) at RT with 150 μL of blocking solution to prevent

non-specific binding. The plates were washed with wash buffer and aspirated and 50 μL of sample supernatant or serial dilutions of standard were added to the plate and incubated for 2 hrs at RT. The plates were subsequently washed again in wash buffer and detection antibody (50 μL /well) was added and the plates incubated for either 1 or 2 hrs at RT depending on the kit. After washing again, HRP-conjugated streptavidin (50 μL/well) was added to the plates and incubated at RT and in the dark for 20 or 30 mins depending on the kit. The plates were washed for a final time and OPD or TMB substrate was added (50 μL/well). The enzyme reaction was stopped by adding 1M H_2SO_4 (25 μL/well) and the optical density (OD) values determined by measuring the absorbance at 492nm (OPD) or 450nm (TMB) using a Versa Max microtiter plate reader. The concentrations of cytokines were determined using a standard curve generated by recombinant cytokines of known concentrations.

2.1.12 Real-time PCR

RNA isolation

Total RNA was isolated from cells using the High Pure RNA Isolation Kit (Roche) following the manufacturer's instructions. Following stimulations and incubation for appropriate time points cells were lysed with buffer RLT and added to a column and incubated with DNAse I to digest any contaminating DNA. After three wash steps the RNA was eluted in RNAse-free H_2O into nuclease-free microcentrifuge tubes. Each RNA sample (1 μL) was added to the Nanodrop spectrophotometer and the absorbance read at 260 nm. The 260/280 nm ratio was used to measure the quality and concentration of RNA. RNA samples were stored at -80˚C for later use.

Reverse transcription

Isolated RNA was used to produce complementary DNA (cDNA). The RNA concentration of each sample was adjusted to 200 ng by adding H2O up to a total volume of 5 μL. cDNA was synthesised by adding 5 μL of master mix to each sample including random hexamers to serve as primers for DNA synthesis, Reverse transcriptase (RT) enzyme to generate cDNA and RNaseOUT to inhibit ribonucleases. To exclude any possible DNA contamination a

random sample without RT enzyme (replaced with nuclease-free H2O) was used as a control with each RT-PCR cycle. The PCR settings used are described in Table below. After the cycle was complete, 20 μL of nuclease-free water was added to dilute the cDNA sample and stored at -20˚C.

Quantitative Real-time PCR

qPCR was performed using cDNA and forward and reverse primers (5 pmol/μL) using the Kapa SYBR® Fast qPCR Kit. In addition to the no RT control, cDNA was replaced with nuclease free H_2O to exclude genomic DNA contamination in the samples or reagents. Samples were run on an Applied Biosystems 7500 Fast system for 40 cycles of 2 mins at 95˚C followed by 3 seconds at 95˚C, and finally by one cycle of 30 seconds at 60˚C. Dissociation curve analysis was performed after a completed real-time qPCR to exclude non-specific products. The change in gene expression was normalised to b-actin expression from the corresponding sample.

2.2.13 Western Blot

Protein extraction from supernatants

BMDMs (1 X 10^6 cells/mL) were plated in 1 mL of cDMEM in a 12-well flat bottom tissue culture plate. Cells were then stimulated at various time points, supernatants were removed and cells washed with PBS. The cell pellet was lysed with 100 μL RIPA lysis buffer (Table) containing protease (1% v/v) and phosphatase inhibitors (1% v/v) on ice for 30 mins with vortexing every 10 mins. The resulting cell lysate was transferred to Eppendorf tubes and frozen at -20˚C for later use or kept on ice for immediate use.

SDS-PAGE

10 μL of sample was mixed with 10 μL of 2X Laemmli sample buffer (approximately 20 μg of protein), boiled for 5-10 mins at 95˚C. Gels were prepared and 20 μL of sample was loaded into each well, in addition to 5 μL Page ruler pre-stained protein ladder (Thermo scientific). Once samples were loaded, the gel was run at 100-120 volts (V) for 90 mins in running buffer.

Transfer of proteins onto polyvinylidene difluoride (PVDF) membrane

Proteins were transferred to a PVDF membrane using a semi-dry blotter (Cleaver Scientific Ltd). The PVDV membrane was activated in methanol by immersion for 30 sec, washed in water for 2 mins and then soaked in transfer buffer for 5 mins. The PVDF membrane was then placed onto a sheet of filter paper that had been soaked in transfer buffer. The gel was carefully placed over the PVDF membrane and an additional sheet of soaked filter paper was placed on top of gel. Any air bubbles were rolled out. The proteins were transferred from the gel to the membrane at 50 milliamperes (mA) per gel for 75 mins.

Immunodetection of proteins

The blotted membrane was removed from the transfer machine and immediately placed in blocking buffer. The blot was incubated for 1 hr at RT with gentle shaking. The membrane was then probed with appropriate dilution of primary antibody in blocking buffer and incubated overnight at 4˚C with gentle shaking. The membrane was washed 3 X 5 mins with 20 mL wash buffer. The membrane was then incubated with recommended dilution of HRP-conjugated secondary antibody (1/10000) in blocking buffer at RT for 1 hr with gentle shaking. The membrane was washed again three times for 5 mins each. Visualised on the Li-cor Odyssey 9120 Imaging System.

2.2.14 NanoString nCounter System

Sample Preparation: BMDM lysis and RNA isolation

On day 7 of the *in vitro* training protocol, alum-trained or DMEM-trained BMDMs were re-stimulated with DMEM or LPS 10 ng/mL for 3 hrs or 8 hrs. The supernatants were removed and cells lysed and homogenized in highly denaturing guanidine-isothiocyanate-containing Buffer RLT Plus (Qiagen) to inactivate RNases. The lysate was then passed through the gDNA eliminator spin column, selectively removing genomic DNA. To allow appropriate binding conditions for RNA ethanol was added and the sample was applied to an RNeasy MinElute spin column containing a silica membrane to specifically bind RNA from cell lysates. Following several wash steps the purified RNA was finally eluted in nuclease-free H_2O.

RNA Quality Control

RNA quality was assessed using the RNA 6000 assay on the Agilent Bioanalyzer,
(all samples were shown to have RIN values greater than 8.5.)

RNA Quantification

RNA quantity was determined using the Qubit High Sensitivity RNA kit and all samples were adjusted to 20.0 ng per μL; 5.0 μL (100ng) was used per NanoString assay.

NanoString Hybridisation Reaction

The hybridization reaction was set up at RT. The mastermix was made up by adding 70 μL of hybridization buffer to the Reporter Codeset tube and inverting it repeatedly. 8 μL of mastermix was added to each of the 12 tubes (12 samples/panel) followed by 5 μL of each sample. The Capture Probeset was then mixed and spun down and 2 μl was added to each tube. The tubes were mixed by repeated inversion, spun down and placed in thermal cycler at 65˚C overnight.

NanoString Prep Station

The NanoString Prep Station is a multi-channel pipetting robot that processes samples to prepare them for data collection on the Digital Analyzer. This automated instrument performs liquid transfers, magnetic bead separations and immobilization of molecular labels on the sample cartridge surface. After sample processing and hybridization at 65˚C overnight, the hybridized samples were inserted into the Prep Station for purification and immobilization onto the internal surface of the sample cartridge.

NanoString Digital Analyzer

The nCounter Digital Analyzer is a multi-channel epifluorescence scanner that is specially designed to image and analyse NanoString's nCounter Cartridges.
Following purification and immobilization steps the sample cartridge was then transferred to the Digital Analyzer for imaging the immobilized fluorescent reporters in the cartridge with a CCD camera through a microscopic lens and analysing the fields of view (FOV) collected for each sample and counting hundreds to thousands of target molecules. The

images were then exported to a comma separated value (CSV) file and analysed using NanoString's nSolver Analysis Software and Advanced Analysis add-on. QC was carried out using nSolver QC tools highlighting targets with an absolute copy number of 20 or lower as flagged (indicated in blue bar on HeatMaps.) Internal reference genes were selected based on nSolver criteria including comparable expression between treatment and control groups and a wide range of Ct values to analyse variabilities in each candidate reference gene. A full list of fold changes and selected internal reference genes are listed in the supplementary section table 1.

2.2.15 Seahorse metabolic flux analyser

For real-time analysis of the extracellular acidification rate (ECAR) and oxygen-consumption rate (OCR) of BMDMs cultured under various conditions, a Seahorse XF-96 Analyzer (Seahorse Bioscience) was used. BMDMs were seeded at 150,000 cells per well in a Seahorse XF-96 plate. Sequential measurements of ECAR and OCR made after the addition of the inhibitors at a final "well" concentration of the following: oligomycin (1 µM), FCCP (1 µM), rotenone plus antimycin A (500 nM) and 2-deoxyglucose (2DG, 25 mM) Rates of basal glycolysis, glycolytic capacity, basal mitochondrial respiration and maximal mitochondrial respiration were calculated using the following equations:

- Basal OCR: (average OCR before Oligomycin) – (average OCR after Rotenone/Antimycin A injection)
- Basal ECAR: (average ECAR before Oligomycin) – (average ECAR after 2-DG injection)
- Maximal Respiration: (average OCR after FCCP injection) – (average OCR after Rotenone/Antimycin A injection)
- Maximal Glycolysis: (average ECAR after Oligomycin) – (average ECAR after 2-DG injection)

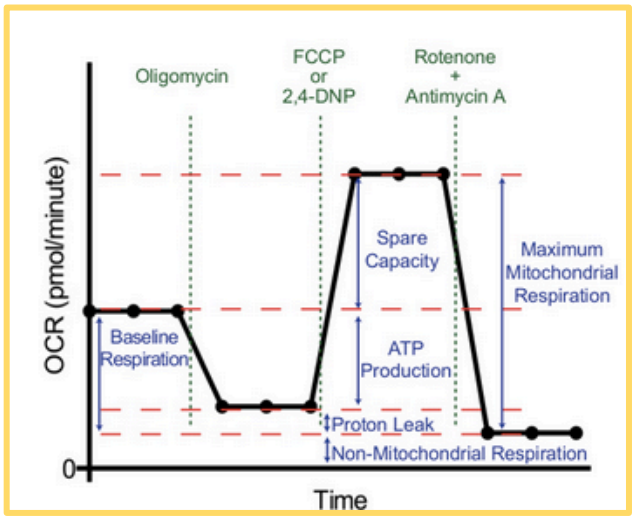

Figure 2.2.2 Analysis of Oxidative Phosphorylation rates using the Seahorse extracellular flux analyser. Basal rates of OxPhos are determined by the amount of oxygen being consumed over time (OCR). ATP synthase, the enzyme that generates ATP from ADP at the end of the electron transport chain (ETC) is inhibited by injection of Oligomycin. FCCP addition disrupts the proton gradient across the inner mitochondrial membrane, which is coupled to electron transport, thus allowing protons to flow freely through the inner mitochondrial membrane. In the presence of FCCP, the rate of OxPhos is thereby maximally increased which can be calculated as Maximum Mitochondrial Respiration. Antimycin A and Rotenone inhibit complex III and I of the ETC respectively, therefore any oxygen consumption after addition of these two compounds is non-mitochondrial respiration.

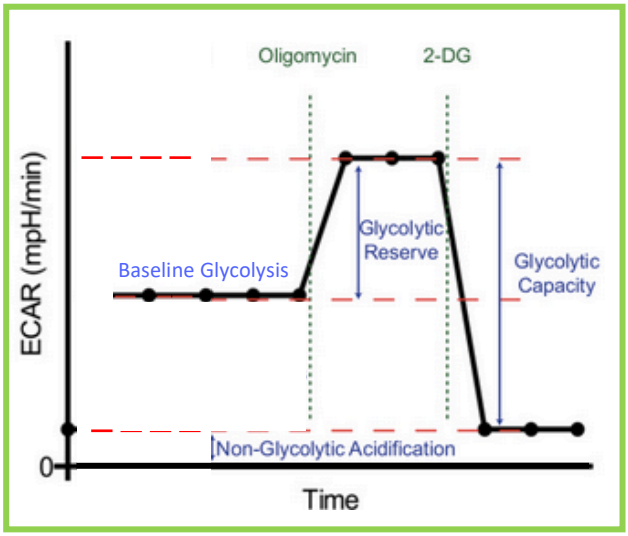

Figure 2.2.3 Analysis of Glycolysis rates using the Seahorse extracellular flux analyser. Basal rates of glycolysis are determined by the change in extracellular acidification in the media over time, resulting from the release of H+ protons during glycolysis (ECAR). ATP synthase, the enzyme that generates ATP from ADP at the end of the electron transport chain (ETC) is inhibited by injection of Oligomycin. Following injection of 2-DG a direct inhibitor of glycolysis media acidification can be attributed to processes other than glycolysis. Glycolytic capacity is the rate at which glycolysis is maximally increased and can be used to calculate the rate of glycolysis.

2.2.16 BCG Infection Assay

Pre-experiment Bacterial Culture (performed by Morgane Mittermite, School of Veterinary Medicine, UCD)

Frozen aliquots of Mycobacterium (BCG Denmark) (1 X 10^7CFU/mL) in 1 mL screw-cap tubes were thawed inside the Class II microbiological safety cabinet (MSC). The 1 mL aliquots were diluted in 9 mL of 7H9 media in a 50 mL tube, sealed and sprayed with 5% Biocleanse. The tubes were allowed to sit for 5 mins in the MSC before being transferred to the 37˚C incubator. They were allowed to grow statically until the optical density was approximately 0.5. The OD was read by adding 1 mL of sample to a cuvette and reading on the spectrophotometer. The culture was up-scaled to a large volume by transferring 4 mL from the starter culture to 46-96 mL of 7H9 Middlebrook broth in a large cell culture roller bottle. The OD of the up-scaled culture was adjusted to 0.1 to correspond to an early lag-phase of bacterial growth. The bottles were placed on rollers in a 37˚C incubator and rotated 1-2 rotations per min and allowed to grow for approximately 5 days until the OD is 0.5-0.8, corresponding to logarithmic phase of bacterial growth.

Bacterial Preparation

When the culture had reached the desired OD, 20 mL aliquots were transferred to a 50 mL centrifuge tube. The tubes were sealed and sprayed with biocleanse and allowed to stand for 5 min in a sealed centrifuge bucket prior to removing from the Class II cabinet. The buckets were carefully transferred to the centrifuge and centrifuged at 1000 x g for 10 mins. After centrifugation the supernatants were discarded by pipetting into 5% Biocleanse in the MSC. Sterile glass beads were added to the tubes and the caps closed tightly and vortexed on full power for 1 min. Pre-warmed cDMEM was then added and the pellet re-suspended by careful pipetting. The tubes were allowed to stand to sediment cells. The 5 mL from the centre of the tube was carefully removed and transferred to another falcon tube while avoiding disruption of pellet. The tube was then transferred to a new 15 mL tube and the bacterial suspension was transferred to a small tissue culture plate and passed slowly and carefully through a 26G needle about 15 times to disaggregate bacterial clumps before being transferred back to the 15 ml tube. The OD was measured as before using the spectrophotometer. An OD of 0.1 corresponds to approximately 10^7 bacteria/mL.

Depending on number of macrophages per well and required MOI dilutions were made in cDMEM for each bacterial culture for 2.5 X 10^6 bacteria/mL and made up to a final volume of 30 mL.

Bacterial Infection

The macrophages were infected with mycobacteria at an appropriate MOI prepared in antibiotic-free culture media. The media was completely removed from the wells and replaced with 1 mL bacteria or media alone. A sample of each MOI was taken to determine the infecting dose by colony forming unit (CFU) counting. The cells were incubated for 3 hrs at 37˚C after which point the media was removed from the 24 and 48 hr plates, the wells washed twice with PBS and fresh media was added before the plates were returned to the incubator for the appropriate incubation time. After 3 hrs of infection the time point was deemed as “0 hrs”.

2.2.17 Confocal Microscopy

BMDMs (0.5 X 10^6 cells/mL) were plated in cDMEM on 35mm glass bottom tissue dishes. Cells were treated with different stimuli for specific times. After several washes with PBS, cells were stained with PI and TMRM and viewed using a Leica SP8 gated STED motorised inverted microscope.

2.2.18 Phase Contrast Microscopy

BMDMs (0.5 X 10^6 cells/mL) were plated in cDMEM in 12 well cell culture dishes and treated with different stimuli for specific times. Cells were visualised using an Olympus IX81 inverted microscope.

2.2.19 Statistical analysis

Statistical analysis was performed using GraphPad Prism V6.04 software and nSolver and nSolver Advanced Analysis software. The means of three or more groups were compared by one-way ANOVA. Where significant differences were found, the Tukey multiple comparisons test was used to identify differences between individual groups. To compare each of a number of treatments to a single control, Dunnett's post hoc test was used. For human monocytes, a paired non-parametric T test was used.

Chapter 3 Alum trains human monocytes and murine BMDMs

3.1 Introduction

Alum has been widely used in several childhood vaccines due to effectiveness in promoting antibody responses and robust safety profile. As a vaccine adjuvant, alum behaves as an immunomodulator, but the mechanisms underlying the ability of alum to modulate innate immune responses remains relatively unresolved. IL-10 is an important cytokine which limits excessive inflammation and promotes repair[144]. Previous data from the Lavelle lab has shown that injection of alum primes draining lymph nodes to produce enhanced IL-10 *ex vivo* in response to a range of stimuli for at least 7 days after vaccination. Importantly, macrophages and DCs at the injection site were found to be major sources of IL-10[141].

The recently coined "trained immunity" challenges the classical view of innate versus adaptive immunity, suggesting that innate cells can retain memory of past immunological insults. This allows for a long-term inflammatory response that can be measured by increased cytokine production upon subsequent stimulation with unrelated stimuli[145].

The ability of alum to enhance IL-10 responses some time following injection led to the hypothesis that alum can train monocytes and macrophages by modulating the inflammatory profile of innate cells when challenged with a secondary, unrelated stimulus. Furthermore, the ability of alum to enhance the production of other anti-inflammatory cytokines such as IL-1Ra by innate immune cells has not been previously explored at a mechanistic level prompting evaluation of its potential involvement as a product of alum-training.

Several studies have demonstrated that innate training with the fungal cell wall component β-glucan, allows cells to respond with an increased production of pro-inflammatory cytokines. In contrast, training innate cells with LPS has been shown to induce tolerance whereby cells become refractory to secondary stimulation[145]. However, several studies have characterised the transcriptional profile of tolerated cells demonstrating a global transcriptional shift including upregulation of anti-inflammatory associated cytokines such as IL-10, TGF-β[75] and IL-1Ra[76].

This study investigates whether alum can train innate immune cells to adopt a distinct phenotype which favours resolution of the initial inflammatory response that is distinct from other known trainers of innate immunity such as β-glucan and BCG.

3.2 Aims

This results chapter aims to identify the following:

- To establish a robust *in vitro* model of trained immunity in both human monocytes and murine bone marrow-derived macrophages
- To investigate the potential of alum to train human monocytes and murine bone marrow-derived macrophages by measuring cytokine responses upon re-stimulation with LPS (or other PRR agonists) 7 days after training
- To evaluate whether macrophages trained by alum for 24hrs adopt and maintain a distinct morphology during the *in vitro* training period
- To evaluate the functional effects of alum-trained BMDMs in an *in vitro* model of infection
- To assess the transcriptional profile of inflammation related genes in murine bone marrow-derived macrophages 7 days after training with alum

3.3 Hypothesis

As a vaccine adjuvant, alum naturally behaves as an immunopotentiator. In the case of vaccines, alum's interaction with innate cells prompts antigen uptake by APCs and favours humoral rather than Th1 cellular responses. How alum influences the innate response is still relatively unresolved. Previous data from the Lavelle lab has shown that injection of alum alone primes draining lymph nodes to produce enhanced anti-inflammatory IL-10 *ex vivo* at least 7 days after vaccination[141]. Macrophages and DCs at the injection site were importantly found to be major sources of IL-10. Alum-induced cell infiltration to the injection site was uncompromised in IL-10 knockout mice, but Th1 antigen-specific responses were markedly boosted.

The ability of alum to enhance IL-10 induction when administered alone prompted us to hypothesise that alum can train monocytes and macrophages (*in vitro* and *in vivo*) by altering the cytokine profile of these innate cells when re-stimulated with PRR agonists. The hypothesis of this chapter is that training by alum causes monocytes/macrophages to become a specialised type of innate cell characterised by an anti-inflammatory phenotype favouring pro-resolution of the initial inflammatory responses that is distinct from other known trainers of innate immunity such as β-glucan and BCG.

3.4 Results

3.4.1 Human PBMC density centrifugation through two Percoll gradients (51% and 42%) and sedimentation through autologous plasma yields a highly purified and viable monocyte population

It has previously been reported that human monocytes can be trained to be more pro-inflammatory with β-glucan, or more tolerant, with LPS[145]. Accordingly, the first step of this project was to reproduce the training model established by Netea *et al* using our stimulus of interest, alum. Monocytes are produced in the bone marrow and then enter the blood, where they account for about 1-10% of the circulating leukocytes. They can be isolated from whole blood or buffy coats using several methods, including density-gradient centrifugation by exploiting the different density properties of immune cells. Leukocyte subpopulations such as peripheral blood mononuclear cells (PBMCs) can be separated from buffy coats by overlaying the buffy coat fraction on a Ficoll-paque gradient (density 1.077 g/mL) to generate a PBMC-enriched fraction between the Ficoll–paque layer and the platelet-rich plasma. Similarly, monocytes can be separated from PBMCs using a Percoll density-gradient, comprising a colloidal solution of silica 15-30 nm in diameter coated with polyvinylpyrrolidone (PVP), which can form gradients with a density range of 1.0 to 1.3 g/mL.

To optimise the monocyte isolation protocol, several challenges were encountered and overcome. The first protocol used for isolating human monocytes from PBMCs, which employs a hyper-osmotic density gradient (Percoll + NaCl), was provided by Professor Mihai Netea's research group in Radboud University. Buffy coats yielded an average of 250 x 10^6 PBMCs per donor by standard Ficoll density centrifugation, however, the hyperosmotic Percoll gradient yielded low monocyte cell counts with poor viability (based on Trypan blue exclusion).

Monocytes become activated by several factors including blood coagulation and alterations in osmolarity. The existing methods can result in cell contamination with lymphocytes, erythrocytes and platelets, in addition to cell clumping, which can result in variability in the yield of viable monocytes. Following several optimisation schemes and extensive research, another protocol from Guilbert *et al*[146] was combined with the original

protocol from Netea's lab to devise an optimal purification procedure to generate monocytes with high viability. In summary, this hybrid monocyte isolation protocol involves separating mononuclear cells from polymorphonuclear leukocytes using a slightly diluted Ficoll gradient (1.5 mL of 1X PBS in 23.5 mL Ficoll-paque), sedimentation through autologous serum to remove platelets and finally separating monocytes from lymphocytes with 42% and 51% Percoll gradients. FACS analysis was carried out to assess the purification protocol. The gating strategy is shown in Figure 3.1 and includes each fraction throughout the purification process including the initial buffy coat fraction Figure 3.1(A), PBMC fraction Figure 3.1(B) and monocyte fraction Figure 3.1(C). This approach yielded a more highly purified monocyte culture (~65%) with a significant increase in the number of viable monocytes per donor Figure 3.1(C). Following 2-3 hours of plastic adherence of the purified monocyte fraction, non-adherent cells are washed away, further purifying the remaining adherent monocyte population. The number of $CD45^+$ cells was comparable between PBMC and monocyte fractions Figure 3.1(D). However, the monocyte fraction yielded twice as many $CD45^+CD11b^+$ cells Figure 3.1(E) when compared with whole PBMCs. Furthermore, there was a significant increase in the number of $CD14^+CD11b^+$ cells in the monocyte fraction Figure 3.1(F) and this monocyte fraction was also highly positive for HLA- DR when compared with the PBMC fraction Figure 3.1(G).

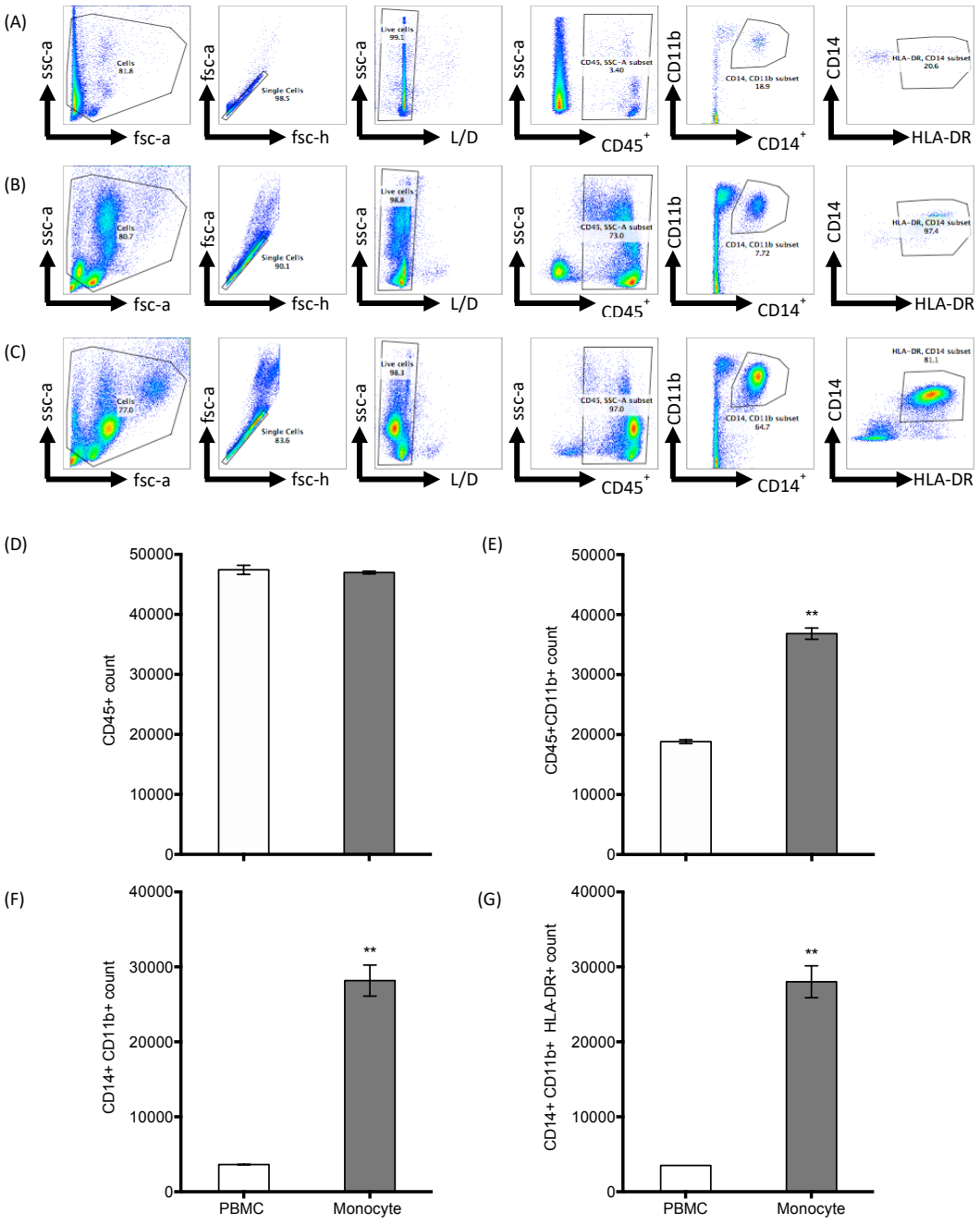

Figure 3.1 FACS analysis of Ficoll and Percoll fractions. Buffy coats from anonymous healthy blood donors were processed by density-gradient centrifugation and each fraction in the isolation process was analysed by FACS. Monocytes were defined as CD11b+CD14+. (A-C) Gating Strategy for buffy coat (A), PBMCs (B), monocytes (C). (D) Total number of lymphoid cells within "PBMC" and "Monocyte" fractions. (E) total number of CD45+CD11b+ cells in each fraction. (F) total number of CD14+CD11b+ monocytes in each fraction. (G) total number of CD14+CD11b+HLA-DR+ monocytes in each fraction. Results are representative of two blood donors. **p<0.01 PBMCs vs Monocytes by unpaired t test.

3.4.2 Alum trains human monocytes to produce more IL-10 and TNF-α upon secondary stimulation with LPS

A paper recently published by the Lavelle lab reported that alum drives IL-10 secretion in human monocytes when co-incubated with LPS[141]. In order to establish if IL-10 could also be induced in human monocytes trained by alum alone, the optimal concentrations for alum were tested in an *in vitro* training model. As alum has been shown to kill cells at high concentrations, cells were stimulated with alum over a range of concentrations from 0.5 ng/mL-100 ng/mL. After 24 h, cells were washed, incubated for 6 days and re-stimulated on day 6 with 1 ng/mL LPS for 24 h. Training of human monocytes with alum for 24 h before a rest period of 6 days did not induce IL-10 or TNF-α production when incubated with medium only Figure 3.2(A)&(C). However, training of human monocytes for 24 h with alum increased the production of IL-10 in a dose-dependent manner upon re-stimulation with LPS Figure 3.2(B). Furthermore, alum-trained cells exhibited enhanced TNF-α secretion upon re-stimulation with LPS when compared with un-trained cells Figure 3.2(D). This effect was dose dependent, however and was reduced at the highest concentrations of alum (100 ng/mL). High concentrations of alum can lead to death in human monocytes[147] and as a result, the optimum alum concentration selected was 100 ng/mL for human studies.

As the buffy coats are sourced from the Irish Blood Transfusion Services in St James' Hospital the only information available on each blood donor was blood type. Vital information such as age, sex and vaccination history could not be obtained for these studies. In order to stratify our results somewhat, donors were selected on the basis of their ability to drive IL-10 cytokine production following *in vitro* training of monocytes with alum. Figure 3.3(B) shows the typical variability observed for LPS-induced IL-10 secretion from trained monocytes in response to alum from eight blood donors compared to cRPMI controls on day 7 Figure 3.3(A). Although the overall response is significantly enhanced across the eight blood donors when PBMCs were trained with alum only 50% of the donors exhibit an enhanced effect on IL-10 secretion upon re-stimulation with LPS, 6 days after alum priming. These results suggest that the responses in the training model are highly variable while using human monocytes isolated from healthy blood donors.

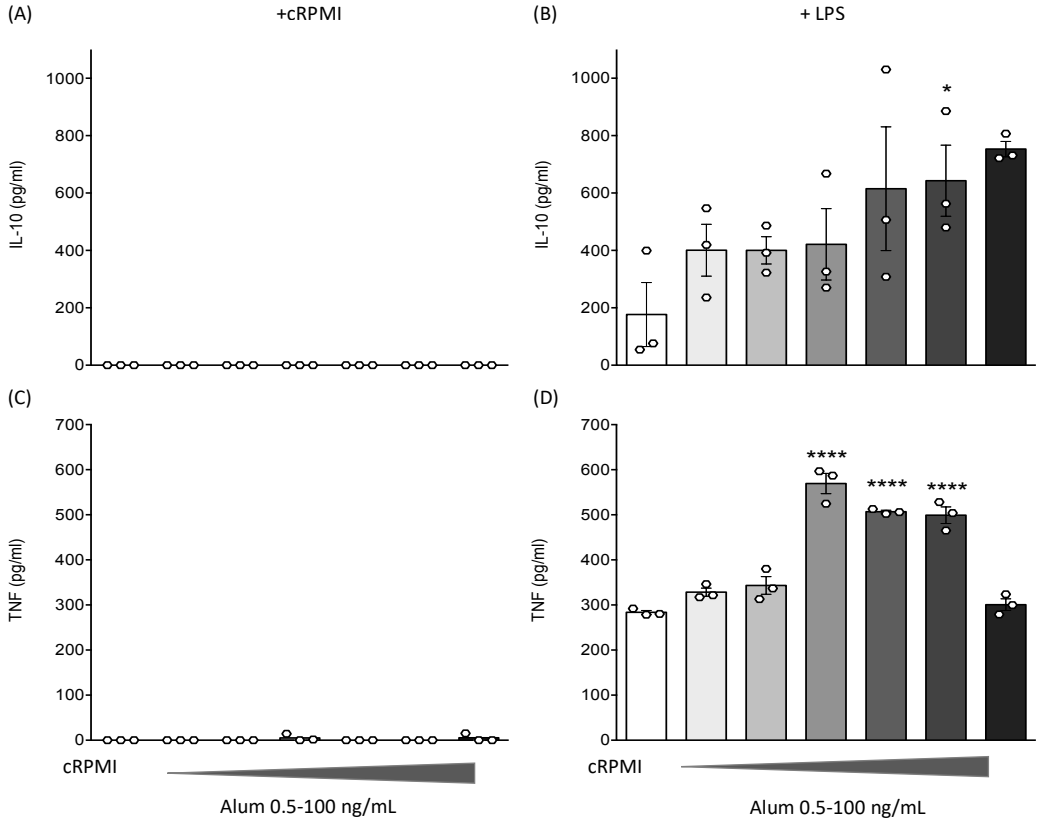

Figure 3.2 Alum-training increased production of IL-10 and TNF-α in human monocytes re-stimulated with LPS 7 days after training. Human monocytes isolated from healthy blood donors were stimulated with cRPMI or alum (at a range of concentrations 0.5-100 ng/mL) for 24 h and re-stimulated for a further 24 h with cRPMI or LPS 1 ng/mL 7 days later. IL-10 production following re-stimulation with cRPMI (A) or LPS (B). TNF-α production following re-stimulation with cRPMI (C) or LPS (D), measured by ELISA. Results are represented as the mean ± SEM of 3 healthy blood donors. *p<0.05, ****p<0.001 un-trained v Alum-trained cells by one-way ANOVA plus Dunnett post-test.

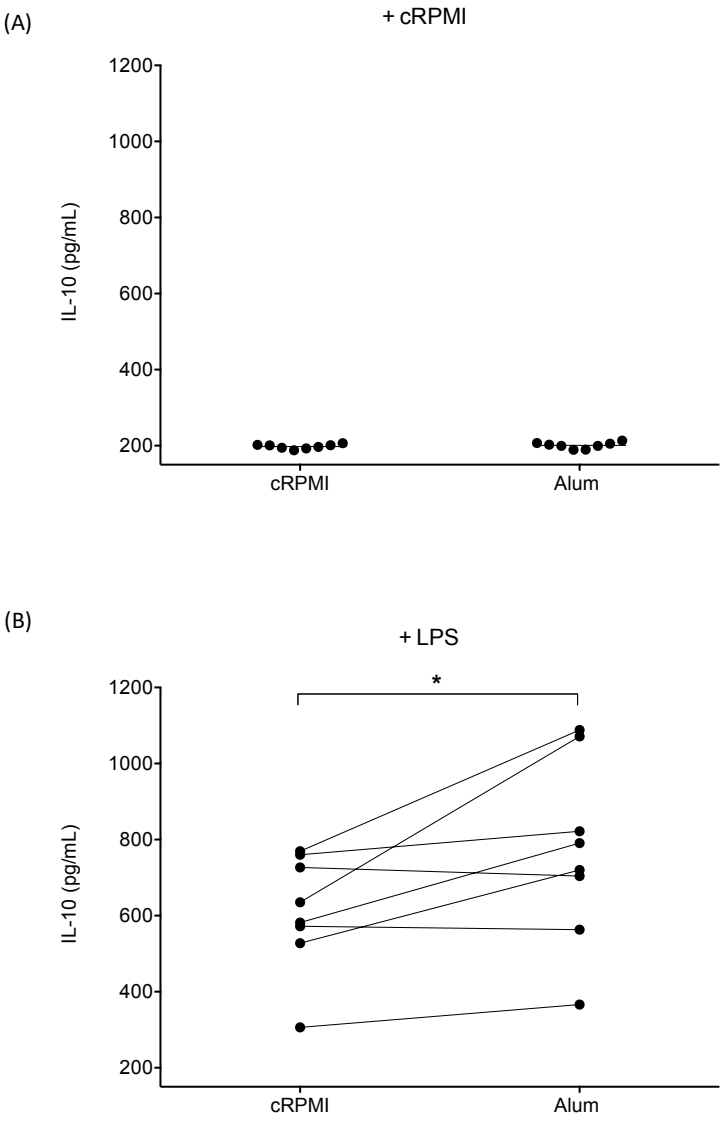

Figure 3.3 Alum-training increased production of IL-10 in 50% of blood donors. Human monocytes isolated from healthy blood donors (n= 8) were un-trained or trained with 100 ng/mL alum for 24 h and re-stimulated after 7 days with (A) cRPMI or (B) 1 ng/mL LPS. After 24 h IL-10 production in alum-trained versus un-trained monocytes was measured by ELISA. Differences were analysed using the Wilcoxon signed-rank test. *p<0.05

3.4.3 Alum-trained murine BMDMs are primed for enhanced secretion of IL-10

Due to the number of limitations encountered when using human monocytes for the *in vitro* training model the project was successfully translated into murine BMDMs. As mentioned, previous data generated in the Lavelle Lab has shown that alum strongly enhances the secretion of IL-10 by macrophages and dendritic cells[141]. As before, a range of alum concentrations were tested in BMDMs to obtain the optimal doses for subsequent training experiments. Concentrations of alum ranging from 1 ng/mL-100 µg/mL were used to stimulate BMDMs for 24 h and after a 6 day rest period the cells were re-stimulated with 10 ng/mL LPS for 24 h. Training of BMDMs with alum for 24 h did not induce IL-10 or TNF-α secretion upon incubation with medium only. However, increased secretion of IL-10 was observed in BMDMs that were trained with alum at 10 µg/mL upon re-stimulation with LPS Figure 3.4(B). As a result, 10 µg/mL was selected as the optimal concentration for alum-training in BMDMs. A slight reduction in TNF-α secretion was observed in BMDMs trained at higher concentrations (500 ng/mL-10 µg/mL) of alum in preliminary experiments Figure 3.4(D). However, due to variable background levels, TNF-α was not used as the primary cytokine readout for alum training *in vitro*.

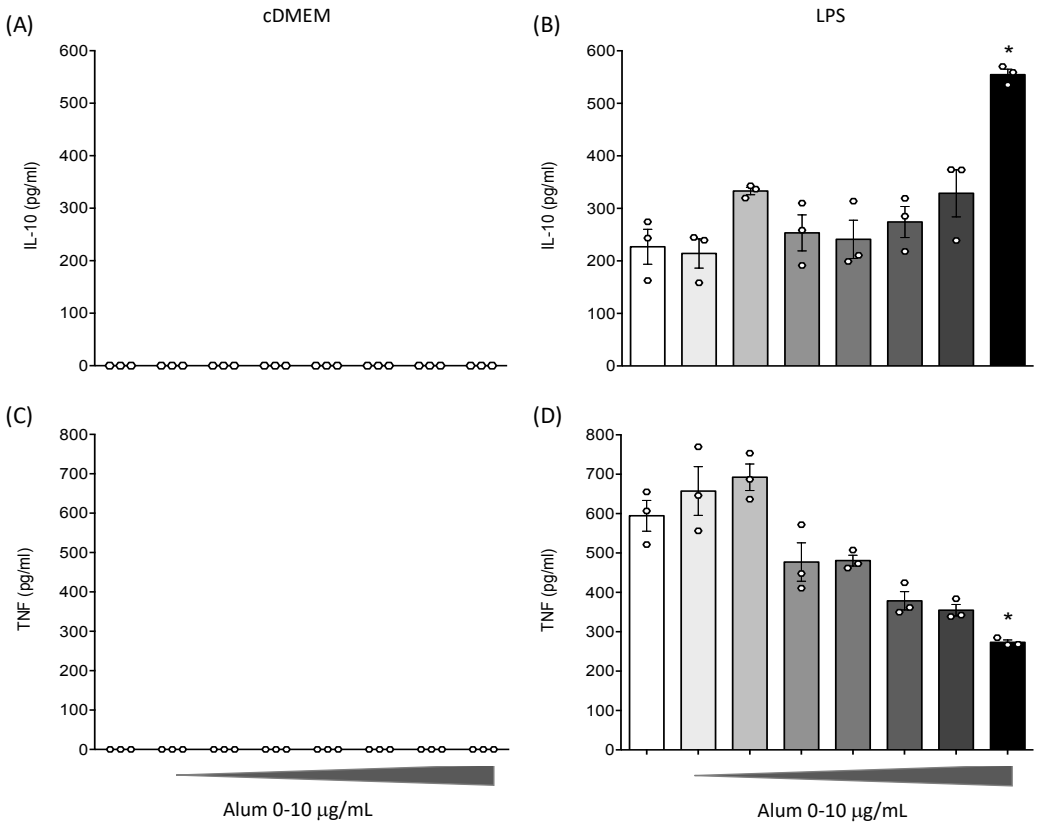

Figure 3.4 Alum-trained murine bone marrow-derived macrophages display altered cytokine secretion when re-stimulated with LPS 7 days post-training. BMDMs were trained with cDMEM or alum (1 ng/mL-10 μg/mL) and re-stimulated 7 days later with cDMEM or 10 ng/mL of LPS. After 24 h IL-10 and TNF-α secretion was measured by ELISA. IL-10 production following re-stimulation with cDMEM (A) or LPS (B). TNF-α production following re-stimulation with cDMEM (C) or LPS (D) measured by ELISA. Results are mean ± SEM of 3 female mice. *p<0.05 DMEM vs Alum-trained cells by one-way ANOVA plus Dunnett post-test.

3.4.4 Alum-training alters the morphology of murine BMDMs

Changes in the membrane morphology of macrophages stimulated with alum for 24 h was observed during routine monitoring of the cells throughout the training period using light microscopy. Furthermore, during the training protocol, increased cell numbers were observed in the wells that were stimulated with alum on day 0. Consequently, the cells were monitored and imaged by phase contrast microscopy. After 24 h of stimulation with alum, before the wash and rest step, the cells were visibly larger than control cells at the highest concentration of alum tested Figure 3.5(A). By day 4 of the training period there was no difference in the morphology or number of BMDMs primed with the lower concentration of alum (100 ng/mL) on day 1 or cDMEM alone on day 1 Figure 3.5(B). However, those stimulated with the highest concentration (10 μg/mL) of alum exhibited a distinct morphology Figure 3.5(B), being larger in size as on day 1 and also displaying a rounded appearance. Interestingly, the concentration of alum that induces these morphological changes is also the optimal concentration for driving alum-trained IL-10 when BMDMs are re-stimulated with LPS on day 6 Figure 3.4(C). By day 7, alum-trained macrophages (10 μg/mL) retained this distinct morphology and appeared to be significantly more abundant than cells stimulated with the lower concentration of alum or cDMEM Figure 3.5(C). Furthermore, this apparent increase in the number of alum-trained macrophages was enhanced when these cells were re-stimulated with LPS for 24 h on day 6 Figure 3.5(D). This increase in the number of cells was observed consistently by eye during routine microscopy analysis and by trypan blue exclusion throughout the *in vitro* training protocol.

The increased cell size observed in trained macrophages by microscopy was further investigated and quantified by FACS analysis. When macrophages were analysed by FACS on day 1 and day 7 of the training period, the cells were notably larger as determined by FSC-A Figure 3.6(B) and more granular by SSC-A Figure 3.6(C) when compared with cells that only received cDMEM during the initial 24 h training stimulation. Furthermore, when macrophages were imaged on day 4 of a typical training experiment, those stimulated with alum on day 0 were larger, more rounded and more abundant than those stimulated with cDMEM or the well-established innate training stimulus, β-glucan Figure 3.6(D). These

results indicate that alum training results in distinct morphological changes in macrophages when compared with un-trained cells.

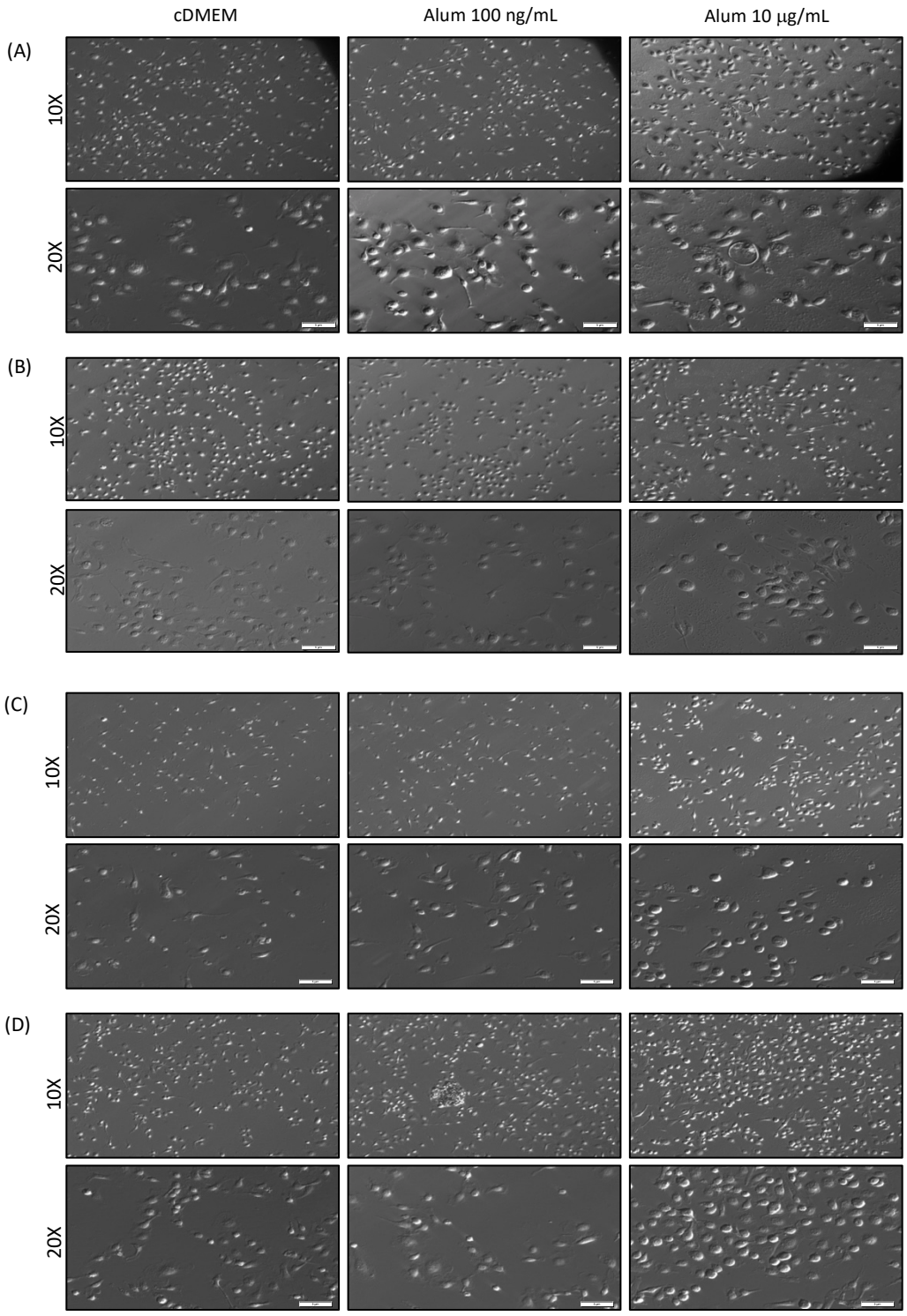

Figure 3.5 Macrophages increase in size and adopt a distinct morphology following 24 h stimulation with alum. Macrophages were stimulated with cDMEM or alum (100 ng/mL or 10 μg/mL) for 24 h and imaged throughout training period by phase contrast microscopy. (A) cDMEM vs alum on day 1 of training protocol. (B) cDMEM vs alum on day 4. (C-D) cDMEM v alum on day 7 after re-stimulated with cDMEM (C) or 10 ng/mL of LPS (D) on day 6. Representative images are shown from 3 independent experiments.

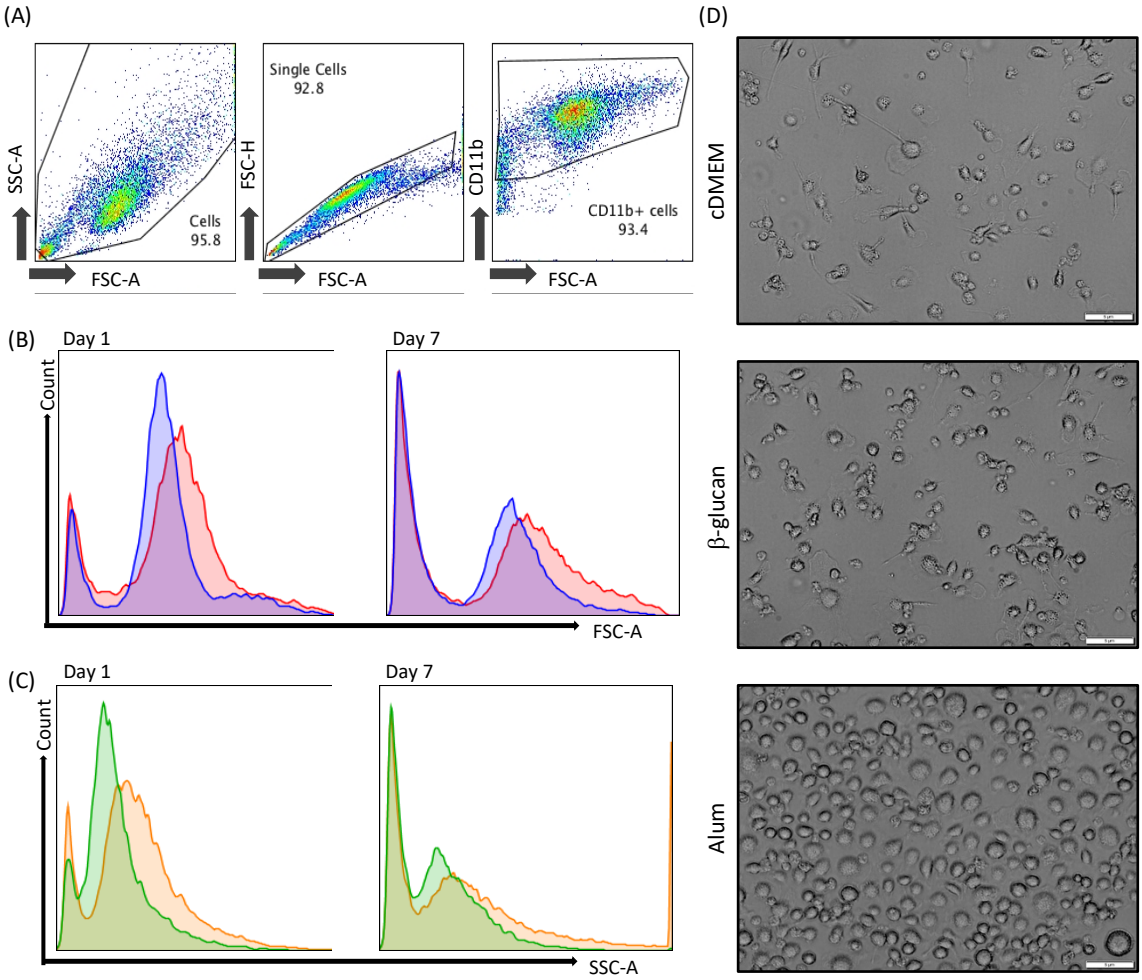

Figure 3.6: Macrophages are larger 24 h after stimulation with alum and maintain this size after 7 days. Macrophages were analysed by flow cytometry 1 and 7 days after stimulation with cDMEM or alum (10 μg/mL). (A) Gating strategy. (B) Macrophage size as measured by FSC-A (red = alum, blue = cDMEM). (C) Macrophage granularity as measured by SSC-A (orange = alum, green = cDMEM). (D) Phase contrast images of macrophages imaged on day 4 after stimulation with cDMEM, β-glucan (10 μg/mL) or alum (10 μg/mL). Representative graphs and images are shown from 4 independent experiments.

3.4.5 BMDMs stimulated with alum on day 0 retain macrophage marker expression throughout the training period

Because of the morphological differences in alum-trained macrophages it was necessary to characterise these cells throughout the training protocol to establish if their macrophage profile had been altered. Cells were stimulated with cDMEM or 10 µg/mL alum for 24 h and analysed by flow cytometry on day 1, 3 and 6 of training. Live cells were gated using Aqua Dead Cell stain and further characterized by CD11b, F480 and Gr1 expression. Doublets were not excluded due to the cell size heterogeneity previously observed. Cells stimulated with alum on day 0 display significant cell death (~40%) throughout the training period Figure 3.7(B) when compared with un-trained cells (~10%) Figure 3.7(A). Interestingly, F480/CD11b expression was consistent between cDMEM- and alum-trained macrophages throughout the protocol (~92-96%), in line with the typical expression profile of BMDMs. Furthermore, expression of Gr1, a protein used to further discriminate macrophage populations from more monocytic-like cells, which are positive for Gr1 in addition to F480/CD11b^{+} was examined. On day 1 of training only a third of untreated cells were Gr1- Figure 3.7(A) when compared with 55% of alum-trained cells Figure 3.7(B). The expression of Gr1 increased in cDMEM stimulated cells by day 3 to 69% and this profile was retained until day 6 Figure 3.7(A). In contrast, Gr1 expression observed on alum-trained cells was similar on day 1 and day 3, with only a slight increase by day 6 Figure 3.7(B). These results suggest that alum-trained cells maintain a macrophage phenotype over a sustained period in culture in contrast to un-trained cells.

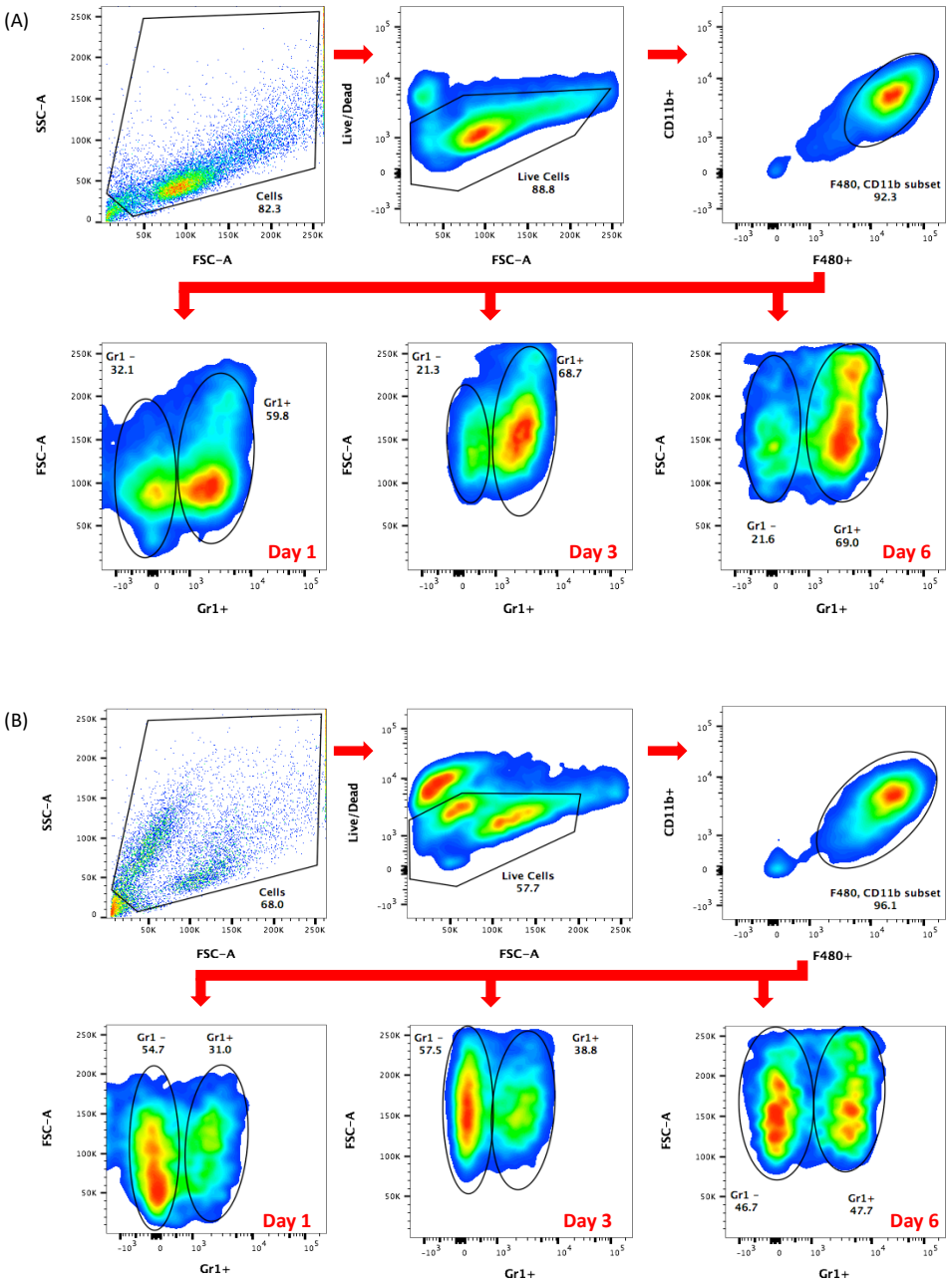

Figure 3.7 Flow cytometric characterization of macrophages in a representative sample of alum *in vitro* training model. Macrophages were analysed by flow cytometry on days 1, 3 and 6 of a typical training protocol. After exclusion of debris and non-viable cells, cells were identified using the following markers; CD11b, F480 and Gr1. Macrophage characterisation on day 1, 3 and 6 following cDMEM stimulation (A) or 10 µg/mL of alum (B) for 24 h. Graphs shown are representative of 2 independent experiments.

3.4.6 Macrophage membrane integrity is maintained following stimulation with alum

Due to the differences in cell numbers observed by phase contrast microscopy when compared to FACS analysis of alum-trained BMDMs, it was important to establish if the decrease in % of live cells observed during FACS analysis was due to the removal protocol of adherent macrophages from the wells to process these cells for FACS. In order to do this, macrophages were stimulated with cDMEM, β-Glucan (10 μg/mL), 10 μg/mL of alum or 100 μg/mL of alum. After 24 h, cells were stained with TMRM; a dye that stains active mitochondria and propidium iodide (PI); a dye that distinguishes live cells from dead cells based on membrane permeability. The limitation of this assay is that both TMRM and PI are the same colour causing the two stains to overlap. To overcome this, TMRM was visualized in the green channel and only viable mitochondrial structures that stained green within the cell were considered TMRM positive. PI was visualized in red and only cells that had taken up PI and the entire cellular contents stained red were considered PI positive. When macrophages were imaged by confocal microscopy, those that received 10 μg/mL of alum Figure 3.8(C) showed viable mitochondria based on structural staining of intact mitochondria with TMRM when visualized in the green channel. Compared to a higher dose of alum (100 μg/mL), the majority of mitochondrial structures within cells were not detectable based on TMRM staining Figure 3.8(D). Furthermore, since PI is impermeable to live cells with a fully intact membrane this stain was used as a means of detecting dead macrophages that were not positive for TMRM staining of viable mitochondrial structures. BMDMs were counted by blind scoring using PI staining (in the red channel) of the entire cell to count dead cells and TMRM staining of viable mitochondrial structures that were not positive for PI to count live cells. PI staining was positive in approximately 25% of macrophages stimulated with 10 μg/mL of alum Figure 3.8(C) when compared with ~95% of those that received the higher dose of alum (100 μg/mL) Figure 3.8(D). In contrast, un-trained Figure 3.8(A) and β-glucan- Figure 3.8(B) stimulated BMDMs were almost completely negative for PI staining after 24 h. In addition, assessment of cell death 30 min after stimulation did not indicate any reduction in viability for cells treated with cDMEM Figure 3.9(A) or either concentration of alum Figure 3.9(C)&(D). Therefore, these results suggest that the dose of alum used for training macrophages induces approximately 25% cell death at 24 h after stimulation.

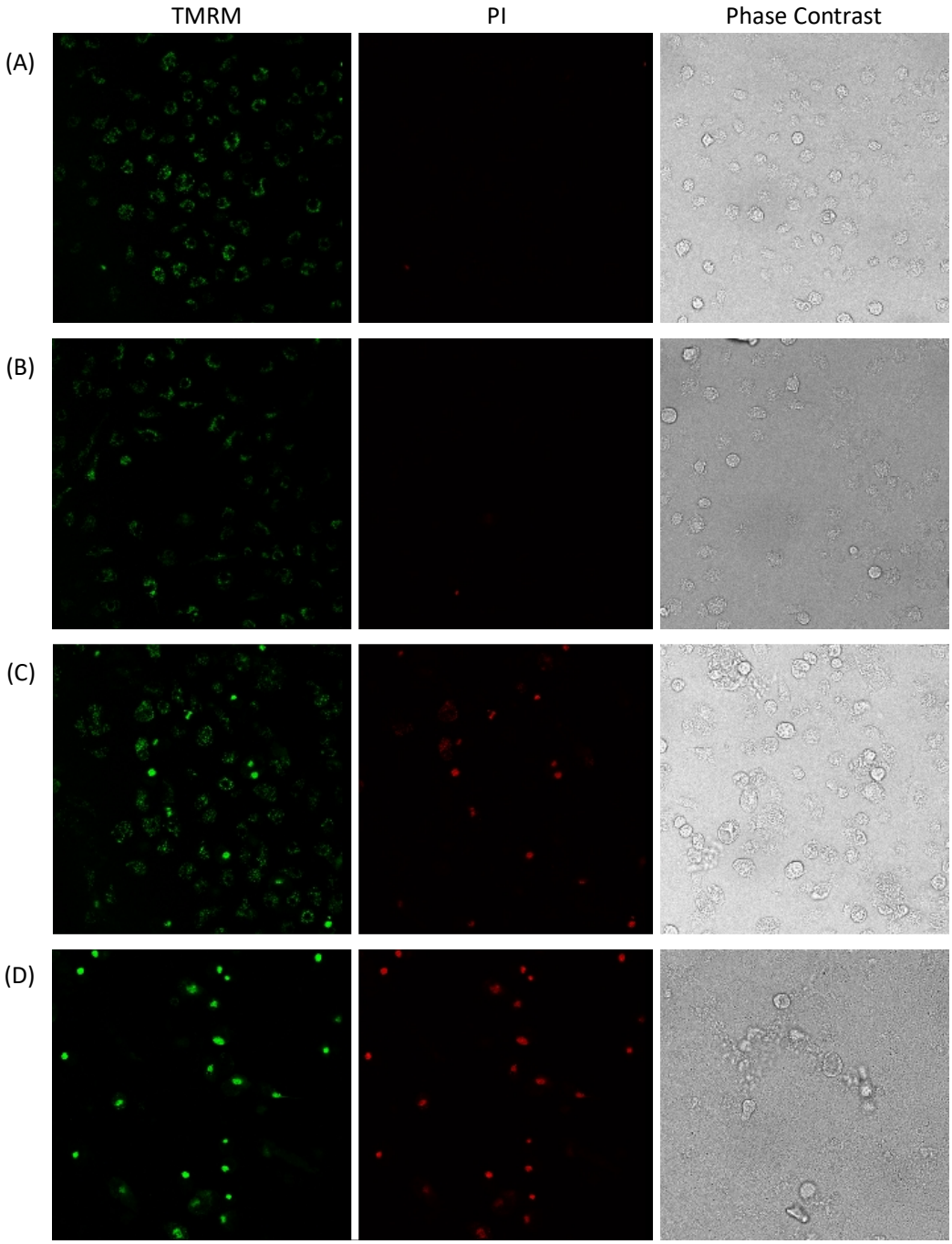

Figure 3.8 Alum does not compromise the cell membranes of viable macrophages following 24 h stimulation. Macrophages were stimulated with (A) cDMEM, (B) β-Glucan (10 μg/mL), (C) alum (10 μg/mL) or (D) alum (100 μg/mL). After 24 h cells were stained with TMRM (shown in green channel) and PI (shown in red channel) and visualized by confocal microscopy. Representative graphs are shown based on 2 independent experiments.

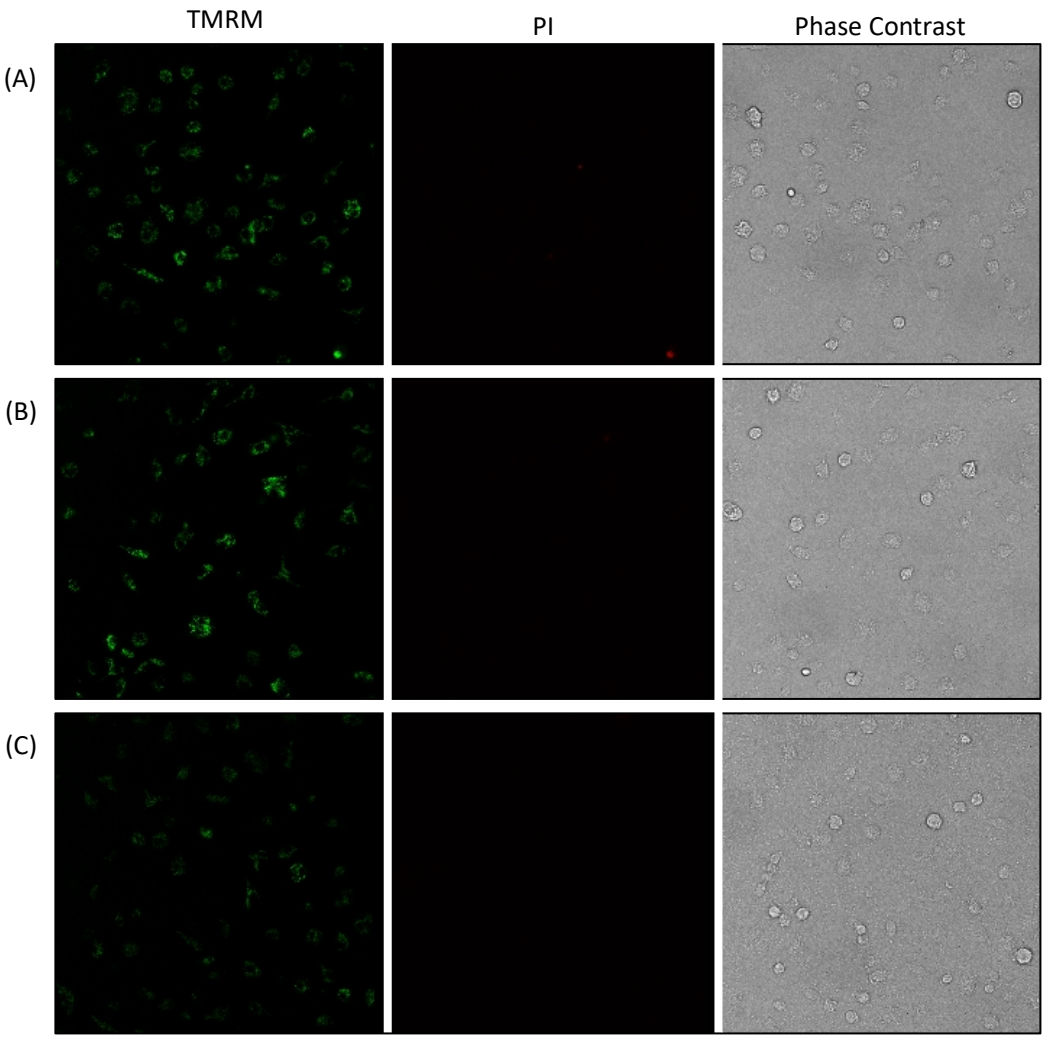

Figure 3.9 Macrophages are viable following short-term stimulation with alum at optimum concentration. Macrophages were stimulated with (A) cDMEM, (B) alum (10 μg/mL) or (C) alum (10 μg/mL). After 30 mins cells were stained with TMRM (shown in green channel) and PI (shown in red channel) and visualized by confocal microscopy. Representative graphs are shown based on 2 independent experiments.

3.4.7 Bone marrow cells isolated from *in vivo* trained mice display increased proliferative capacity

It has been shown that mice injected with alum are primed for enhanced production of IL-10[141]. Furthermore, the results in this chapter have shown that alum can train macrophages to secrete higher concentrations of IL-10 upon re-stimulation. Therefore, it was necessary to establish if injection of alum could train bone marrow cells *in vivo* and if these cells have an ability to produce enhanced levels of anti-inflammatory cytokines *ex vivo*. Mice were injected intraperitoneally with 1 mg of alum in 200 mL PBS or equivalent volume of PBS alone and bone marrow cells were isolated 3- and 7-days post treatment. Bone marrow cells from PBS and alum-injected mice were isolated and differentiated into BMDMs in large petri dishes. The differentiated BMDMs were subsequently recovered from the petri dishes and re-plated on day 6 of differentiation and stimulated with a range of PRR agonists (day 0 of typical training protocol). These PRR agonists were: Zymosan (1 μg/mL), Poly (I)(C) (1 μg/mL), β-Glucan (10 μg/mL), LPS (10 ng/mL), R848 (1 μg/mL) or CpG (1 μg/mL).

Bone marrow cells isolated from the femur and tibia of alum- or PBS-injected mice were counted prior to plating for the macrophage differentiation protocol. Mice injected 7 days prior to bone marrow isolation, with alum yielded almost three times more cells than PBS injected mice Figure 3.10(A). These cells were seeded at the same density and differentiated for 7 days in the presence of L929-conditioned media.

During the differentiation of these BMDMs, the cells from bone marrow of alum injected mice were noticeably more abundant than those isolated from PBS mice (images not shown). This was particularly evident when these cells were recovered from petri dishes on day 6 of differentiation, at which stage they were counted and re-plated. Mice injected with alum 3 days before euthanisation yielded twice as many BMDMs as PBS-injected mice while mice injected with alum 7 days prior to bone marrow collection yielded almost three times as many macrophages Figure 3.10(B), indicating enhanced proliferation or expansion. BMDMs differentiated from the bone marrow of PBS- or alum-treated mice were re-plated in 96 well plates at the same seeding density and stimulated for 24 h with the aforementioned PRR agonists. The results showed enhanced IL-10 secretion by BMDMs generated from the bone marrow of mice taken 3 days Figure 3.10(C) when re-stimulated with poly(I)(C) or R848. BMDMs generated from mice70 7 days after PBS or alum injection

following re-stimulation with a range of PRR agonists showed no significant enhancement in IL-10 Figure 3.10(D). However, higher bone marrow (and BMDM) cell counts from alum injected mice suggest that alum may be enhancing the proliferative capacity of bone marrow cells, an effect that is retained by macrophages differentiated from alum-trained bone marrow cells. This effect suggests that some of the enhancement in IL-10 that was previously seen *in vitro* may have been partially due to differences in cell numbers during the training period.

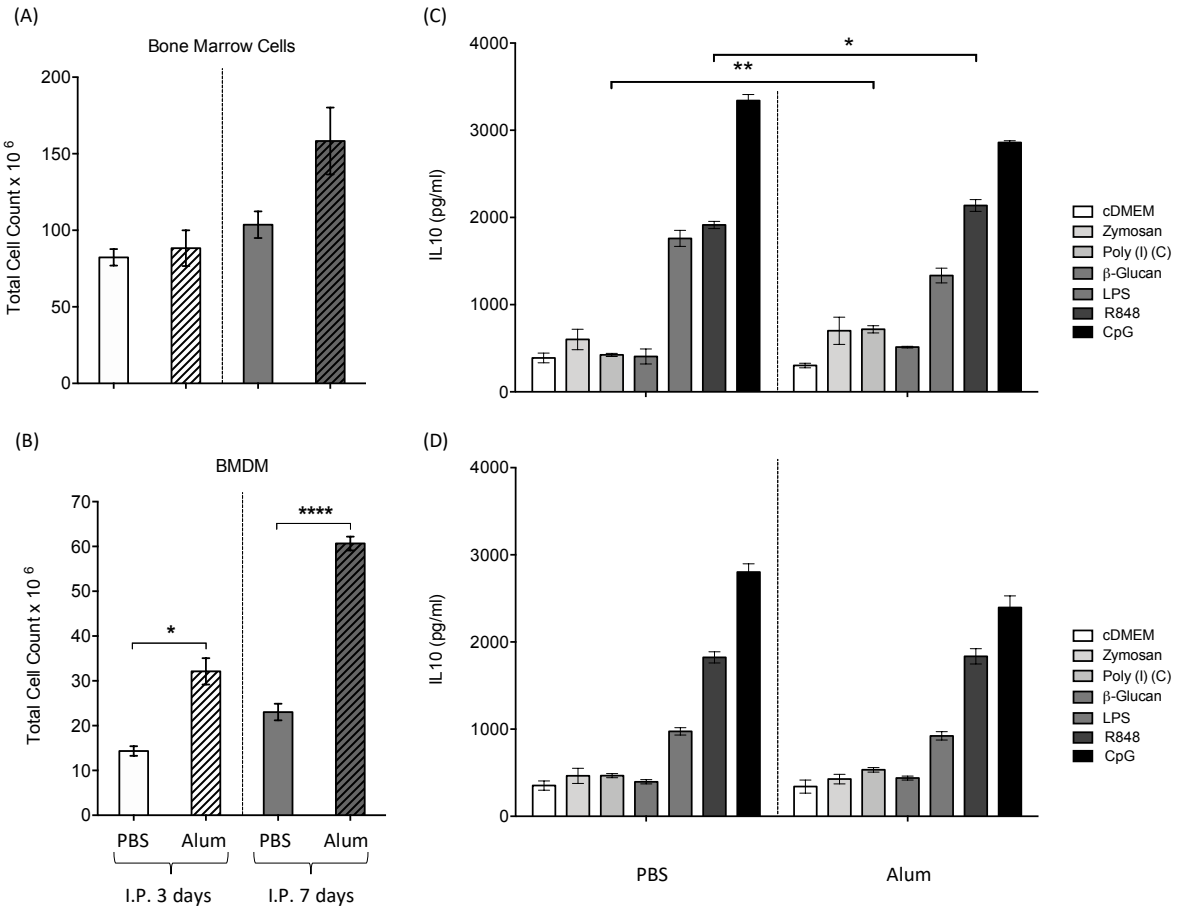

Figure 3.10 Intraperitoneal injection of alum increases the proliferative capacity of bone marrow cells *in vivo* and BMDMs *in vitro.* Mice were immunised I.P. with PBS or 1 mg of alum 3 or 7 days prior to euthanisation. Bone marrow cells were counted before plating for differentiation. After 7 days, BMDMs from either PBS or alum-injected mice were re-stimulated with a range of PRR agonists including: Zymosan (1 μg/mL), Poly (I)(C) (1 μg/mL), β-Glucan (10 μg/mL), LPS (10 ng/mL), R848 (1 μg/mL) or CpG (1 μg/mL). (A) Bone marrow cell counts from bone marrow of PBS or alum-injected mice. (B) BMDMs cell counts from PBS or alum-injected mice on day 7 after differentiation in L929-conditioned media. IL-10 production by BMDMs re-stimulated with different PRR agonists from mice immunized I.P. 3 days (C) or 7 days (D) prior to euthanisation. Results are mean ± SEM of 3 female mice. *p<0.05, **p<0.01, ****p<0.001.(A&B) PBS-immunised vs alum-immunised for cell counts by unpaired t test. (C&D) cDMEM vs PRR agonists re-stimulation after differentiation by one-way ANOVA plus Dunnett post-test.

3.4.8 Alum-training strongly enhances secretion of the anti-inflammatory cytokines IL-10 and IL-1Ra following infection with BCG

In order to further elucidate the functional properties of alum in the training model, macrophages were incubated with cDMEM or alum (10 μg/mL), as before, and infected with live BCG on day 6 of training at an MOI of 5:1. Colony forming units (CFUs) were determined to assess bacterial uptake and the killing ability of these cells when infected with live mycobacteria. The % CFU difference at all time-points indicated that bacterial uptake and bactericidal capacity were comparable for alum-trained and un-trained macrophages Figure 3.11(A). In terms of total CFUs there was a slight increase in the number of bacteria in alum-trained macrophages by 48 h. However, the most striking differences were observed in the supernatants from macrophages 24 h after infection. While secretion of TNF-α following BCG infection was slightly increased in macrophages generated from the bone marrow of alum injected mice compared with un-trained cells Figure 3.11(C), IL-10 Figure 3.11(D) and particularly IL-1Ra Figure 3.11(E) secretion was strongly enhanced. These results suggest that although training with alum induced a proliferative but anti-inflammatory phenotype in BMDMs, this does not impede uptake of bacteria. There appeared to be an effect on bactericidal capacity, but future work would be required to substantiate this observation.

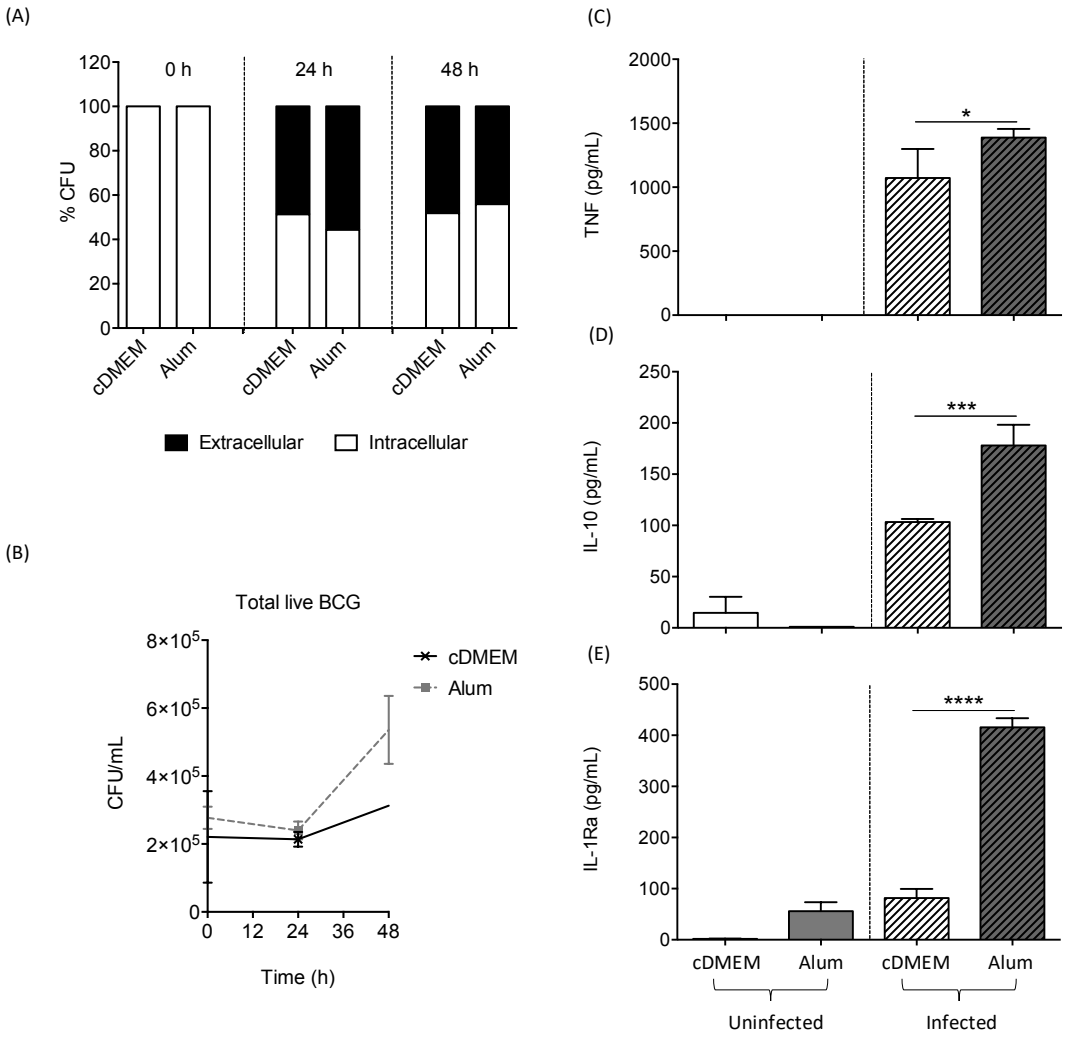

Figure 3.11 Macrophages trained with alum *in vitro* secrete anti-inflammatory cytokines in response to infection with BCG. Macrophages were stimulated for 24 h with cDMEM or 10 μg/mL alum (w/o pen/strep), washed and rested for 5 days. On day 6 macrophages were infected with live BCG at MOI of 5:1 (5 live bacilli to 1 macrophage) for 3 h (time 0) before being washed and rested for 48 h. Supernatants were taken after 24 h for ELISA while CFU counts were set up using supernatants and cell lysates at 0, 24 and 48 h timepoints. (A) % CFUs of extracellular (supernatant) vs intracellular (cell lysate) in macrophages trained with cDMEM or alum followed by BCG infection. (B) Total CFU of live BCG (intra- and extracellular) over 48 h in un-trained v alum-trained macrophages. TNF-α (C), IL-10 (D) and IL-1Ra (E) production by un-trained macrophages or macrophages trained or alum 24 h after re-stimulation with cDMEM or infection with live BCG. Representative graphs are mean ± SD from two individual experiments with two mice/group. *p<0.05, ****p<0.001 DMEM vs alum-trained macrophages by unpaired t test.

3.4.9 Alum-training appears to globally down-regulate pro-inflammatory gene transcription in macrophages

Having successfully optimized the *in vitro* training protocol in BMDMs, the transcriptional profile of cytokines and other immunomodulatory mediators was explored. The NanoString Murine Inflammation V2 panel containing 254 genes (248 inflammation-associated genes + 6 internal reference genes) was selected for characterizing alum-dependent transcriptional rewiring in trained macrophages. A full list of genes and selected internal reference genes are listed in supplementary table 1. NanoString's nCounter Analysis System employs the use of digital barcode technology for directly measuring multiple analytes allowing a high sensitivity of <1 copy per cell. These molecular barcodes are colour-coded and attached to a single target-specific probe which are then imaged to detect hundreds of unique transcripts in a single reaction.

BMDMs from 3 female C57BL/6 mice were stimulated for 24 h with alum (10 μg/mL) or cDMEM as before, and one week later, RNA was isolated, quantified and normalised to 100 ng. The RNA samples were then hybridized over night with NanoString Reporter and Capture Probesets, inserted into the automated Prep Station and analysed by the Digital Analyzer system the following day. Following normalisation by background subtraction of the sample counts to 6 reference genes (verified by GeneNorm software) differential expression between samples could be analysed using nSolver and Advanced Analysis software. Alum stimulated macrophages are predominantly transcriptionally repressed based on the 248 inflammatory genes assessed in this experiment Figure 3.12(A). The majority of these pro-inflammatory genes are down-regulated with the exception of a small group of up-regulated genes following BMDM stimulation with alum.

As an additional quality control step, qPCR verification of three genes, *H2eb1, Ccl2* and *Tlr5* was carried out by Dr. John Browne from UCD to rule out any potential issues related to the particular NanoString Codeset used, the NanoString nCounter MAX Analysis system or the nSolver software used to analyse the data. The expression of these three genes across all samples by qPCR was found to be 92-99% correlated with the expression profile generated by NanoString Figure 3.12(B-D). Pathway analysis was further assessed using the nSolver Advanced Analysis software and from the smaller group of upregulated genes several potential pathways were highlighted. Of these potential pathways the chemokine

family was found to be one of the most upregulated (Figure 3.13 A) and included both Ccl (Figure 3.13 B) and Cxcl (Figure 3.13 C) family members. Other noteworthy pathways identified include positive regulation of proliferation and antioxidant response (Figure 3.14 A). The proliferation associated genes highlighted in this pathway include prosurvival genes *Jun*, *Myc*, *Bcl2l1, Csf1* and *Tnf* (Figure 3.14 B). The antioxidant response includes members of the Nrf2 pathway, *Nfe2l2* itself and genes encoding the small Maf proteins *Mafk* and *Maff* (Figure 3.14 C). Finally, the regulation of inflammation pathway is shown in Figure 3.15 A. Within this pathway, *I1rn,* the gene encoding IL-1Ra, the antagonist of the IL-1 receptor, was found to be the most highly expressed gene in alum-trained macrophages. This gene expression profile was also associated with down regulation of *Il1a*, *Il1b* and *Il18* (Figure 3.15 B). The IL-1Ra protein was also shown to be strongly induced when these cells were infected with live BCG Figure 3.11(E). This confirms the results observed during the BCG infection experiment, which highlights IL-1Ra as a key anti-inflammatory target in alum-trained cells.

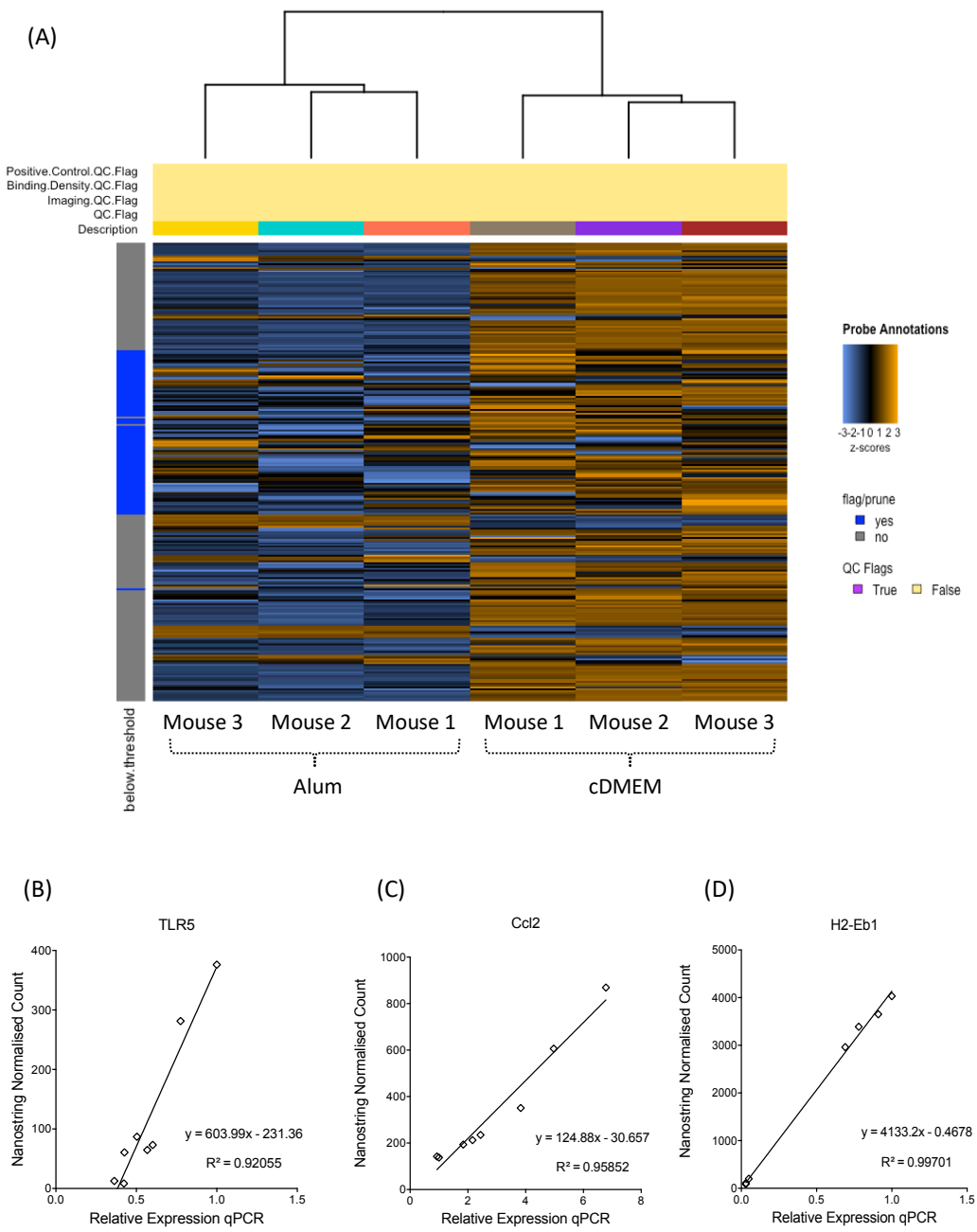

Figure 3.12 NanoString HeatMap of overall differential gene expression in trained macrophages BMDMs from 3 female C57BL\6 mice were stimulated with alum (10 µg/ml) or cDMEM for 24 h, washed and rested for 6 days. On day 7, RNA was isolated and normalised to 100ng, hybridized over night with NanoString Reporter and Capture Probesets, inserted into the automated Prep Station and analysed by the Digital Analyzer system the following day. Differential gene expression was analysed using nSolver and normalised to 5 selected internal reference genes using GeneNorm software. Genes flagged in blue bar were below detection limit of 20 mRNA counts. (A) HeatMap showing differential expression of all data (249 genes) in alum-trained v cDMEM BMDMs, blue = downregulation, orange = upregulation based on mRNA counts. (B) qPCR analysis of *Tlr5* (B) *Ccl2* (C) and *H2-Eb1* (D) correlated with the NanoString normalised counts. N=3 mice. Experiment was performed once.

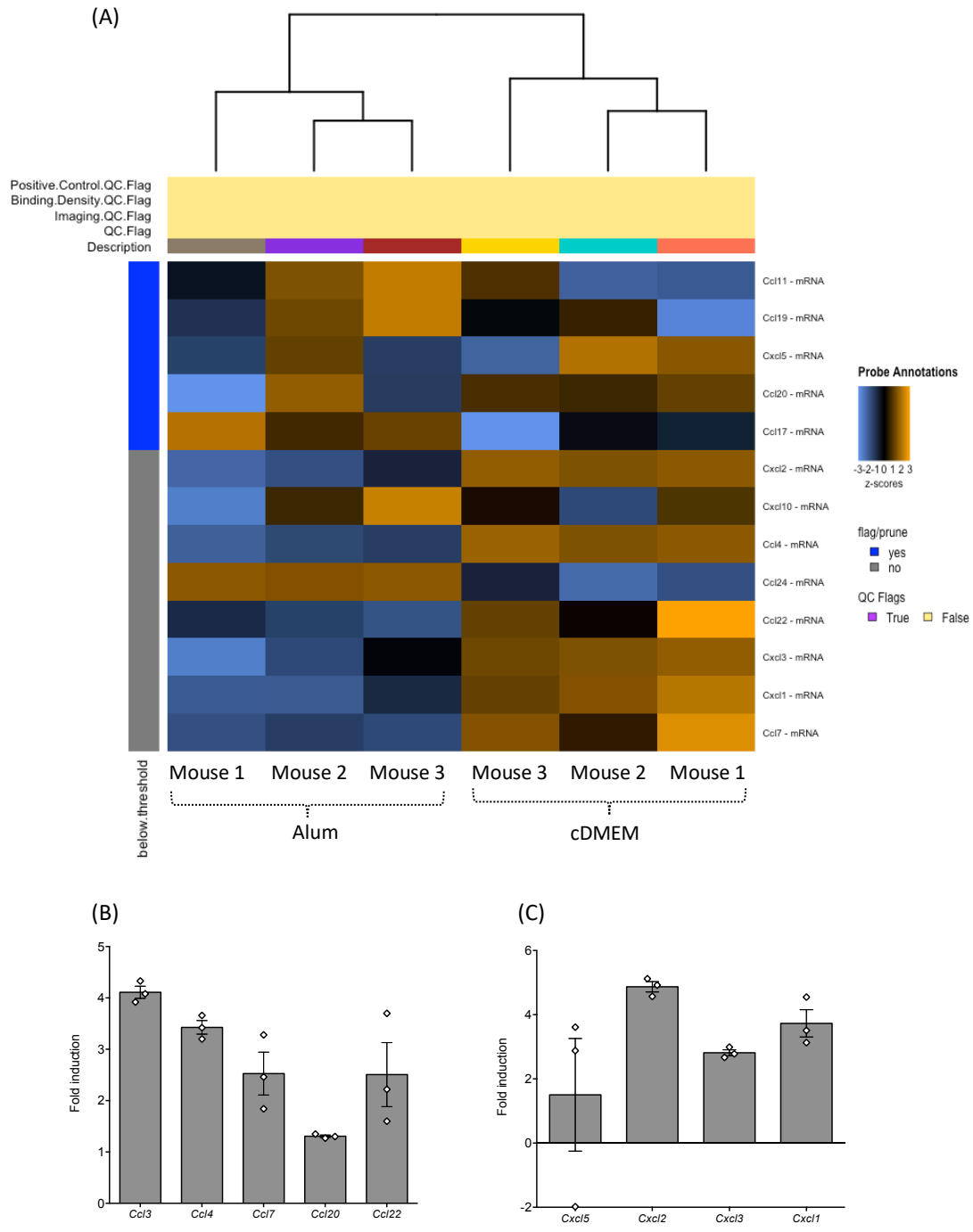

Figure 3.13 Pathway analysis of chemokine activity in trained macrophages BMDMs from 3 female C57BL\6 mice were stimulated with alum (10 µg/ml) or cDMEM for 24 h, washed and rested for 6 days. On day 7, RNA was isolated and normalised to 100ng and NanoString was performed as previously described. Differential gene expression was analysed using nSolver Advanced Analysis and normalised to 5 selected internal reference genes using GeneNorm software. (A) HeatMap showing differential expression of 13 genes associated with chemokine activity in alum-trained v cDMEM BMDMs, blue = downregulation, orange = upregulation based on mRNA counts. Genes flagged in blue bar were below detection limit of 20 mRNA counts. (B) Fold change of CCL chemokine family member and (C) CXCL chemokine family member gene expression in alum-trained BMDMs compared to un-trained controls. N=3 mice. Experiment was performed once.

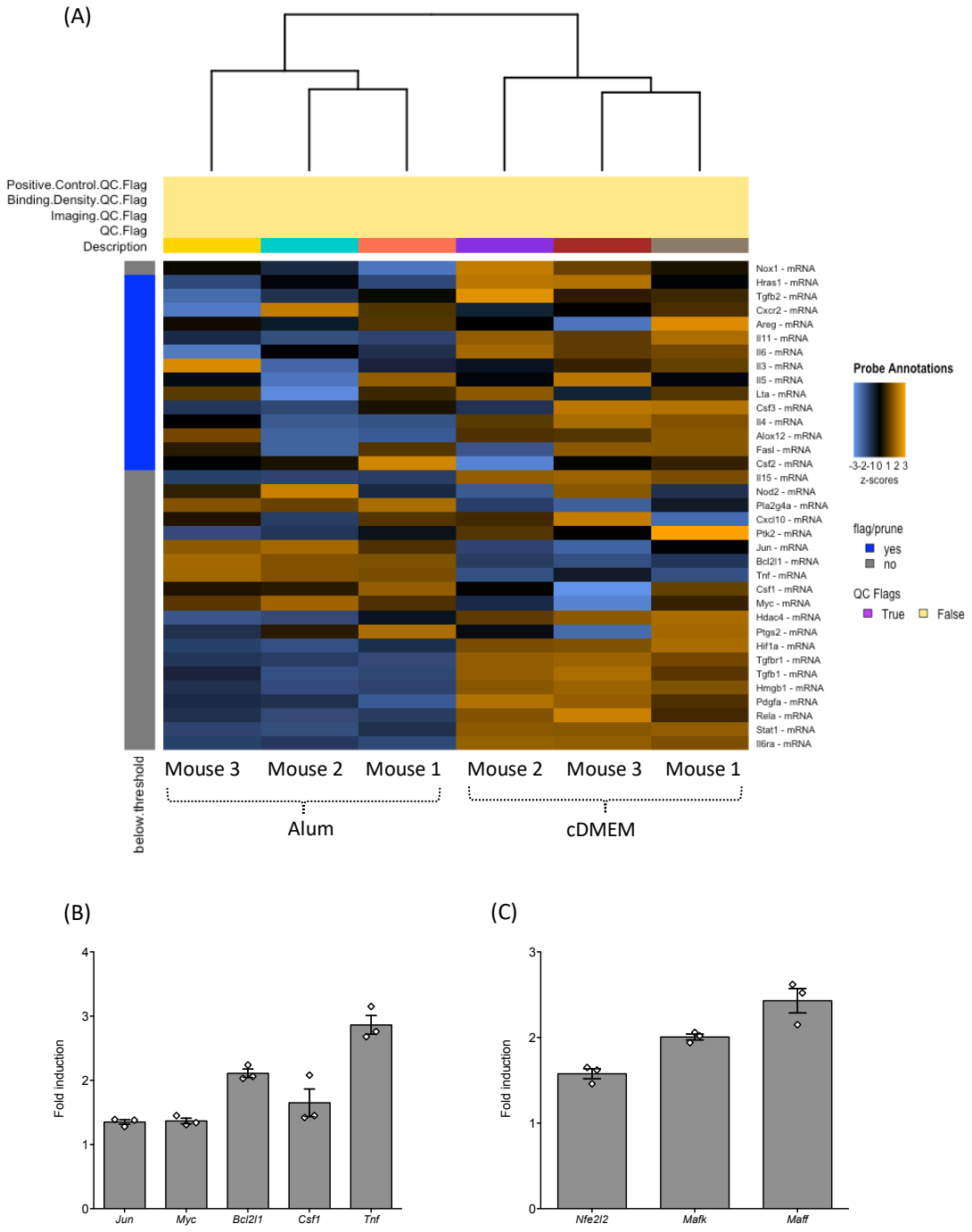

Figure 3.14 Pathway analysis of positive regulation of cell proliferation and anti-oxidant response in trained macrophages BMDMs from 3 female C57BL\6 mice were stimulated with alum (10 µg/ml) or cDMEM for 24 h, washed and rested for 6 days. On day 7, RNA was isolated and normalised to 100ng and NanoString was performed as previously described. Differential gene expression was analysed using nSolver Advanced Analysis and normalised to 5 selected internal reference genes using GeneNorm software. (A) HeatMap showing differential expression of 35 genes associated with positive regulation of proliferation in alum-trained v cDMEM BMDMs, blue = downregulation, orange = upregulation based on mRNA counts. Genes flagged in blue bar were below detection limit of 20 mRNA counts. (B) Fold change of proliferation and prosurvival-associated gene expression and (C) Nrf2 anti-oxidant and prosurvival associated gene expression in alum-trained BMDMs compared to un-trained controls. N=3 mice. Experiment was performed once.

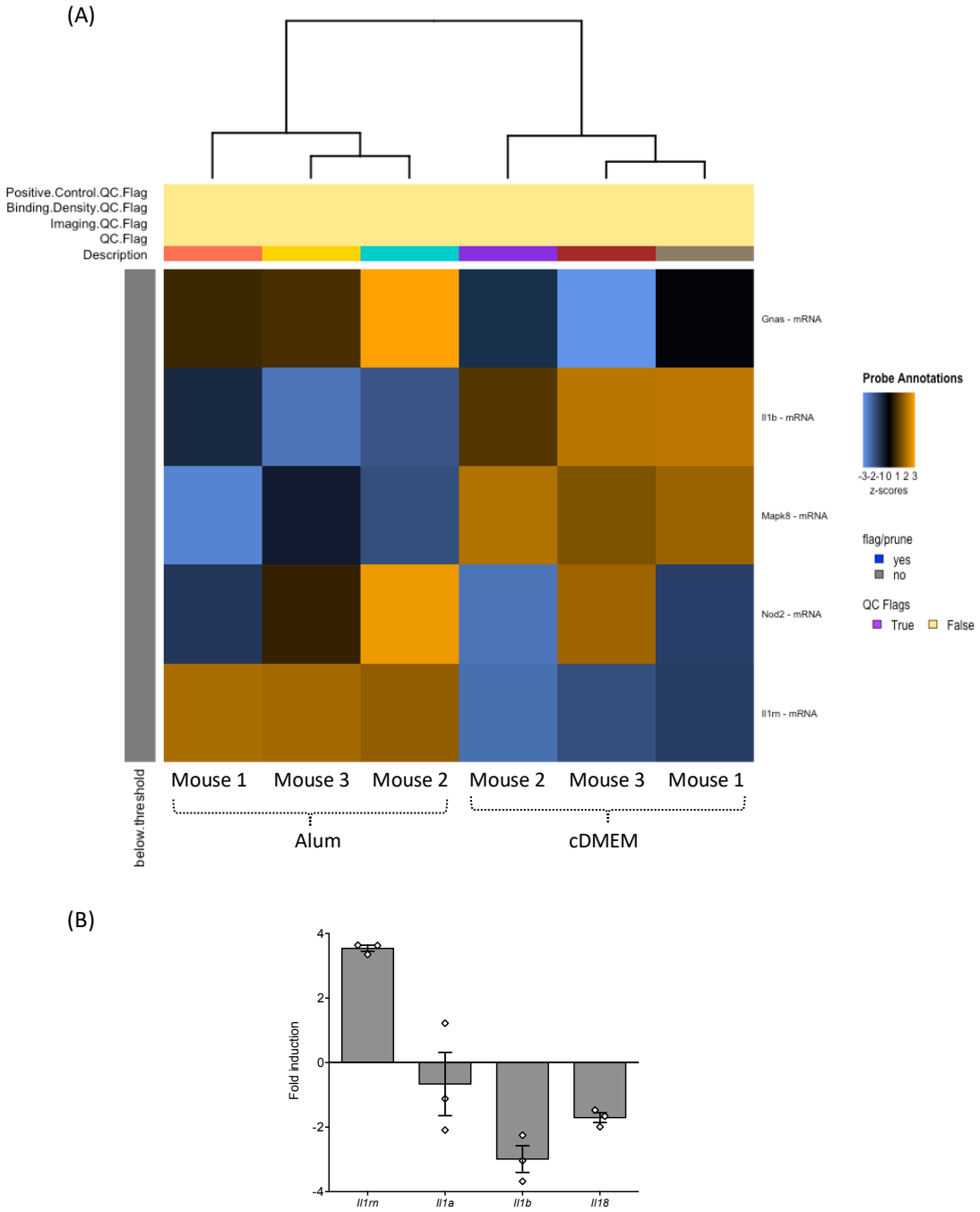

Figure 3.15 Pathway analysis of regulation of inflammation in trained macrophages BMDMs from 3 female C57BL\6 mice were stimulated with alum (10 µg/ml) or cDMEM for 24 h, washed and rested for 6 days. On day 7, RNA was isolated and normalised to 100ng and NanoString was performed as previously described. Differential gene expression was analysed using nSolver Advanced Analysis and normalised to 5 selected internal reference genes using GeneNorm software. (A) HeatMap showing differential expression of 5 genes associated with regulation of inflammation in alum-trained v cDMEM BMDMs, blue = downregulation, orange = upregulation based on mRNA counts. Genes flagged in blue bar were below detection limit of 20 mRNA counts. (B) Fold change of IL-1 family member gene expression in alum-trained BMDMs compared to un-trained controls. N=3 mice. Experiment was performed once.

3.5 Discussion

The classical view of innate immunity is that it lacks the ability to retain immunological memory, unlike its adaptive counterpart[2]. The dogma has recently been challenged by several research groups that have postulated the existence of a type of innate immune memory whereby organisms, including mammals, are protected from a broad range of infections in a manner independent of T and B cells[148]. This process coined "trained immunity" allows for primed cellular responses to secondary infections and has been shown to be mediated by innate immune cells, such as monocytes and macrophages[149]. Innate immune memory to infection has been well documented in plants and has also been the subject of intensive investigation in invertebrate models[150]. Of note, neither plants nor invertebrates possess an adaptive immune system, which was classically regarded as the sole means of conferring protection against reinfection in vertebrates. While it has been shown that certain live vaccines, such as BCG, can induce trained immunity[142], the training effects of non-living vaccines incorporating the widely used vaccine adjuvant alum have not been addressed.

Adjuvants have been essential in the development of many vaccines[151] due to the fact that most subunit antigens possess relatively poor immunogenicity[15]. Alum remains the most widely used vaccine adjuvant as it provides protection through the induction of antibody-mediated immunity along with a robust safety profile[152]. Although it has been in use for almost 100 years, the mechanism of action of alum has not been fully resolved, in particular, its effects on innate immune cells.

The observation that alum increases the induction of IL-10 when co-incubated with LPS has previously been shown in the Lavelle lab for both human monocytes and murine macrophages[141]. This effect was reproduced in the *in vitro* model of training for both cell types, demonstrating for the first time that alum can train innate immune cells to produce more IL-10 upon re-stimulation with LPS one week after initial stimulation. These trained cells were also shown to secrete higher concentrations of TNF-α, however, due to variability in background levels, TNF-α was not a reliable cytokine readout in order to measure the innate training potential of alum. The results in this chapter demonstrated that monocytes isolated from healthy human blood donors display a highly variable response to alum training, with only 50% of donors displaying increased IL-10 production.

As these monocytes were isolated from blood donors obtained through the Irish Blood Transfusion Services it was not possible to acquire important stratifying information such as age, sex and vaccination history. As a result, the innate training model was subsequently translated into murine BMDMs.

Phase contrast microscopic analysis throughout the *in vitro* training period revealed a distinct morphology in alum-trained BMDMs, characterised by a highly abundant population of rounded macrophages. FACS analysis further confirmed this, showing a population of macrophages that were both larger and more granular than controls. Due to the distinct differences in morphology between alum-trained and un-trained macrophages, it was important to establish the macrophage marker expression profile of these cells throughout the training period. FACS analysis of alum-trained cells required attention to FSC and SSC voltages to allow for the analysis of the broad range of cell sizes (including the large cells observed in the phase contrast images).

Mature BMDMs and activated macrophages can be identified by flow cytometry analysis for expression of surface antigens including CD11b and F4/80. Furthermore, monocytic-macrophages can be discriminated based on Gr1 expression, represented by the two molecules, Ly-6G and Ly6C. BMDMs are F4/80^{med}Gr1$^{low/neg}$, while mature macrophages are F4/80^{high}Gr1^{neg} cells. F4/80 and CD11b expression was comparable between cDMEM and alum-stimulated cells, however, Gr1 expression was much higher in the un-trained cells throughout the training period when compared with alum-trained cells. These results suggest that un-trained cells revert to a more monocyte-like phenotype during the 6/7-day training protocol. In contrast, the majority of alum-trained cells retain their macrophage properties, even by day 7.

Live/dead staining during FACS analysis suggested that there was a significant degree of cell death in the alum treated cultures, however, no indication of cell death was evident when cells were assessed using light microscopy. For FACS staining, cells were recovered from the dishes using PBS:EDTA on ice before being counted using trypan blue exclusion. As the cells appeared viable and adherent when imaged *in situ* by phase contrast microscopy throughout the 7 day training period, it was important to establish if the membrane was being permeabilised by the initial interaction of the cells with alum, without affecting the viability, an effect that is well documented in certain pore-forming bacteria[153]. PI is a dye that binds to double-stranded DNA by intercalating between base pairs following

uptake by cells with a compromised membrane, which for the most part, is a shared property of dead cells[154]. Similarly, Aqua Dead Stain reacts with free amines both in the cell interior and on the cell surface, which are only accessible on cells with compromised membranes. In order to distinguish viable cells with a compromised membrane from dead cells an alternative method for staining viable cells was required. TMRM is a cell-permeant dye that accumulates in active mitochondria with intact membrane potentials[155]. Therefore, if the cells are healthy and have functioning mitochondria, bright staining will be seen. Using confocal microscopy, TMRM was used to distinguish healthy viable cells, while PI was used to identify if the membranes of viable cells were permeabilised. Cells stimulated with both concentrations of alum for 30 minutes were negative for PI staining . However, some cells stimulated with the training concentration of alum (10 μg/mL) for 24 h displayed positive PI staining without TMRM staining, therefore, distinguishing them as dead cells. In contrast, the higher concentration of 100 μg/mL of alum killed all the cells after 24 h, which has previously been shown by several research groups[140]. Furthermore, un-trained and β-glucan-stimulated cells were almost completely negative for PI, indicating minimal cell death. It must be noted that a limitation of this assay is that both TMRM and PI are the same colour causing the two stains to overlap therefore only differences in structural staining can be used to show TMRM staining of viable mitochondria. These results suggest that macrophages stimulated with the training concentration of alum undergo a limited degree of cell death. However, this contrasts with the significant cell death observed during FACS analysis. The results suggest that cells that take up alum possess a larger, more rounded morphology that may result in membrane sensitivity during the recovery of adherent BMDMs for FACS analysis. These data highlight the importance of evaluating cell viability in a number of ways and also emphasizes the value of microscopy.

A key observation in these initial exploratory studies, in addition to the effects of alum on cell morphology, was the increase in cell numbers during training following initial stimulation with alum. This effect was also seen *in vivo* when mice were injected with alum 3 or 7 days prior to harvesting bone marrow. Mice injected intraperitoneally with alum 7 days prior to collecting bone marrow yielded more bone marrow cells when compared with PBS-injected mice. Furthermore, when bone marrow cells were differentiated into BMDMs for 6 days, those isolated from mice injected with alum were significantly more abundant than those from mice injected with PBS. In this model, there was no indication that alum

injection primed bone marrow cells for enhanced IL-10 secretion when re-stimulated with individual PRR ligands. It is important to note that although there was an increase in differentiated BMDMs from the bone marrow of mice injected with alum, cell numbers were normalized prior to stimulation with PRR agonists. This increase in the number of trained macrophages may be important in the context of cytokine production by these cells. It is possible that increased survival of alum-trained cells and/or increased proliferation is responsible for the elevated levels of IL-10 following LPS stimulation observed during the *in vitro* training model. Furthermore, it is also important to consider the difference between *in vivo* training effects of alum with regard to IL-10 secretion from BMDMs after re-stimulation *ex vivo*, which may be less pronounced when compared with direct stimulation of macrophages with alum *in vitro*.

Recently several studies have shown that macrophages trained with BCG or β-glucan possess heightened responses to secondary infection through the increased production of pro-inflammatory cytokines such as TNF-α and IL-6 which support enhanced protection during pathogen infection[44]. Furthermore, TNF-α production is key in host defence against mycobacterial infection[156]. Accordingly, alum-trained macrophages were infected with live BCG to ascertain the effects of alum training in an *in vitro* infection model. CFU percentages revealed more live bacteria present in alum-trained macrophages in the later time-point of infection. These results indicate that training with alum does not impede uptake of bacteria, however, alum-trained macrophages, may not be effective in killing bacteria once inside the cell. Furthermore, the most striking observation was the altered cytokine profile of these macrophages in response to mycobacterial infection. As seen before, TNF-α secretion was comparable between both treatments, however, the production of anti-inflammatory cytokines was dramatically enhanced in alum-trained macrophages 24 h after infection with BCG. A significant increase in the secretion of IL-10 was observed as in previous experiments. All data were normalised for differences in cell numbers, therefore this increase in IL-10 was a result of enhanced secretion by macrophages and not due to enhanced cell numbers. Furthermore, IL-1Ra was included in this experiment as an additional anti-inflammatory cytokine as it has recently been shown to be an important cytokine induced during innate immune training in response to helminths[157]. Substantial evidence shows that IL-1Ra functions exclusively as a competitive inhibitor of IL-1 by

binding to IL-1 cell-surface receptors[158]. Importantly, a balance between the ratio of IL-1β and IL-1Ra is vital *in vivo* to dampen excessive inflammation and prevent damage to tissues[159]. In this study, IL-1Ra secretion was four-fold higher in BCG-infected macrophages trained with alum. This is a key finding as alum has not previously been shown to enhance production of this cytokine by macrophages. The beneficial innate immune training effects of vaccines has been specific to live vaccines such as BCG, measles and the oral polio vaccine[42]. Therefore, alum-adjuvanted vaccines in this context may exert a "damage control" effect through the resolution of inflammation to prevent unnecessary tissue injury, which supports its widely established safety profile.

In order to characterise the transcriptional profile of alum-trained BMDMs the NanoString nCounter Analysis system was used to examine differential expression of a group of 249 inflammation-associated genes. Alum-trained macrophages display a global downregulation of pro-inflammatory genes compared to un-trained cells. Most of the literature on alum has presented this adjuvant as an inducer of inflammation through necrosis, DAMP release[160], IL1-β induction[161] and activation of DCs to polarise Th2 responses, supporting protective humoral immunity[162]. A small cluster of upregulated genes was observed following training, offering some interesting insights into the underlying mechanisms behind the establishment of this unexpected phenotype in alum stimulated macrophages. These upregulated genes were further explored using nSolver's Advanced Analysis software to generate potential pathways of interest.

From this analysis several pathways were highlighted including a potential role for chemokine expression during alum training in macrophages. Known for their effects on cellular migration, the chemokines comprise a large family of secreted proteins that signal through G protein-coupled heptahelical receptors and can be protective or damaging depending on the context of their activation[138]. A few hours after administration of alum several cells are recruited to the site of injection including neutrophils, eosinophils, monocytes, DCs, NK and NKT cells. This recruitment coincides with the production of several cytokines and chemokines including CCL2, CCL11, CXCL3 and CXCL2[163]. Crucially, chemokines are key regulators of wound healing and resolution of inflammation through tailored promotion and inhibition of angiogenesis. Furthermore these proteins recruit cells that are vital sources of growth factors and anti-inflammatory cytokines during the resolution phase of infection[138]. The process of wound healing is complex and multifaceted

with four interconnected phases: haemostasis, inflammation, proliferation and remodelling. The macrophage is a key cell within this multistep process. During monocyte-to-macrophage differentiation it is necessary for these cells to generate an increased resistance to apoptotic mediators[164]. Several genes involved in anti-apoptotic and proliferation pathways were upregulated in alum-trained BMDMs from the NanoString data supporting our previous observations that suggest alum induces a pro-survival signal and enhances proliferative capacity. Both *Bcl2l11* and *Csf1* are important genes in macrophage apoptosis and pro-survival pathways[165]. Bcl2L1 or Bcl-xL, a member of the BCL-2 family of proteins, is involved in the apoptotic pathway by inhibiting the action of pro-apoptotic BCL-2 family members such as BH3-only activators by binding and sequestering them, thereby preventing their interaction with pore-forming effectors[91]. Macrophage colony-stimulating factor 1 (CSF-1) is a key growth factor involved in regulating the migration, proliferation and survival of macrophages. CSF-1 is involved in several pathways such as PI3K[166], JAK-STAT[167] and the Ras signalling pathways[168].

Another gene expression signature from analysis of the transcriptional profile of alum-trained cells was the upregulation of genes involved in the antioxidant response to reactive oxygen species which includes the nuclear factor erythroid 2 (NFE2)-related factor 2 (*Nfe2l2*) or Nrf2 and the small Maf proteins, *MafK* and *MafF*[169]. One of the major features of Nrf2 is its role in the antioxidant response to reactive oxygen species and subsequent downregulation of pro-inflammatory cytokines. Under normal conditions Nrf2 is constitutively degraded through binding to Keap1 (Kelch-like ECH-associated protein 1), an adaptor protein of E3 ubiquitin ligase. However during oxidative stress the degradation of Nrf2 is prevented causing it to accumulate and subsequently translocate to the nucleus. Within the nucleus Nrf2 forms heterodimers with one of the small Maf proteins and finally binds to regulatory regions of ARE-target genes involved in the anti-oxidant response eliciting an anti-inflammatory expression profile that is vital for the initiation of healing[170]. Preliminary data also suggests that mitochondrial ROS production is induced in BMDMs stimulated with alum for one hour at the same concentration required to train these cells. Finally, IL-1Ra was strongly upregulated in alum-trained BMDMs, further supporting previous data showing a robust enhancement of the IL-1Ra protein in response to BCG infection. This upregulation coincided with a downregulation of *Il-1a*, *Il-b* and *Il-18*. Although IL-1Ra exerts its effects through competitive inhibition of IL-1R signalling it is

interesting that the expression of these pro-inflammatory members of the IL-1 family was decreased in alum-trained BMDMs 7 days after initial exposure to this adjuvant.

These results suggest that alum training may favour a pro-resolution phenotype by generating more anti-inflammatory myeloid cells possessing enhanced survival and proliferative capacity. The extensive downregulation of pro-inflammatory genes observed by NanoString analysis seven days following innate training further supports this theory.

Chapter 4 Alum induces metabolic re-wiring and anti-inflammatory cytokine secretion through mTOR

4.1 Introduction

In Chapter 3 we showed the anti-inflammatory expression profile of alum-trained macrophages in addition to an enhanced proliferation and survival capacity. During the infection model of BCG, alum-trained macrophages secreted enhanced levels of IL-10 and IL-1Ra compared to un-trained cells.

Enhanced proliferation through cell cycle progression critically depends on the availability of nutrients and metabolites, while cell cycle machinery is indispensable for the regulation of metabolic networks to allow this survival and proliferation. An important pathway involved in this regulation between cellular metabolism and cell cycle machinery is the PI3K/Akt/mTOR pathway. The PI3K/Akt/mTOR pathway is a signal transduction pathway that regulates cell growth and survival in response to nutrient and growth factor availability. Several studies have also recently demonstrated the importance of metabolism for the polarisation of macrophages and macrophage functional responses. The mTOR pathway has also been shown to be involved in innate immune training as inhibition of mTOR blocked β-glucan-mediated training of human monocytes. Accordingly, the next step in this project was to investigate the metabolic profile of BMDMs stimulated with alum, in particular how the involvement of PI3K and mTOR might influence this metabolism and the anti-inflammatory response induced by alum.

4.2 Hypothesis

As alum was found to enhance secretion of anti-inflammatory cytokines such as IL-10 and IL-1Ra it was important to identify the upstream mechanism of this response. Several studies have identified an important link between the polarisation of macrophages and the underlying metabolic rewiring that facilitates these responses. The ability of alum to enhance an anti-inflammatory macrophage with enhanced proliferative/survival capacity prompted the hypothesis that alum may train macrophages through alterations to the metabolic machinery that support sustained energy demands required for these processes. Furthermore, the involvement of metabolic regulators such as mTOR was also proposed as a key signalling pathway involved in alum's ability to modulate macrophage responses that might enhance proliferation and anti-inflammatory responses.

4.3 Aims

This results chapter aims to identify the following:

- To investigate the anti-inflammatory profile of BMDMs stimulated by alum, in particular the kinetics of IL-1Ra secretion during the training model
- To evaluate if macrophages trained by alum for 24hrs adopt and maintain a distinct metabolic profile
- To assess the potential involvement of distinct metabolic pathways involved in innate immune training including the role of the regulatory protein mTOR
- To quantify gene expression associated with the metabolic response in BMDMs stimulated by alum

4.4 Results

4.4.1 Alum induces potent and sustained IL-1Ra secretion by macrophages

Results presented in Chapter 3 demonstrated that IL-1Ra gene expression and protein secretion was enhanced in alum-trained BMDMs, both basally and in response to infection with BCG. Here, this was investigated in greater detail to address kinetics and the underlying mechanism. Fully differentiated BMDMs were stimulated with cDMEM or alum (10 μg/mL) and IL-1Ra secretion was assessed 24 h later by ELISA. Alum was found to significantly enhance IL-1Ra secretion when compared with un-stimulated cells Figure 4.1(A). BMDMs were also trained, as previously described, with cDMEM or alum (10 μg/mL) for 24 h, followed by a rest period of 6 days. On day 6, the trained macrophages were re-stimulated for 24 h with cDMEM or LPS (10 ng/mL). Interestingly, increased secretion of IL-1Ra was retained 7 days later when alum-trained cells were incubated in cDMEM. Furthermore, re-stimulation with LPS on day 6 further enhanced alum-induced IL-1Ra secretion by trained macrophages Figure 4.1(B). This result supports the anti-inflammatory profile of alum-stimulated BMDMs observed in earlier experiments and demonstrates that this phenotype is established during initial exposure to alum and retained until the end of the training protocol. Furthermore, these BMDMs are primed for enhanced secretion of IL-1Ra upon re-stimulation with LPS on day 6.

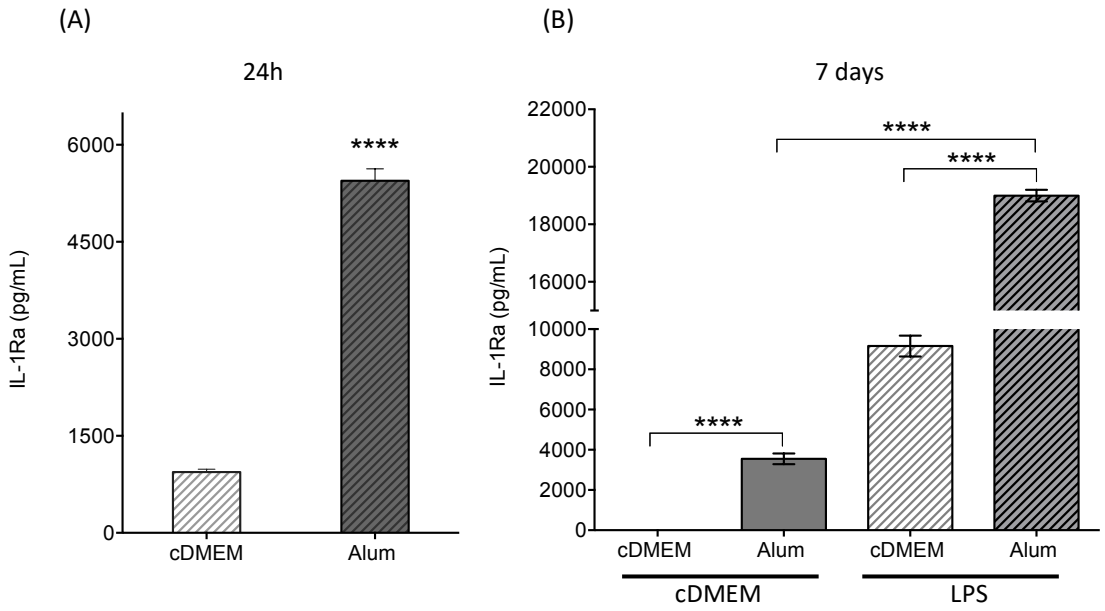

Figure 4.1 Alum drives sustained secretion of IL-1Ra by macrophages. (A) BMDMs were seeded at equal numbers and stimulated with alum (10 µg/mL) and supernatants were collected after 24 h. (B) BMDMs were un-trained or trained with alum (10 µg/mL) for 24 h, rested and re-stimulated 6 days later with cDMEM or LPS (10 ng/mL) and supernatants were collected after 24 h. IL-1Ra secretion was measured by ELISA. Results are mean ± SEM from 3 female mice. ****p<0.001 Un-stimulated vs Alum-stimulated cells after 24 h (A) by unpaired t test. ****p<0.001 (B) by one-way ANOVA with Tukey post-test.

4.4.2 Macrophages display enhanced metabolic activity 7 days after training with alum

IL-1Ra and IL-10 have recently been shown to be associated with the metabolic reprogramming of macrophages[171]. Therefore, it was important to evaluate the metabolic profile of alum-trained macrophages. BMDMs were trained with alum (10 μg/mL), β-glucan (10 μg/mL) or un-trained for 24 h, rested for 6 days and re-plated in a Seahorse XF96 well plate and allowed to recover overnight. The Seahorse extracellular flux assay measures the oxygen consumption rate (OCR) and the extracellular acidification rate (ECAR). For OCR readings, trained BMDMs were treated sequentially with Oligomycin (1 mM), FCCP (1 mM) and finally Antimycin A/Rotenone (500 nM). For ECAR readings, trained BMDMs were treated sequentially with Oligomycin (1 mM) and 2-DG (25 mM). Representative traces for both OCR and ECAR are shown in Figure 4.2(A)&(C). These two readouts allow real time quantification of metabolic cellular functions, such as mitochondrial respiration and glycolysis, respectively. Both basal OCR Figure 4.2(B) and ECAR Figure 4.2(D) readouts were significantly enhanced in alum-trained BMDMs when compared with β-glucan-trained or un-trained cells. Using an energy plot of OCR vs ECAR readings, alum was found to train macrophages to adopt a highly energetic state compared to a more oxidative profile in β-glucan-trained cells while un-trained cells displayed a quiescent metabolic profile Figure 4.2(E).

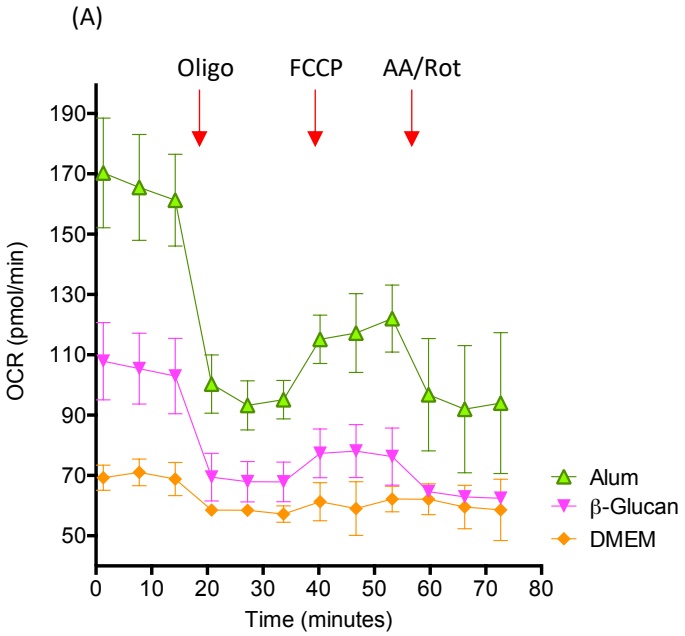
(A)
Oligo
FCCP
AA/Rot
OCR (pmol/min)
190
170
150
130
110
90
70
50
0
10
20
30
40
50
60
70
80
Time (minutes)
Alum
β-Glucan
DMEM

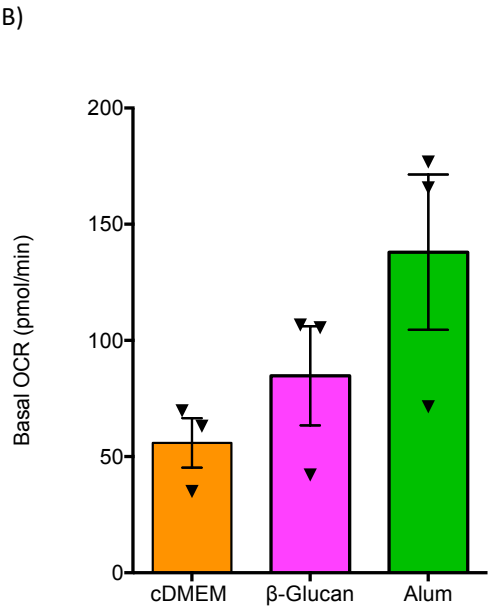
(B)
Basal OCR (pmol/min)
200
150
100
50
0
cDMEM
β-Glucan
Alum

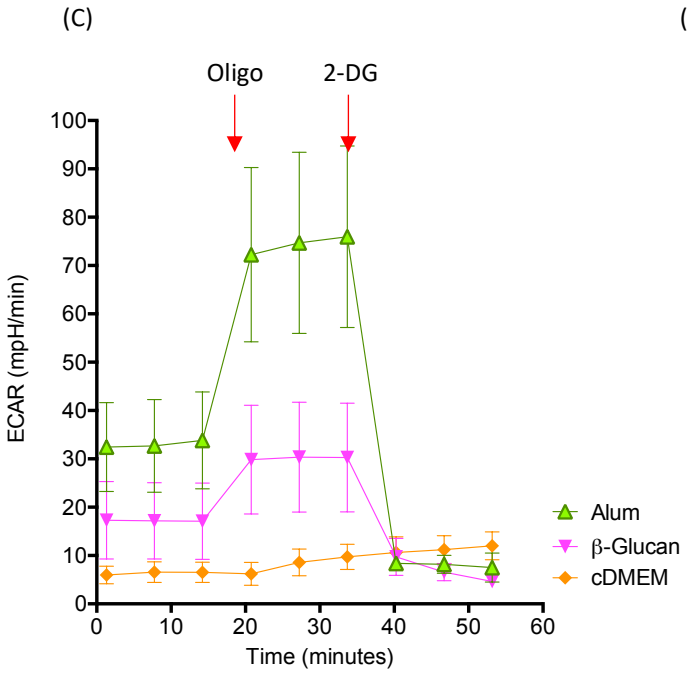
(C)
Oligo
2-DG
ECAR (mpH/min)
100
90
80
70
60
50
40
30
20
10
0
0
10
20
30
40
50
60
Time (minutes)
Alum
β-Glucan
cDMEM

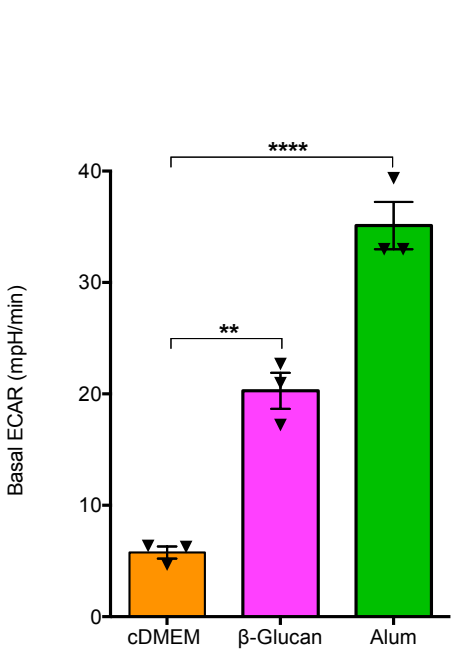
(D)
Basal ECAR (mpH/min)
****
**
40
30
20
10
0
cDMEM
β-Glucan
Alum

(E)

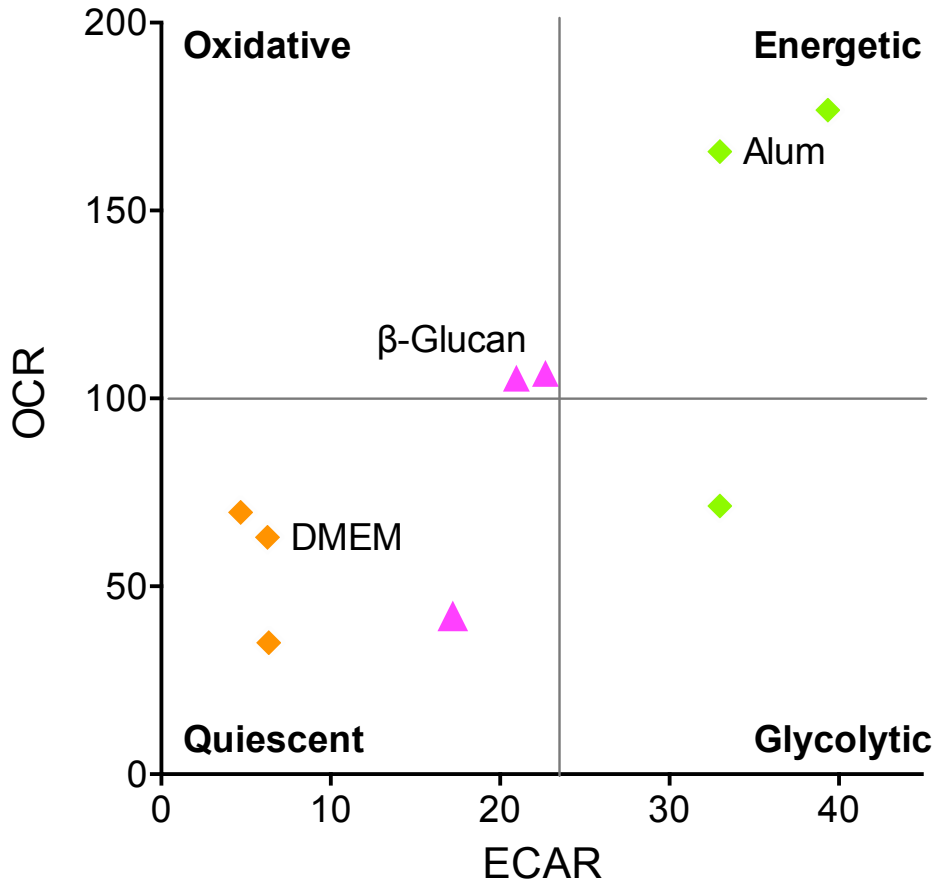

Figure 4.2 Macrophages display enhanced metabolic activity 7 days after training with alum. BMDMs were un-stimulated, stimulated for 24 h with β-glucan (10 μg/mL) or alum (10 μg/mL), rested for 6 days and re-plated in a Seahorse XF96 well plate at a seeding density of 150,000 cells/well and allowed to recover overnight. A. Seahorse extracellular flux assay was carried out. For OCR readings, trained macrophages were treated sequentially with Oligomycin (1 μM), FCCP (1 μM) and finally Antimycin A/Rotenone (500 nM). Representative traces are presented for OCR readings (A). Basal OCR for pooled data is shown in (B). For ECAR readings, trained macrophages were treated sequentially with Oligomycin (1 μM) and 2-DG (25 mM). Representative traces for ECAR (C). Basal ECAR for pooled data is shown in (D). The rates of ECAR were compared with the rates of OCR for un-trained, β-glucan-trained and alum-trained and plotted on an energy map (E). Results are mean ± SEM for three mice from three individual experiments. **p<0.01 ****p<0.001 un-trained vs alum or β-glucan-trained cells by one-way ANOVA with Dunnett post-test.

4.4.3 IL-1Ra secretion by alum-stimulated BMDMs is reduced by inhibition of the PI3K/mTOR pathway

Metabolic analysis of innate immune training has revealed a cellular reprogramming from oxidative phosphorylation towards enhanced glycolysis mediated by mTORC1. Furthermore, in myeloid cells the PI3K/mTOR pathway has been strongly implicated in the upregulation of anti-inflammatory cytokines such as IL-10 and inhibition of pro-inflammatory cytokines[122]. It was therefore important to investigate the role of PI3K and mTOR in the increased secretion of IL-1Ra observed in response to alum. The LDH cytotoxicity assay was used to preclude alterations in cytokine profiles due to cell death when BMDMs were pre-treated with inhibitors. The class I PI3K inhibitor, ZSTK474, was used as it has been shown to block tumour cell proliferation through G1 arrest of the cell cycle without inducing apoptosis *in vitro.* BMDMs were pre-treated with a range of ZSTK474 concentrations (0.1-20 μM) or cDMEM for 1 h prior to stimulation with alum (10 μg/mL) *or* cDMEM for 24 h. Supernatants were collected and LDH was measured and compared to the positive control (SDS lysis buffer). The lowest concentration of ZSTK474 (0.1 μM) caused no detectable cell death in BMDMs stimulated with cDMEM Figure 4.3(A). Furthermore, the addition of alum did not enhance LDH release from BMDMs pre-treated with 0.1 μM of ZSTK474. However, higher concentrations of the inhibitor (0.5, 5 and 20 μM) alone induced approximately 20% LDH release compared to SDS-lysed cells and this was unchanged when cells were stimulated with alum Figure 4.3(A).

Rapamycin, a macrocyclic triene antibiotic, is an inhibitor of mTOR with immunosuppressive and anti-proliferative properties in mammalian cells.

BMDMs were pre-treated with a range of concentrations of rapamycin (1-50 nM) and stimulated with alum or cDMEM as previously described for ZSTK474. All concentrations tested induced minimal cell death (<10%) in cells that were incubated in cDMEM Figure 4.3(B). Furthermore, when BMDMs were stimulated with alum for 24 h, the lower concentrations of rapamycin (1, 10 nM) induced <20% cell death, however, the highest concentration (50 nM) induced approximately 25% cell death when compared with the positive control.

ELISA was carried out on supernatants to test the effects of ZSTK474 and Rapamycin on the secretion of IL-1Ra after 24 h of stimulation with alum. In addition, rapamycin also

significantly reduced alum-enhanced IL-1Ra secretion consistently across all concentrations tested Figure 4.3(D). This finding suggests a novel role for the PI3K/mTOR pathway in the enhancement of IL-1Ra secretion by alum-stimulated macrophages.

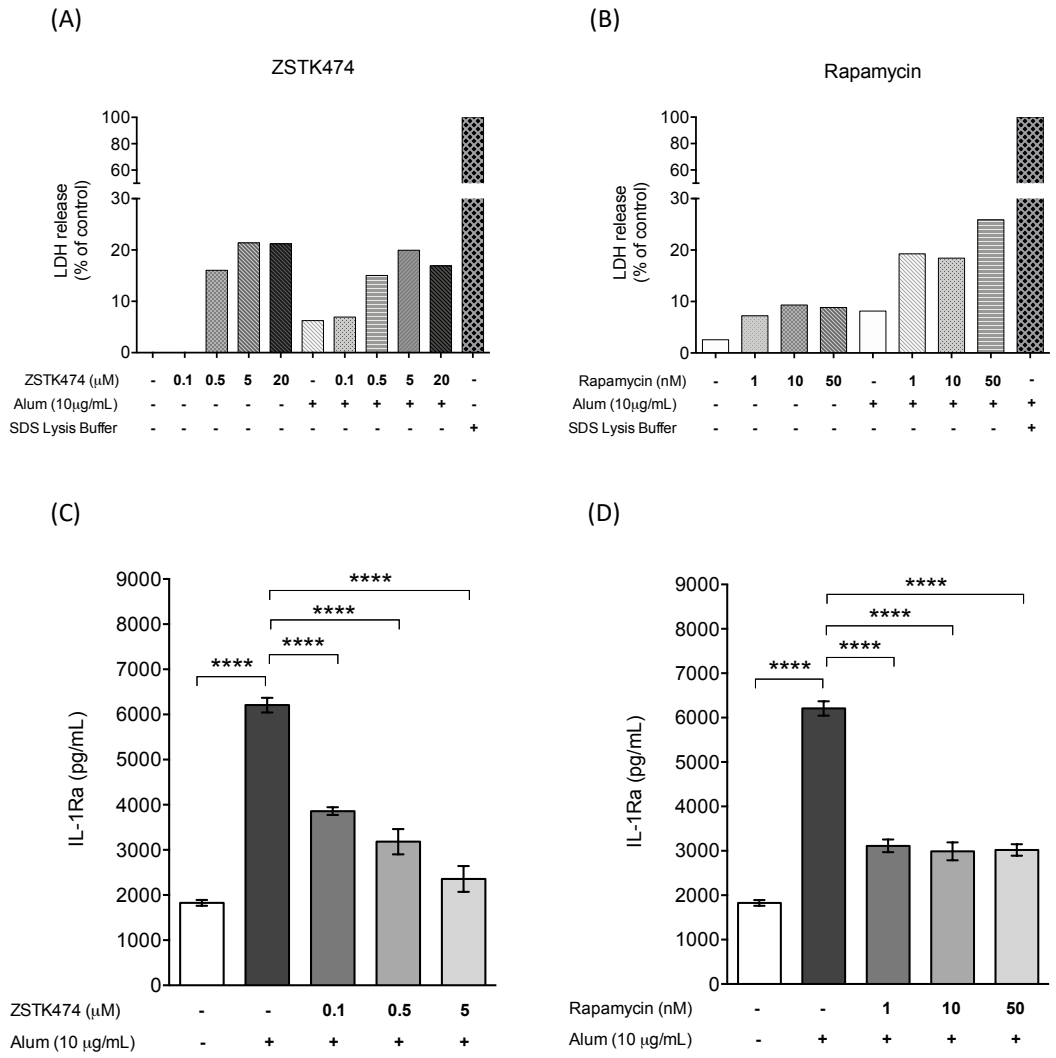

Figure 4.3 IL-1Ra secretion by alum-stimulated BMDMs is reduced by inhibition of the PI3K/mTOR pathway. BMDMs were pre-incubated with a range of concentrations of the PI3K Class I inhibitor, ZSTK474 (0.1-5 μM) or the mTOR inhibitor, rapamycin (1-50 nM) for 1 h prior to stimulation with alum (10 μg/mL) for 24 h. Supernatants were collected and LDH (to assess cytotoxicity) was measured for ZSTK474 +/- alum (A) and Rapamycin +/- alum. (B). Results show %LDH released compared to SDS-lysed cells. Supernatants were also recovered after 24 h and IL-1Ra secretion was measured by ELISA for ZSTK474 +/- alum (C) and Rapamycin +/- alum (D). Results are mean ± SD for technical triplicates and representative of 3 experiments. ****p<0.001 vs Alum-stimulated cells by one-way ANOVA plus Dunnett post-test.

4.4.4 Rapamycin reduces alum-induced IL-1Ra secretion by BMDMs after 24 h and 7 days

The metabolic basis of innate immune training with β-glucan has previously been shown to be mTOR-dependent induction of glycolysis. It was therefore necessary to investigate the potential role of this pathway in the long-term effects observed in alum-stimulated BMDMs. As all concentrations of rapamycin tested significantly reduced the secretion of IL-1Ra, 24 h after stimulation with alum, the lowest concentration of 1 nM was selected as it had a limited effect on cell death. BMDMs were pre-incubated with rapamycin (1 nM) or cDMEM for 1 h prior to stimulation with alum (10 μg/mL) or cDMEM for 24 h. Supernatants were taken after 24 h and cells were given fresh media. Supernatants were also taken after 7 days and ELISA for IL-1Ra was carried out on samples collected at both time points. As seen before, alum-induced IL-1Ra secretion was significantly reduced when mTOR was inhibited prior to stimulation Figure 4.4(A). Furthermore, after 7 days in culture, alum-trained BMDMs that were pre-incubated with rapamycin secreted significantly less IL-1Ra Figure 4.4(B). These results indicate that the mTOR pathway is important for the sustained effects of alum on IL-1Ra secretion by macrophages.

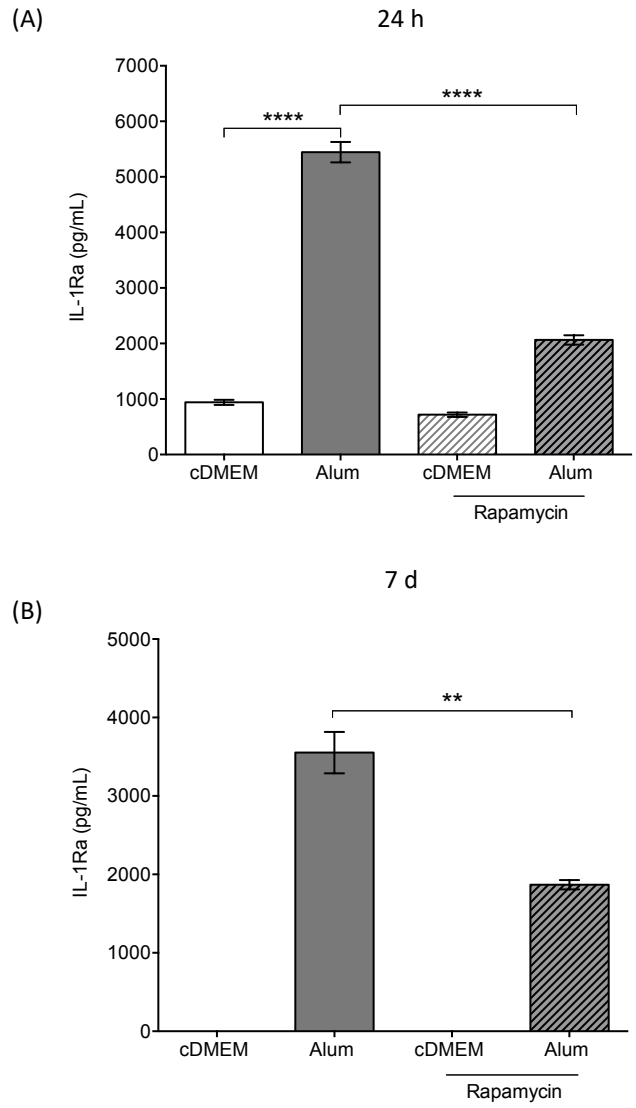

Figure 4.4 The inhibitory effect of rapamycin on alum-induced IL-1Ra secretion by BMDMs is sustained for up to 7 days. BMDMs were pre-incubated with rapamycin (1 nM) for 1 h prior to stimulation with alum (10 μg/mL) for 24 h and supernatants were collected. Fresh medium was added and cells were then rested for 7 days and supernatants were collected again on day 7. IL-1Ra was measured by ELISA after the initial 24 h stimulation (A) and after 7 days (B). Results are mean ± SEM from 3 female mice. ****$p<0.001$ **$p<0.01$ by one-way ANOVA plus Tukey post-test.

4.4.5 Sustained secretion of IL-1Ra over time in response to alum is reduced by rapamycin

Enhanced production of IL-1Ra was consistently observed in BMDMs as early as 24 h and as late as 7 days following initial stimulation with alum. As cells receive fresh media during the training protocol and prior to re-stimulation on day 6 it is difficult to quantify the cumulative secretion of IL-1Ra during training before and after re-stimulation. Accordingly, a time course was carried out on IL-1Ra accumulation in supernatants over 14 days from initial stimulation with alum. BMDMs were pre-incubated for 1 h with rapamycin (10 nM) or cDMEM followed by incubation of cells with alum or cDMEM for 24 h, after which the cells were given fresh medium. On day 6, trained macrophages were re-stimulated with LPS (10 ng/mL) or cDMEM, as before. Supernatants were collected on days 1, 2, 3, 4, 5, 7, 10 and 14 of training. IL-1Ra accumulation in supernatants was assessed by ELISA and a time course of its secretion is presented in Figure 4.5(A). In un-trained controls, IL-1Ra production was undetectable until cells were re-stimulated with LPS on day 7. However, concentrations of IL-1Ra increased progressively in supernatants of BMDMs that were trained with alum over the 14-day period, which was dramatically amplified when cells were re-stimulated with LPS on day 7. Rapamycin pre-treatment reduced IL-1Ra secretion throughout the 14-day period, with a statistically significant difference observed on day 10 and 14. Furthermore, rapamycin significantly reduced alum-induced secretion of IL-1Ra on day 10 and 14 when cells were re-stimulated on day 7 with LPS. These results suggest that IL-1Ra is cumulatively secreted throughout the training protocol when BMDMs are stimulated with alum on day 0. This effect was strongly enhanced by re-stimulation with LPS on day 7 and significantly inhibited by pre-treatment of cells with rapamycin on day 0.

(A)

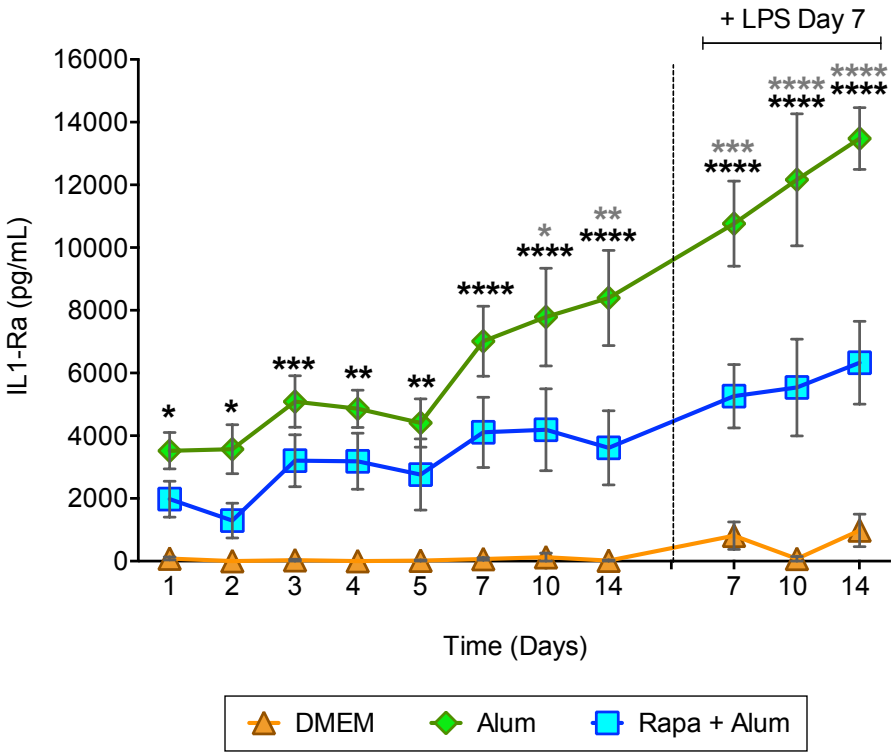

Figure 4.5. Alum induced sustained and primed secretion of IL-1Ra is reduced by rapamycin. BMDMs were pre-incubated with rapamycin (10 nM) for 1 h prior to stimulation with alum (10 μg/mL) for 24 h, rested for 7 days and re-stimulated for 24 h with cDMEM or LPS (10 ng/mL). Supernatants were collected on days 1, 2, 3, 4, 5, 7, 10 and 14 and IL-1Ra secretion over 14 days was measured by ELISA. Results are mean ± SEM from 3 female mice. *p<0.05 **p<0.01, ***p<0.005, ****p<0.001 un-trained vs Alum-trained. *p<0.05, **p<0.01***, p<0.005, ****p<0.001 Alum-trained vs Rapamycin + Alum-trained by two-way ANOVA with Tukey post-test. Experiment was performed once in 3 mice.

4.4.6 Secretion of IL-1Ra by human monocytes is enhanced by training with alum and this effect is reversed by rapamycin

It was demonstrated in Chapter 3 that human monocytes trained with alum exhibited enhanced IL-10 production. However, due to issues with variability in donor responses to alum the training protocol was translated into murine BMDMs. Having shown the involvement of another anti-inflammatory cytokine (IL-1Ra) in response to alum-training, it was important to investigate if this response was similar in human monocytes. Human monocytes were isolated from one healthy blood donor by MACS through CD14 negative selection. Adherent monocytes were pre-incubated with rapamycin (1 nM) or cRPMI for 1 h prior to stimulation with alum (100 ng/mL) or cRPMI for 24 h. Trained monocytes were rested for 5 days and re-stimulated on day 6 with cRPMI, Heat-killed *Mtb* (25 μg/mL) or LPS (100 ng/mL) for 24 h. ELISA carried out on supernatants revealed enhanced IL-1Ra in alum-trained human monocytes, which was significantly reduced by pre-incubation with rapamycin Figure 4.6(A). Furthermore, alum-trained monocytes secreted significantly higher concentrations of IL-1Ra in response to re-stimulation with Heat-killed *Mtb* and LPS and this effect was reversed by pre-incubation with rapamycin Figure 4.6(B) and (C). These finding support the previous results (Figures 3.2 and 3.4) in human monocytes and BMDMs and demonstrate that alum alters the inflammatory profile of innate immune cells by enhancing secretion of the IL-1 receptor antagonist both basally and following secondary challenge with unrelated stimuli. Furthermore, this innate immune training effect induced by alum appears to be mTOR dependant.

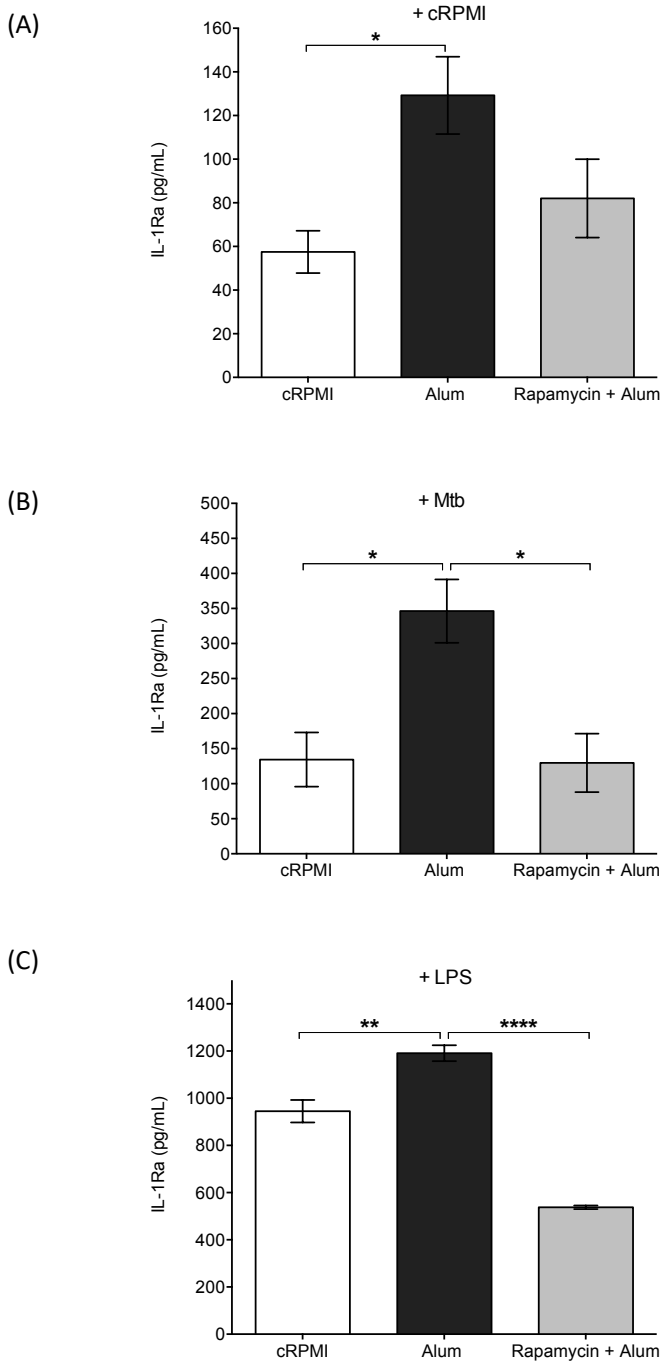

Figure 4.6 IL-1Ra is enhanced in alum-trained human monocytes in response to *Mtb* or LPS and is reversed by rapamycin. Human monocytes were isolated from one healthy blood donor by MACS using negative selection for CD14+ cells. Sorted monocytes were pre-incubated for 1 h with cRPMI or rapamycin (1 nM), stimulated for 24 h with cRPMI or alum (100 ng/mL) before being rested for 5 days and re-stimulated with cRPMI, irradiated *Mtb* (25 mg/mL) or LPS (100 ng/mL). Supernatants were collected after 24 h and ELISA was performed. IL-1Ra was measured for trained BMDMs re-stimulated on day 5 with cRPMI (A), irradiated *Mtb* (25 mg/mL) (B) or LPS (100 ng/mL) (C) . Results are mean ± SD of one blood donor. *p<0.05 **p<0.01 ****p<0.001 vs Alum-trained monocytes by one-way ANOVA plus Dunnett post-test. Experiment was performed once in triplicate.

4.4.7 The enhanced metabolic activity of alum-stimulated BMDMs is inhibited by rapamycin

We previously observed that alum-trained BMDMs displayed a highly energetic phenotype using OCR and ECAR readings from the Seahorse extracellular flux assay. Enhancement of IL-1Ra secretion by alum is observed as early as 24 h after stimulation and is partially dependent on PI3K/mTOR at this stage. Following on from these results, the next step was to assess the metabolic profile of these cells after initial stimulation with alum and investigate the potential role of mTOR. BMDMs were seeded in Seahorse XF96 well plates and pre-incubated for 1 h with cDMEM or rapamycin (1 nM) and then stimulated with cDMEM or alum (10 μg/mL) for 24 h. The Seahorse extracellular flux assay was carried out. For OCR readings, cells were treated sequentially with Oligomycin (1 μM), FCCP (1 μM) and finally Antimycin A/Rotenone (500nM). Representative traces can be found in Figure 4.7(A). Basal OCR was calculated and alum-stimulated BMDMs displayed significantly enhanced basal OCR when compared with un-stimulated controls. When alum-stimulated cells were pre-treated with rapamycin the basal OCR was comparable to un-stimulated macrophages Figure 4.7(B). Maximal respiration or maximal oxygen consumption rate revealed a similar result with alum-stimulated cells displaying significantly enhanced respiration when compared with media stimulated cells and this was reversed by the addition of rapamycin Figure 4.7(C). For ECAR readings, macrophages were treated sequentially with Oligomycin (1 μM) and 2-DG (25 mM). A representative ECAR trace is shown in Figure 4.8(A). Basal ECAR was calculated and alum-stimulated BMDMs showed significantly enhanced basal ECAR when compared with un-stimulated cells. While rapamycin significantly inhibited basal ECAR in alum-stimulated cells, it was still slightly higher than un-stimulated cells Figure 4.8(B). Maximal glycolysis (or glycolytic capacity) was calculated and alum-stimulated BMDMs had higher glycolytic capacity than media stimulated cells. However, when alum-stimulated BMDMs were pre-incubated with rapamycin glycolytic capacity was significantly inhibited to levels lower than media stimulated cells Figure 4.8(C). The energy plot in Figure 4.8 (D) displays energetic metabolic profile of alum-stimulated macrophages, which was previously seen for alum-trained macrophages. This energetic phenotype reverts to a similar profile as the un-stimulated cells (quiescent) upon pre-treatment with rapamycin. These findings demonstrate the highly energetic profile of macrophages during

initial stimulation by alum and suggest an important role for mTOR activation in the establishment of this enhanced metabolic capacity.

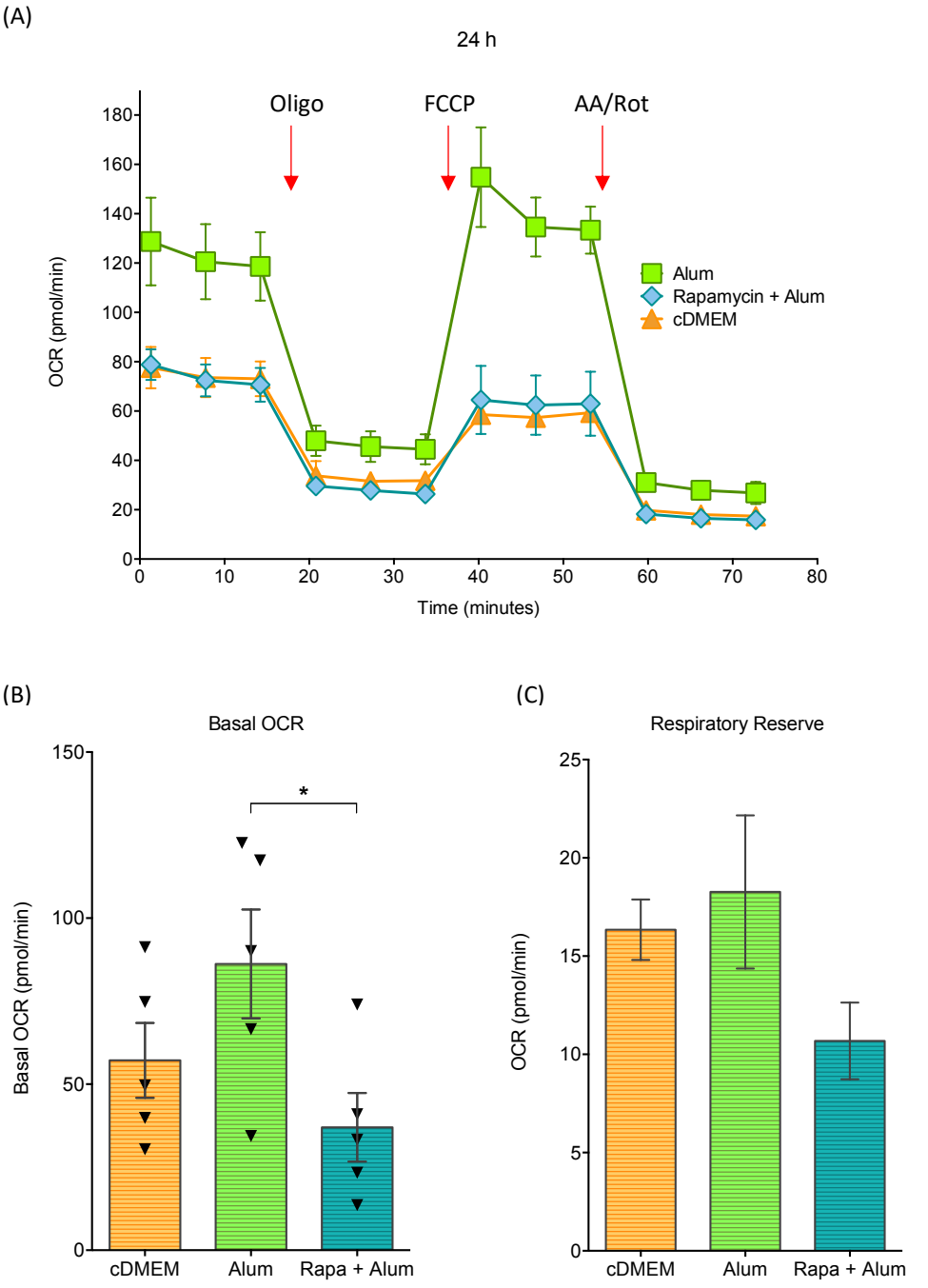

Figure 4.7 Enhanced OXPHOS in alum-stimulated BMDMs is inhibited by rapamycin. BMDMs were pre-incubated for one hour with cDMEM or rapamycin (1 nM) and stimulated for 24 h with cDMEM or alum (10 μg/mL) in Seahorse XF96 well plates at a seeding density of 150,000 cells/well. Seahorse extracellular flux assay was carried out. For OCR readings, BMDMs were treated sequentially with Oligomycin (1 μM), FCCP (1 μM) and finally Antimycin A/Rotenone (500 nM). Representative OCR trace (A), basal OCR with pooled data (B) and representative respiratory reserve (or maximal respiration) (C) Pooled data are mean ± SEM of 5 mice from 3 independent experiments. *$p<0.05$ alum- vs alum + rapamycin-stimulated cells by one-way ANOVA with Dunnett post-test.

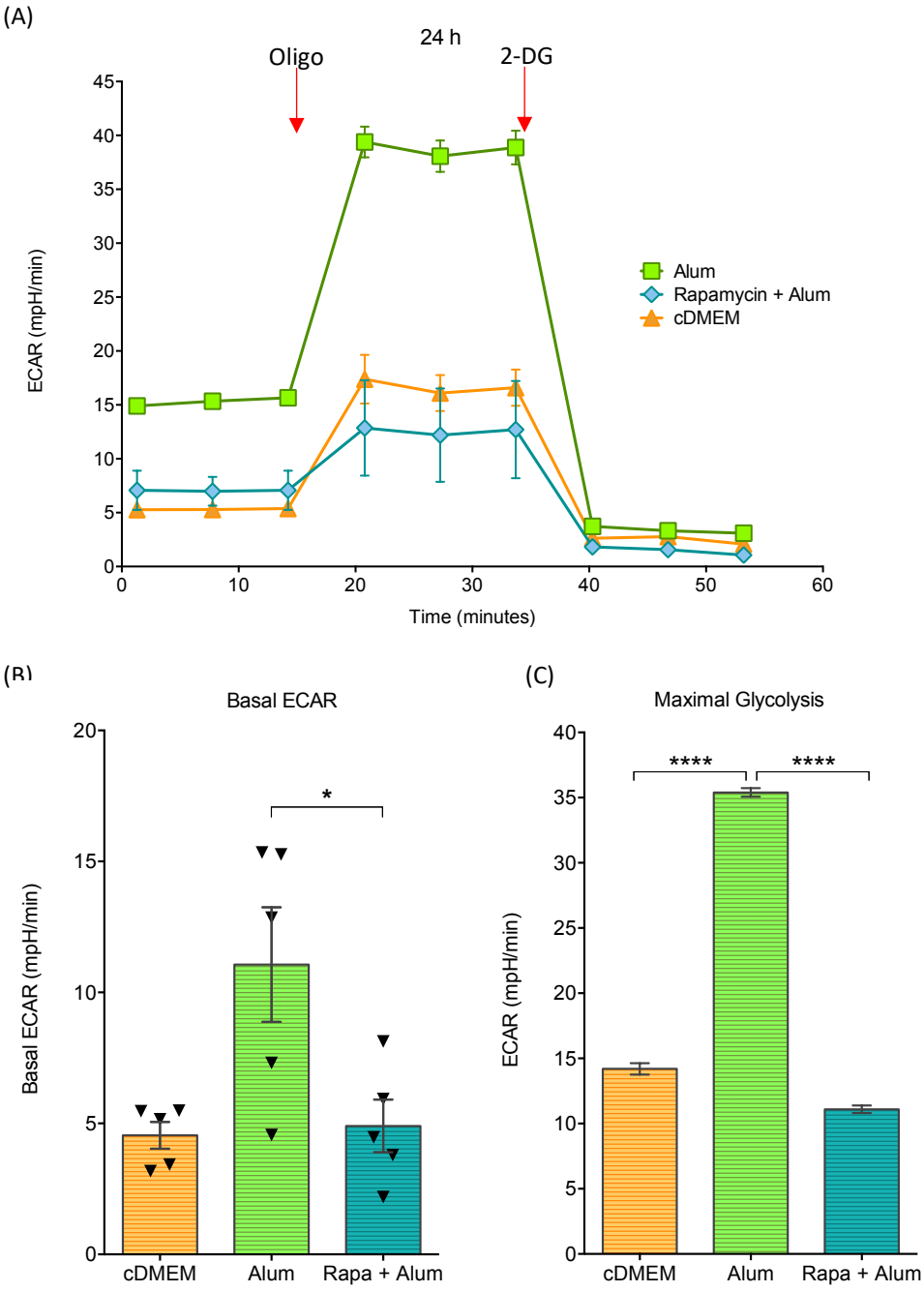
(A)
Oligo
24 h
2-DG
ECAR (mpH/min)
Time (minutes)
Alum
Rapamycin + Alum
cDMEM
(B)
Basal ECAR
Basal ECAR (mpH/min)
cDMEM
Alum
Rapa + Alum
(C)
Maximal Glycolysis
ECAR (mpH/min)
****
****
cDMEM
Alum
Rapa + Alum

(D)

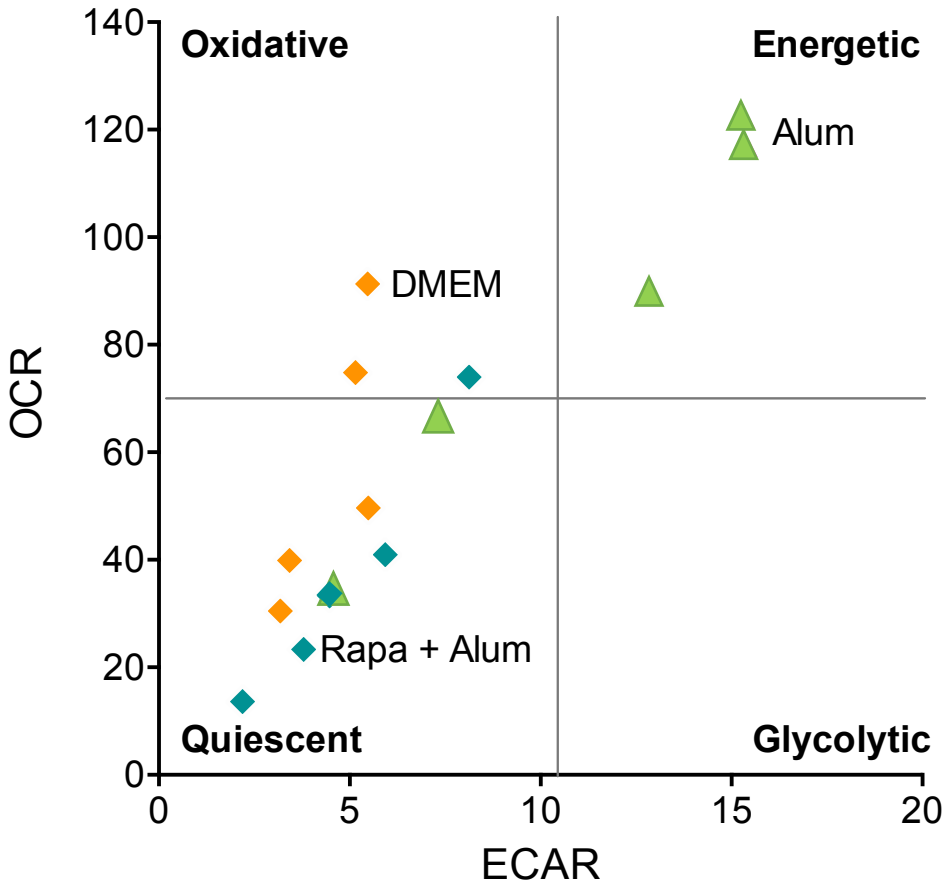

Figure 4.8 Alum increases the glycolytic capacity of BMDMs and this is inhibited by rapamycin. BMDMs were pre-incubated for one hour with cDMEM or rapamycin (1 nM) and stimulated for 24 h with cDMEM or alum (10 μg/mL) in Seahorse XF96 well plates at a seeding density of 150,000 cells/well. Seahorse extracellular flux assay was carried out. For ECAR readings, macrophages were treated sequentially with Oligomycin (1 mM) and 2-DG (25 mM). Representative ECAR trace (A), basal ECAR with pooled data (B) and representative maximal glycolysis (C) Pooled data are mean ± SEM of 5 mice from 3 independent experiments, The rates of ECAR were compared with the rates of OCR for un-stimulated, alum-stimulated and rapamycin + alum stimulated and plotted on an energy map (D). *p<0.05 alum- vs alum + rapamycin-stimulated cells by one-way ANOVA with Dunnett post-test. Maximal glycolysis results are mean ± SD and are representative of 3 independent experiments, ****p<0.001 by one-way ANOVA with Dunnett post-test.

4.4.8 Alum-dependent survival of BMDMs is markedly reduced by rapamycin

Results from Chapter 3 have shown changes in the abundance and morphology of macrophages trained with alum. Consequently, BMDMs were routinely visualised by phase contrast microscopy during the training protocol when rapamycin (1 nM) was given to cells prior to stimulation with cDMEM or alum (10 μg/mL). As shown previously, alum stimulation caused changes in the abundance and morphology of BMDMs when compared with media-stimulated cells on day 2 of the training protocol and this was unchanged by the addition of rapamycin Figure 4.9(A). However, when cells treated with alum were pre-incubated with rapamycin there was a considerable difference in the number and morphology of cells present. Cells pre-treated with rapamycin were less abundant and slightly smaller than alum-stimulated cells that were pre-treated with medium Figure 4.9(B). This observation suggests that mTOR activation is involved in imparting the characteristic morphology and enhanced survival capacity of alum-trained macrophages.

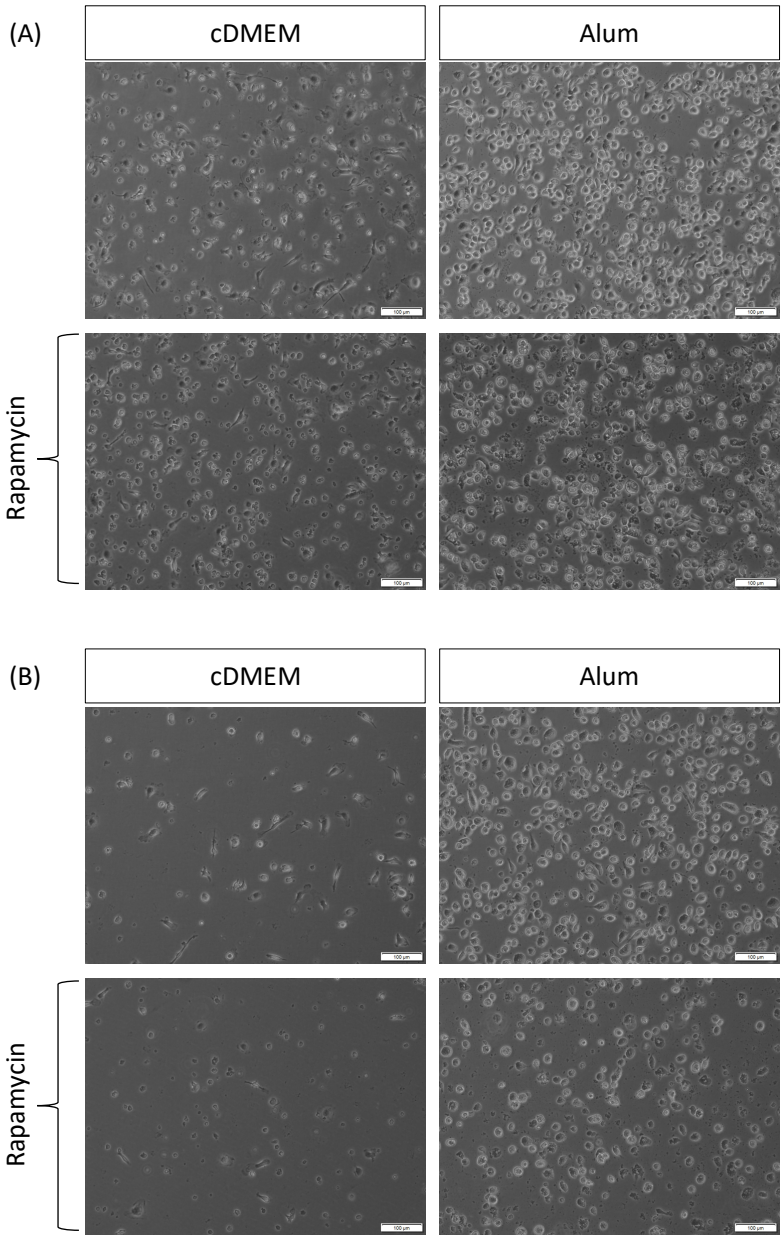

Figure 4.9 The survival of alum-trained BMDMs is markedly reduced by rapamycin. BMDMs were pre-incubated with cDMEM or rapamycin (1 nM) for 1 h prior to stimulation with cDMEM or alum (10 μg/mL) for 24 h before cells were rested for 5 days. Phase contrast images were captured on day 2 (A) and day 5 (B) after initial stimulation. Representative images shown from 3 independent experiments with 2 mice/experiment.

4.4.9 Alum rapidly induces mTORC1 activation in BMDMs

As the effects of alum on BMDMs is inhibited by rapamycin it is reasonable to assume a strong role for mTORC1 activation by this adjuvant. However, mTORC1 activation requires protein expression analysis to validate a role for this protein complex. mTORC1 activity can be assessed by analysing phosphorylation of the mTORC1 substrate S6 kinase (p70S6K) and the phosphorylation of its downstream substrate S6 ribosomal protein (pS6).

Consequently, a time-course experiment was performed whereby BMDMs were stimulated with alum for 15-, 30-, 60- and 180-minute intervals and lysed for protein extraction. BMDMs stimulated with alum were compared to un-stimulated cells and the mTOR positive control PMA/Ionomycin.

Western blot analysis of macrophages stimulated with alum show significantly enhanced pS6 compared to untreated cells only 15 minutes after stimulation with alum, the expression of which is retained at 30 minutes and begins to decrease after 60 mins. p70S6K displays slightly enhanced expression at 15 mins, however the protein expression signal was less pronounced for this western blot.

(A)

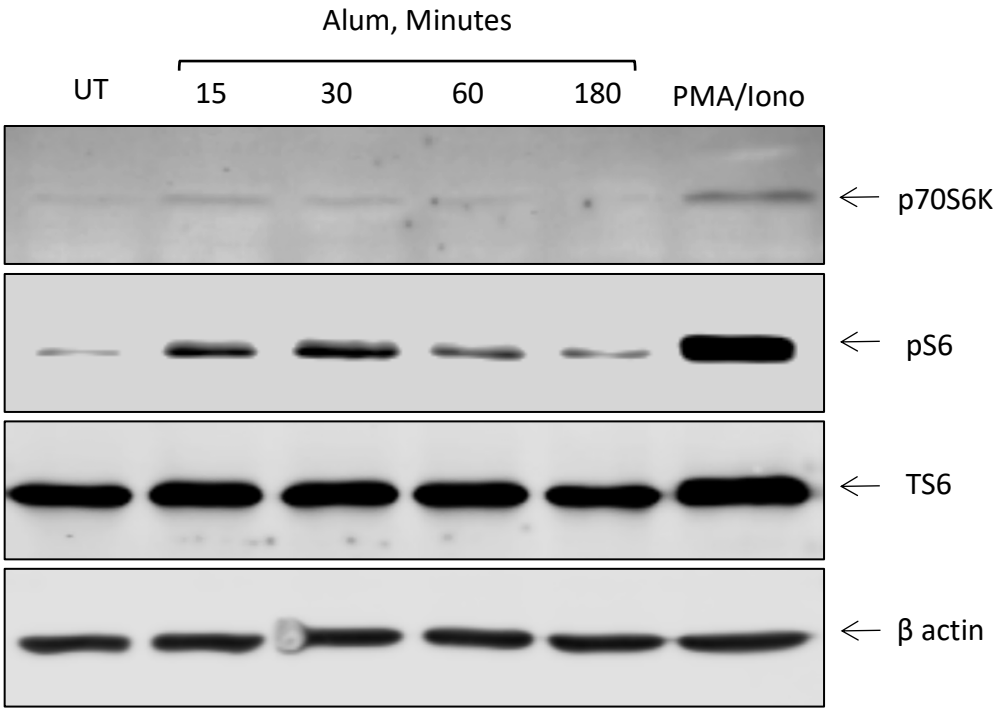

Figure 4.10 Alum upregulates expression of mTOR targets p70S6K and pS6 BMDMs were untreated (UT), stimulated with alum (10 μg/mL) for 15, 30, 60, 180 minutes, or stimulated with PMA(50 ng/mL) + Ionomycin (1 ug/mL) for 60 minutes and subsequently lysed to evaluate protein expression. mTORC1 targets p70S6K and pS6 were assessed by western blot analysis. TS6K and β-actin were used as loading controls. Results are from one mouse and are representative of 2 independent experiments.

4.4.9 Alum upregulates expression of *Myc* and *Bcl2* in an mTOR dependent manner

mTOR is known to target several downstream genes involved in cell growth and proliferation via the regulation of protein synthesis. The data point to mTOR activation by alum and a role for this pathway in imparting the characteristic metabolic and inflammatory profile of alum-stimulated cells. The next step was to assess if alum could also upregulate expression of genes that are associated with mTOR activation. BMDMs were pre-incubated with cDMEM or rapamycin (1 nM) for 1 h and then stimulated with cDMEM or alum (10 μg/mL). After 30 mins of stimulation, cells were lysed and RNA was isolated. Following normalisation of gene expression against the internal reference gene β-actin, real-time PCR revealed that there is a trend towards alum enhancing fold increase expression of *Myc* Figure 4.11(A) and *Bcl2* Figure 4.11(B). These effects were reduced by pre-treatment with rapamycin. The increased expression of genes associated with the mTOR pathway further supports the role of mTOR activation by alum in BMDMs.

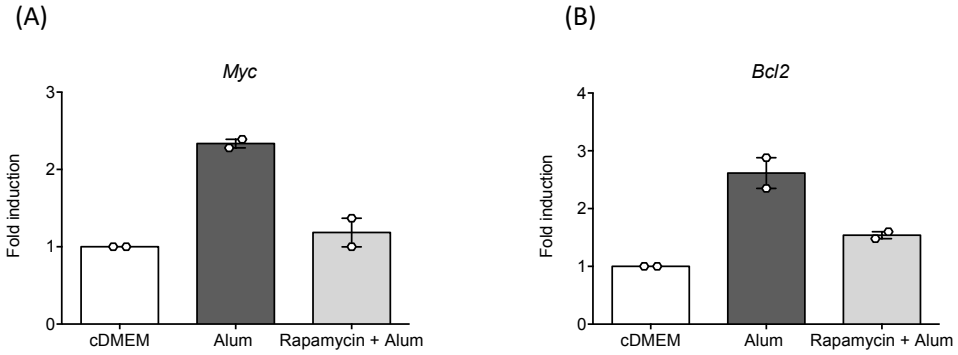

Figure 4.11 Alum upregulates expression of mTOR gene targets *Myc* and *Bcl2* BMDMs were pre-incubated with cDMEM or rapamycin (1 nM) for 1 h prior to stimulation with alum (10 μg/mL). Cells were lysed 30 mins later for RNA. Expression of (A) *Myc* and (B) *Bcl2* was evaluated by qRT-PCR relative to cells cultured in medium, following normalisation to the endogenous control *Actb.* Results are mean+/-error of 2 female mice.

4.5 Discussion

The NanoString panel revealed an anti-inflammatory gene expression profile in alum-trained macrophages which included significant upregulation of the IL-1 receptor antagonist, *il-1rn.* The IL-1Ra protein was also strongly enhanced by alum priming following BCG infection. Alum has not been previously shown to induce production of IL-1Ra by macrophages so it was important to pursue this observation in detail. In fact, incubation of macrophages with alum alone did not induce detectable secretion of any other cytokine tested. This correlates with previous studies on enhanced secretion of IL-1α [172] , IL-1β[173] and IL-10[141] by alum where co-stimulation with LPS is required. Enhanced secretion of IL-1Ra was detectable after 24 h of exposure to alum and at the end of the training protocol and was further elevated in response to re-stimulation with LPS on day 6. As we have previously demonstrated enhanced secretion of another potent anti-inflammatory cytokine, IL-10, this result supports the hypothesis that alum induces a pro-resolution response in macrophages. Enhanced secretion of IL-10 and IL-1Ra has been shown to be associated with an M2 or M2-like macrophage repertoire which is frequently found during containment of parasitic infections and importantly promotes tissue remodelling[174]. Resolution of inflammation is a highly energetic process which requires efficient metabolic rewiring to fuel phagocytosis, proliferation and survival[133]. Accordingly, the metabolic phenotype of alum-trained BMDMs was assessed by the SeaHorse extracellular flux assay which measures oxygen consumption rate (OCR) and extracellular acidification rate (ECAR). We find alum trained BMDMs to be highly energetic through enhanced oxygen consumption and glycolytic capacity compared to the well-characterised innate immune training stimulus, β-glucan, which displayed a more oxidative phenotype. An important consideration in the metabolic training effects of β-glucan is the particular source of this polysaccharide which can be isolated from the cell walls of several organisms including bacteria, fungi, yeast and some cereals. The different metabolic response of β-glucan trained BMDMs in our model compared to other studies may be due to the variation in the sourcing of glucans. M1-polarized macrophages require an increase in their glycolytic capacity in order to activate microbicidal responses and rapidly release pro-inflammatory cytokines. On the other hand, M2 cells possess an intact TCA cycle to provide necessary substrates for the ETC complexes[89]. This dependency on oxidative phosphorylation in M2-

like macrophages facilitates the sustained energy demands during tissue remodelling and repair through enhanced proliferation and survival[175]. Although ATP production is reduced, glycolysis is also advantageous during proliferation due to the generation of metabolic precursors required for biosynthetic pathways[176]. The immunometabolic profile of macrophages trained by alum which encompasses enhanced respiratory and glycolytic capacity may support survival and proliferation induced by alum (Figure 4.2) compared to un-trained or β-glucan-trained cells in addition to the amplified anti-inflammatory cytokine profile observed.

Overall, the extracellular flux assay suggests a metabolically anergic profile in un-trained cells which may be due to decreased viability after the significant period in culture without a stimulatory signal. In contrast the trained macrophage data demonstrate the high metabolic demands required by these cells, particularly innate training by alum.

The extracellular flux assays performed on trained BMDMs suggest that the addition of FCCP did not increase the OCR value above basal rates of respiration. There are some limitations when using this inhibitor as high FCCP concentrations (in comparison to the number of viable cells in a well) can suppress respiration due to toxicity[177]. Therefore a titration for this inhibitor should be carried out for additional innate training experiments in which cell viability may be reduced due to long term *in vitro* culture, particularly for un-trained control cells.

Metabolic reprogramming of macrophages through inhibition of succinate oxidation by dimethyl malonate has recently been shown to promote anti-inflammatory responses by upregulating IL-1Ra and IL-10[171]. The PI3K pathway has been implicated in the production of IL-1Ra by macrophages in response to LPS, as inhibition of PI3K activity decreases the production of this anti-inflammatory cytokine and enhances the production of IL-1β[178]. Furthermore, inhibition of mTOR, which lies downstream of PI3K, results in enhanced pro-inflammatory cytokine production via NFκB in PTEN-deficient cancer cells through dissociation of Raptor from mTOR[179]. Interestingly, TLR-activated DCs have increased IL-12 and reduced IL-10/type I interferon expression when mTOR is blocked by rapamycin resulting in their enhanced T cell stimulatory capacity[122]. This may shed some light on the downstream effects of alum during vaccination as our lab have previously shown that induction of IL-10 by alum suppresses Th1 responses and may explain the inability of alum to induce protective Th1 immunity[141].

In order to investigate the potential role of the PI3K/mTOR pathway in alum-induced IL-1Ra secretion, BMDMs were pre-incubated with the class I PI3K inhibitor, ZSTK474, significantly reducing the secretion of IL-1Ra by BMDMs stimulated with alum, demonstrating an important role for this pathway. An important consideration for this result is alternate activation of mTOR in addition to the PI3K/Akt pathway. Phosphorylation of S6K can occur independently of Akt activity and has been shown in cells from both mammals and Drosophila[180]. Interestingly, amino acids alone can activate mTORC1 in the absence of growth factors and occurs independent of TSC-RHEB[181]. Amino acids such as Leucine, Glycine and Arginine are sufficient to activate mTOR when growth factors are unavailable, but growth factors alone cannot activate this pathway when amino acids are limiting[109]. Furthermore, mTORC1 is inhibited through AMP-activated protein kinase activation of TSC during nutrient deficiency[182].

The mTOR targeting antibiotic, rapamycin, was also found to significantly reduce the secretion of IL-1Ra by BMDMs stimulated with alum. In the model of training, rapamycin also reduced the secretion of IL-1Ra in BMDMs 7 days after stimulation with alum.

Finally, the time course of IL-1Ra secretion by alum-trained cells revealed progressive accumulation of this cytokine in supernatants over the course of 14 days after initial exposure to alum. The secretion of IL-1Ra was significantly amplified by re-stimulation of trained cells with LPS on day 6. Pre-treatment of macrophages with rapamycin reduced this effect over the 14-day period even when alum-trained cells were subsequently re-stimulated with LPS.

It was shown in Chapter 3 that training of human monocytes with alum primed the cells for enhanced secretion of IL-10 upon subsequent re-stimulation. Enhanced secretion of IL-1Ra in the murine model of training prompted us to revisit the human model of training and investigate the role of the mTOR pathway in monocytes. Secretion of IL-1Ra was significantly enhanced in alum-trained monocytes which was further amplified when trained monocytes were re-stimulated with Heat-killed *Mtb* or LPS. Secretion of IL-1Ra was reduced by inhibition of mTOR in alum-trained monocytes. Pre-treatment of cells with rapamycin blocked the alum induced enhancement in IL-1Ra secretion that was seen when cells when re-stimulated with Heat-killed *Mtb* or LPS. This result requires further investigation as it is representative of one blood donor and as highlighted in the previous chapter, human monocytes display highly variable responses to alum. However, this

supports the murine data and is an interesting observation in the context of vaccination as mTOR-dependent IL-1Ra secretion by alum may limit excessive tissue damage at the site of injection through competitive inhibition of IL-1 signalling[159].

Macrophages can adopt different functional states depending on the context in which they are activated. The mTOR pathway was shown to be involved in the anti-inflammatory profile of cells stimulated with alum after 24 h and retained by trained macrophages up to 14 days after initial stimulation. Several studies have demonstrated the involvement of metabolic shifts in the regulation of the effector functions of innate immune cells in specific contexts[122]. mTOR is a major regulator of macrophage metabolism and activation and consequently the role of this pathway in the metabolic effects of alum-stimulated BMDMs was assessed by Seahorse. Alum significantly enhanced the oxidative and glycolytic capacity of BMDMs after just 24 h compared to un-stimulated cells. Pharmacological inhibition of mTOR by rapamycin reversed this effect, restoring the metabolic profile of alum-stimulated cells to that of un-stimulated cells. Furthermore, phase contrast images on day 5 after stimulation showed increased cell numbers indicative of enhanced cell proliferation and/or survival in alum-trained cells compared to un-stimulated cells. This was partially lost when mTOR was inhibited by rapamycin before training with alum. As previously mentioned mTOR activation is an anabolic pathway resulting in enhanced biogenesis of macromolecules including nucleotides, proteins and lipids to aid cell growth and proliferation[136]. Interestingly, Thompson *et al* found that rapamycin diminished the Akt-mediated increase in cell size , mitochondrial membrane potential and cell survival in a murine prolymphocytic cell line, FL5.12, stimulated with doxycycline[183].

Located upstream of mTOR, Akt is involved in growth factor signal transduction cascades that regulate cell growth and survival[109]. Increased surface expression of nutrient transporters through Akt allows increases in cell size and survival[183].

In Chapter 3 we showed an increase in the size of alum-trained macrophages as well as enhanced survival and abundance compared to un-trained cells. We have also shown that this is partially dependent on mTOR activation as inhibition of this regulatory protein impacted on the alum-dependent metabolic rewiring of macrophages which may also influence the size and survival capacity of these cells. Whether alum induces mTOR dependent proliferation or enhanced cell survival requires further exploration. It is likely that due to the activation of mTOR and downstream genes such as *Bcl2* and *Myc*, a

combination of enhanced proliferation and prosurvival is occurring in these cells under the appropriate conditions for growth factor and nutrient availability.

Western blot analysis further supports a role for mTOR activation by alum. The mTORC1 target pS6 was upregulated as early as 15 minutes after exposure to alum. However, it is important to note that S6 can be phosphorylated downstream of the MAPK/ERK pathway through the alternative S6 kinase, p90-ribosomal S6 kinase (p90RSK)[184] in addition to PI3K-dependent and independent mTOR activation[185].

A consideration for future experiments is to include rapamycin as an additional control to validate the role of mTOR activation in the phosphorylation of S6. Other phosphorylation targets of mTOR should also be investigated such as 4-EBP1. Finally, phosphorylation of S6 can also be analysed by flow cytometry to further validate this finding.

Having shown the activation of mTOR through p-S6 expression, the downstream genes involved in this metabolic pathway were analysed by real-time PCR. Alum upregulated the expression of *Bcl2* and *Myc* 1 h after stimulation. This effect was restored to the expression levels of control cells when BMDMs were pre-treated with rapamycin. In Chapter 3, data presented on NanoString analysis revealed upregulation of *Bcl2l1* (BCL2 Like 1) in alum-trained cells. The Bcl-2 family includes pro- and anti-apoptotic members, the latter of which includes Bcl-2 itself. Expression of these proteins is regulated by mTOR via the upstream effectors PI3K and AKT[186]. Importantly, the ratio of pro- to anti-apoptotic Bcl-2 family members determines, to some extent, the survival outcome of the cell. AKT upregulates the transcription of anti-apoptotic Bcl-2 and inactivates the pro-apoptotic member, Bad, by mTOR-dependent phosphorylation to promote cell survival[187]. The survival and proliferation of the cell is highly dependent on the availability on nutrients, fatty acids and other vital metabolites[188]. It is therefore logical that the nutrient-sensing PI3K/AKT/mTOR pathway is involved in regulating the expression of *Bcl2* and other survival/proliferation genes. As previously mentioned, the anabolic processes of cell growth, proliferation and survival are energetically demanding and require efficient metabolic flux to fuel the necessary pathways required for macromolecule biosynthesis[188]. Alum-stimulated macrophages displayed enhanced oxygen consumption and glycolytic capacity. One of the main functions of the mTOR pathway is to stimulate enhanced protein synthesis following innate cell activation[122]. Central to this metabolic pathway is the induction of anabolic responses through the transcription factor, c-Myc[134]. c-Myc induces the synthesis of nucleic

acids, proteins and lipids via upregulation of both glycolytic gene expression and mitochondrial respiration[189].

In order to fully validate the mTOR-dependent gene expression of *Myc* following stimulation with alum, western blot analysis of protein expression should be carried out. c-Myc expression is generally controlled post-transcriptionally. For example, mRNA expression of c-Myc in HSCs is comparable to committed progenitor cells and the transition from HSC renewal towards differentiation is heavily reliant on this gene. However, while mRNA expression is equivalent, the protein expression in reduced in HSCs and increases gradually during progenitor cell differentiation[190]. Bcl-2 is also regulated post-transcriptionally[191] and therefore should also be validated by western blot analysis.

In Chapter 3, it was shown that alum-trained macrophages enhanced expression of several genes involved in the anti-oxidant response pathway including *Nfe2l2*, *Maff* and *Mafk*. Alum was also found to induce mitochondrial ROS production 1 h after stimulation (supplementary figure 1). The Nrf2 master transcription factor recognises and binds antioxidant response elements (AREs) on gene promoters in response to cellular stress such as excessive ROS production[192]. Moderate levels of ROS can be beneficial during proliferation and as a means of cellular defence, however excessive levels can lead to cellular damage and the induction of cell death[193]. Interestingly, Nrf2 antioxidant signalling was also found to attenuate NFκB-mediated inflammation in a colitis-induced colorectal cancer model[194].

Cells have evolved several ways to limit excessive production of ROS, intracellular metabolites and inflammatory mediators. These pathways are tightly regulated and can allow cellular survival and proliferation during damage-associated inflammation by enhancing tissue remodelling and limiting inflammation. A study by Piantadosi *et al* found that during sepsis IL-10 and IL-1Ra were associated with preservation of mitochondrial function and survival by enhancing mitochondrial biogenesis. Both cytokines were shown to limit NFκB-dependent IL-1β production during disease via heme oxygenase-1 activation of Nrf-2. In this study, increased nuclear accumulation of Nrf2 was also associated with Bcl2 expression[195].

Chapter 5 General Discussion

In addition to clean water and general sanitation, the introduction of protective vaccines against a multitude of infectious diseases is the most significant medical intervention in the last century. It was recently estimated that since 1924, vaccines have prevented over 103 million cases of childhood diseases in the US alone with the WHO reporting that vaccination prevents 2.5 million deaths each year[196]. The first vaccines introduced at a time when there was only a rudimentary understanding of the immune system, paved the way for the development of the class of vaccines used in immunisation schemes across the globe today and for a new generation of rationally designed vaccines under development.

Many of these would not be as successful without the essential addition of adjuvants due to the fact that most non-live vaccines possess relatively poor immunogenicity. Over the past 90 years alum has been the most widely used vaccine adjuvant and largely provides protection through the induction of antibody-mediated immunity[152]. The mechanism of action of alum has not been fully resolved, in particular, its effects on innate cells.

The classical view of innate immunity until recently was that it lacks the ability to retain immunological memory, unlike its adaptive counterpart. This dogma has recently been challenged by several research groups that have postulated the existence of a type of innate memory that results from innate training whereby mammals are protected from secondary infections in a manner independent of T and B cells. This cross-protection is believed to be orchestrated by innate cells such as monocytes and macrophages. Innate memory to infection has been well documented in plants and is the subject of intensive investigation in invertebrate models. Of note, neither plants nor invertebrates possess an adaptive immune system, which is classically accepted as the sole means of conferring protection against reinfection in vertebrates[197]. The research findings of this project present some of the potential ways in which alum can induce trained immunity in human monocytes and murine macrophages.

The observation that alum increases the induction of the immunomodulatory cytokine, IL-10, when co-incubated with LPS has previously been shown in the Lavelle lab for both human monocytes and murine macrophages[141]. We have recapitulated this result in the *in vitro* model of training for both cell types to show that alum can train innate cells to produce more IL-10 upon re-stimulation with LPS one week later. Monocytes isolated from

healthy blood donors display a highly variable response to alum training with 50% of donors displaying increased IL-10. However as these monocytes were isolated from human blood donors obtained through the Irish Blood Transfusion Services, we were unable to acquire important stratifying information such as age, sex and vaccination history.

In addition to the enhanced secretion of IL-10 by murine BMDMs trained with alum, distinct morphological changes in these cells were observed during phase contrast microscopy imaging throughout the *in vitro* training period. Alum-trained BMDMs were found to be a highly abundant population of rounded macrophages that are larger and more granular, as confirmed by FACS analysis.

Data generated following the injection of alum supported the microscopy data showing enhanced proliferation and/or survival of these trained macrophages when bone marrow from mice injected intraperitoneally with alum 7 days earlier yielded more bone marrow cells compared to PBS-injected mice. When these cells were re-plated on the last day of differentiation, BMDMs isolated from mice injected with alum were 2-3 times more abundant than those from mice immunised with PBS for both time points.

To characterise the functional effects of these findings, alum-trained BMDMs were infected with live BCG to assess their bacterial killing ability through analysis of CFU counts and cytokine secretion during the infection assay. Alum training did not affect bacterial uptake, however CFU counts indicate that these macrophages may have a compromised killing ability once the bacteria are internalised. The enhanced secretion of IL-10 in the initial training experiments was reproduced in the BCG infection model as well as a second anti-inflammatory cytokine, IL-1Ra. This natural inhibitor of IL-1 signalling was dramatically upregulated in alum-trained macrophages in this model. This cytokine was also highly upregulated in alum-trained BMDMs characterised by the NanoString Inflammation panel. Remarkably, NanoString also revealed global downregulation of pro-inflammatory genes in alum-trained BMDMs compared to un-trained cells. Most of the literature on alum has presented this adjuvant as an inducer of inflammation through necrosis, DAMP release[160], IL1-β induction[161] and activation of DCs to polarise Th2 responses, inducing protective humoral immunity during vaccination[162]. In addition to IL-1Ra, a small group of upregulated genes was observed following training with alum including other anti-inflammatory mediators and several targets involved in cell proliferation and survival.

The recent surge in immunometabolism research prompted us to investigate the potential metabolic rewiring of macrophages underlying the anti-inflammatory effects of macrophages stimulated with alum. Innate immune training has been found to be heavily reliant on metabolic reprogramming to facilitate specific functional requirements of cells in a given context. Alum-trained macrophages were found to exhibit enhanced oxygen consumption and glycolytic capacity compared to β-glucan. β-glucan-trained cells have also been shown to have enhanced metabolic machinery and favour a switch from oxidative phosphorylation to glycolysis according to several papers[198]. Macrophages that have been polarised towards the M1 end of the hypothetical polarisation continuum tend to have an increased glycolytic capacity to fuel rapid responses such as enhanced secretion of inflammatory mediators during infection[88]. On the other end of the scale the more M2-like cells require an intact TCA cycle to provide substrates for ETC complexes which fuel oxidative phosphorylation[89]. This facilitates the sustained energy requirements of cells during the resolution phase of inflammation, particularly through enhanced proliferation and survival. A key regulator in the control of cellular growth and proliferation is the nutrient and growth factor sensor, mTOR[109]. The PI3K/mTOR pathway is fundamental in the biosynthesis of macromolecules so it was unsurprising that inhibition of mTOR by rapamycin reversed the metabolic profile of alum-stimulated BMDMs to that of un-stimulated cells. Inhibition of both PI3K and mTOR also significantly reduced the secretion of IL-1Ra and the pro-survival effects of alum training as seen by phase contrast imaging. Furthermore, mTOR inhibition has been shown to enhance pro-inflammatory cytokine production via NFκB in certain cancers[199] while DCs have enhanced IL-12 and reduced IL-10/type I interferons when pre-treated with rapamycin, causing enhanced T cell responses[200]. Another study found that inhibition of mTOR in monocytes and DCs stimulated with TLR ligands enhanced differentiation of pro-inflammatory, anti-tumour Th1 cells[131].

Our findings on alum-dependent mTOR activation and subsequent enhancement of IL-1Ra secretion in macrophages are particularly exciting in the context of vaccination. As mentioned, alum is known to enhance the secretion of inflammatory mediators during vaccination, including IL-1β which is dependent on activation of the NLRP3 inflammasome[173]. However, several studies have also shown that this inflammatory response through NLRP3 is not required for enhanced IgG antibody responses which is

primarily how alum induces its adjuvanticity. McKee *et al* showed that the inflammation induced by alum *in vivo* is caspase-1-independent and that the endogenous T cell and antibody responses as well as Th2 bias were unaffected by the absence of caspase-1 or NLRP3[163]. Alum has retained its position as the most widely used vaccine adjuvant for almost a hundred years. This is primarily due to its effectiveness at driving protective humoral responses, but crucially, with the strongest safety record of any human adjuvant, the widespread use of alum is due to its robust safety profile.

After the initial adjuvant-driven immunostimulatory response following vaccination, the prevention of damage is ensured by the resolution phase of inflammation which promotes repair mechanisms for wound healing.

The process of wound healing following injury or vaccination is a multistep cascade of events and is mediated by several growth factors, cytokines and chemokines[201]. The three overlapping phases of wound healing include the inflammatory phase, the proliferative phase and finally the tissue remodelling phase[67]. Initially, inflammatory mediators such as chemokines and cytokines allow recruitment of cells to the site of injury and subsequent polarisation of these cells into functional effectors to prevent infection[202]. Production of reactive oxygen species (ROS) is part of this inflammatory phase particularly following damage to blood vessels. To circumvent the toxic effects of ROS, scavenger proteins and detoxifying enzymes are enhanced during normal wound healing[203]. This is supported by anti-oxidant response pathways such as the Nrf2 pathway which also downregulates pro-inflammatory cytokines and enhances anti-inflammatory mediators such as IL-10 and IL-1Ra[195]. Interestingly a study characterising the wound healing properties of Acemannan, a bioactive polysaccharide derived from aloe vera found that the expression of the proliferation associated antigen Ki67 was enhanced in mouse fibroblasts when treated with this polysaccharide. Furthermore activation of AKT/mTOR signalling in these cells lead to enhanced eIF4F and increased cyclin D1 translation, a marker of cell proliferation. When mTOR was inhibited by rapamycin the enhanced translation of cyclin D1 was lost[204]. Finally, constitutive activation of mTOR was found to enhance the wound healing process in mice with epithelial-specific knock down of *Pten* and *Tsc1* genes[205].

During the onset of repair, myeloid cells at the injection site such as tissue-resident macrophages and monocyte-derived macrophages recruited during the acute phase response, switch to more anti-inflammatory, M2-like effectors[206]. These anti-inflammatory

macrophages enhance healing through enhanced secretion of IL-10[202] and IL-1Ra[207] and are metabolically rewired to provide this tailored cytokine response as well as the initiation of proliferation and cell growth through mTOR-dependent macromolecular biosynthesis[208]. Based on the results in this thesis, it can be proposed that alum trains macrophages through metabolic rewiring via mTOR activation to enhance secretion of anti-inflammatory cytokines including IL-10 and IL-1Ra and provide the metabolic machinery favoured by proliferating macrophages to promote resolution and repair. In the context of vaccination, this effect may shed light on the robust safety profile of this widely used adjuvant.

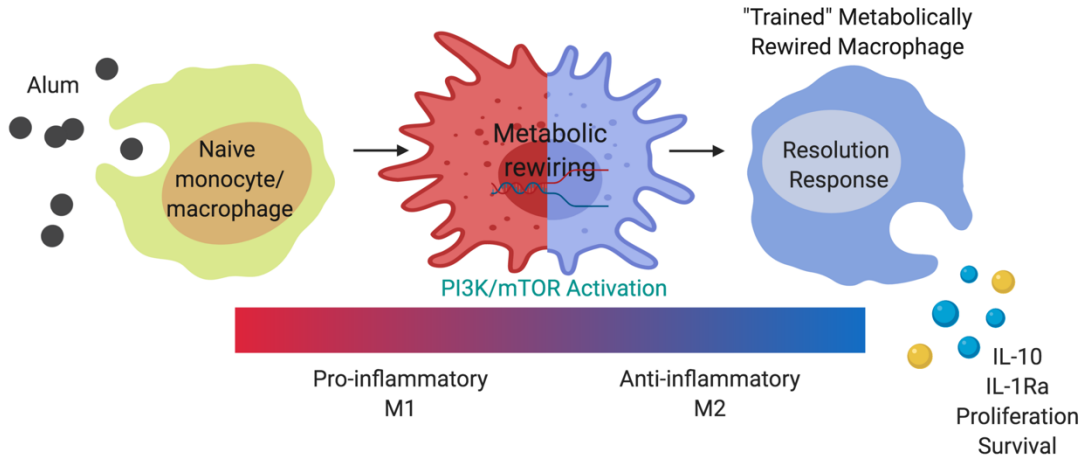

Figure 5.1 Schematic of alum trained macrophage. Naïve monocytes/macrophages exposed to alum induce activation of mTOR resulting in metabolic rewiring. Alum-trains macrophages to be highly energetic coupled with the secretion of anti-inflammatory cytokines including IL-10 and IL-1Ra and provide the metabolic machinery through enhanced glycolysis and oxidative phosphorylation favoured by proliferating macrophages to promote resolution and repair

References

1. Buchmann, K. Evolution of Innate Immunity: Clues from Invertebrates via Fish to Mammals . *Frontiers in Immunology* **5**, 459 (2014).
2. Netea, M. G. *et al.* Trained immunity: A program of innate immune memory in health and disease. *Science* **352**, 427 (2016).
3. Sánchez-Sampedro, L. *et al.* The evolution of poxvirus vaccines. *Viruses* **7**, 1726–1803 (2015).
4. Brimnes, N. Variolation, vaccination and popular resistance in early colonial south India. *Med. Hist.* **48**, 199–228 (2004).
5. Morgan, A. J. & Parker, S. Translational mini-review series on vaccines: The Edward Jenner Museum and the history of vaccination. *Clin. Exp. Immunol.* **147**, 389–394 (2007).
6. Riedel, S. Edward Jenner and the history of smallpox and vaccination. *Proc. (Bayl. Univ. Med. Cent).* **18**, 21–25 (2005).
7. Smith, K. A. Louis pasteur, the father of immunology? *Front. Immunol.* **3**, 68 (2012).
8. Horwitz, M. A., Harth, G., Dillon, B. J. & Maslesa-Galić, S. Commonly administered BCG strains including an evolutionarily early strain and evolutionarily late strains of disparate genealogy induce comparable protective immunity against tuberculosis. *Vaccine* **27**, 441–445 (2009).
9. Norrby, E. Yellow fever and Max Theiler: the only Nobel Prize for a virus vaccine. *J. Exp. Med.* **204**, 2779 LP – 2784 (2007).
10. Plotkin, S. Vaccines : past , present and future Early successes. *Nat. Med.* **11**, 5–11 (2005).
11. Coffman, R. L., Sher, A. & Seder, R. A. Vaccine adjuvants: putting innate immunity to work. *Immunity* **33**, 492–503 (2010).
12. Moyle, P. M. & Toth, I. Modern Subunit Vaccines: Development, Components, and Research Opportunities. *ChemMedChem* **8**, 360–376 (2013).
13. Awate, S., Babiuk, L. A. & Mutwiri, G. Mechanisms of action of adjuvants. *Front. Immunol.* **4**, 114 (2013).
14. Ho, N. I., Huis In 't Veld, L. G. M., Raaijmakers, T. K. & Adema, G. J. Adjuvants Enhancing Cross-Presentation by Dendritic Cells: The Key to More Effective Vaccines?

Front. Immunol. **9**, 2874 (2018).

15. Di Pasquale, A., Preiss, S., Tavares Da Silva, F. & Garçon, N. Vaccine Adjuvants: from 1920 to 2015 and Beyond. *Vaccines* **3**, 320–343 (2015).
16. Christensen, D. Vaccine adjuvants: Why and how. *Hum. Vaccin. Immunother.* **12**, 2709–2711 (2016).
17. Munks, M. W. *et al.* Aluminum adjuvants elicit fibrin-dependent extracellular traps in vivo. *Blood* **116**, 5191 LP – 5199 (2010).
18. Lee, S. & Nguyen, M. T. Recent advances of vaccine adjuvants for infectious diseases. *Immune Netw.* **15**, 51–57 (2015).
19. Wen, Y. & Shi, Y. Alum: an old dog with new tricks. *Emerg. Microbes Infect.* **5**, e25–e25 (2016).
20. Hutchison, S. *et al.* Antigen depot is not required for alum adjuvanticity. *FASEB J.* **26**, 1272–1279 (2012).
21. Maisonneuve, C., Bertholet, S., Philpott, D. J. & De Gregorio, E. Unleashing the potential of NOD- and Toll-like agonists as vaccine adjuvants. *Proc. Natl. Acad. Sci.* **111**, 12294 LP – 12299 (2014).
22. Krishnaswamy, J. K., Chu, T. & Eisenbarth, S. C. Beyond pattern recognition: NOD-like receptors in dendritic cells. *Trends Immunol.* **34**, 224–233 (2013).
23. Jo, E.-K., Kim, J. K., Shin, D.-M. & Sasakawa, C. Molecular mechanisms regulating NLRP3 inflammasome activation. *Cell. Mol. Immunol.* **13**, 148–159 (2016).
24. Li, H., Nookala, S. & Re, F. Aluminum Hydroxide Adjuvants Activate Caspase-1 and Induce IL-1β and IL-18 Release. *J. Immunol.* **178**, 5271 LP – 5276 (2007).
25. Martinon, F., Pétrilli, V., Mayor, A., Tardivel, A. & Tschopp, J. Gout-associated uric acid crystals activate the NALP3 inflammasome. *Nature* **440**, 237–241 (2006).
26. Kingsbury, S. R., Conaghan, P. G. & McDermott, M. F. The role of the NLRP3 inflammasome in gout. *J. Inflamm. Res.* **4**, 39–49 (2011).
27. Marrack, P., McKee, A. S. & Munks, M. W. Towards an understanding of the adjuvant action of aluminium. *Nat. Rev. Immunol.* **9**, 287–293 (2009).
28. Oleszycka, E. *et al.* IL-1α and inflammasome-independent IL-1β promote neutrophil infiltration following alum vaccination. *FEBS J.* **283**, 9–24 (2016).
29. Kuroda, E., Coban, C. & Ishii, K. J. Particulate adjuvant and innate immunity: past achievements, present findings, and future prospects. *Int. Rev. Immunol.* **32**, 209–

220 (2013).

30. Flach, T. L. *et al.* Alum interaction with dendritic cell membrane lipids is essential for its adjuvanticity. *Nat. Med.* **17**, 479–487 (2011).
31. Mócsai, A., Ruland, J. & Tybulewicz, V. L. J. The SYK tyrosine kinase: a crucial player in diverse biological functions. *Nat. Rev. Immunol.* **10**, 387–402 (2010).
32. Ghimire, T. R. The mechanisms of action of vaccines containing aluminum adjuvants: an in vitro vs in vivo paradigm. *Springerplus* **4**, 181 (2015).
33. Meeusen, E. N. T., Walker, J., Peters, A., Pastoret, P.-P. & Jungersen, G. Current Status of Veterinary Vaccines. *Clin. Microbiol. Rev.* **20**, 489 LP – 510 (2007).
34. Goodridge, H. S. *et al.* Harnessing the beneficial heterologous effects of vaccination. *Nat. Rev. Immunol.* **16**, 392–400 (2016).
35. Zwerling, A. *et al.* The BCG World Atlas: A Database of Global BCG Vaccination Policies and Practices. *PLOS Med.* **8**, e1001012 (2011).
36. Askeland, E. J., Newton, M. R., O'Donnell, M. A. & Luo, Y. Bladder Cancer Immunotherapy: BCG and Beyond. *Adv. Urol.* **2012**, 181987 (2012).
37. Netea, M. G. & van Crevel, R. BCG-induced protection: Effects on innate immune memory. *Semin. Immunol.* **26**, 512–517 (2014).
38. Sankoh, O. *et al.* The non-specific effects of vaccines and other childhood interventions: the contribution of INDEPTH Health and Demographic Surveillance Systems. *Int. J. Epidemiol.* **43**, 645–653 (2014).
39. Benn, C. S., Netea, M. G., Selin, L. K. & Aaby, P. A small jab – a big effect: nonspecific immunomodulation by vaccines. *Trends Immunol.* **34**, 431–439 (2013).
40. Fotso, J.-C., Ezeh, A. C., Madise, N. J. & Ciera, J. Progress towards the child mortality millennium development goal in urban sub-Saharan Africa: the dynamics of population growth, immunization, and access to clean water. *BMC Public Health* **7**, 218 (2007).
41. Aaby, P., Mogensen, S. W., Rodrigues, A. & Benn, C. S. Evidence of Increase in Mortality After the Introduction of Diphtheria–Tetanus–Pertussis Vaccine to Children Aged 6–35 Months in Guinea-Bissau: A Time for Reflection? *Front. Public Heal.* **6**, 79 (2018).
42. Uthayakumar, D. *et al.* Non-specific Effects of Vaccines Illustrated Through the BCG Example: From Observations to Demonstrations. *Front. Immunol.* **9**, 2869 (2018).

43. Kleinnijenhuis, J. *et al.* Bacille Calmette-Guérin induces NOD2-dependent nonspecific protection from reinfection via epigenetic reprogramming of monocytes. *Proc. Natl. Acad. Sci.* **109**, 17537 LP – 17542 (2012).
44. Rusek, P., Wala, M., Druszczyńska, M. & Fol, M. Infectious Agents as Stimuli of Trained Innate Immunity. *Int. J. Mol. Sci.* **19**, 456 (2018).
45. Quintin, J. *et al.* Candida albicans infection affords protection against reinfection via functional reprogramming of monocytes. *Cell Host Microbe* **12**, 223–232 (2012).
46. Crișan, T. O., Netea, M. G. & Joosten, L. A. B. Innate immune memory: Implications for host responses to damage-associated molecular patterns. *Eur. J. Immunol.* **46**, 817–828 (2016).
47. Arts, R. J. W., Joosten, L. A. B. & Netea, M. G. The potential role of trained immunity in autoimmune and autoinflammatory disorders. *Frontiers in Immunology* **9**, (2018).
48. Buffen, K. *et al.* Autophagy Controls BCG-Induced Trained Immunity and the Response to Intravesical BCG Therapy for Bladder Cancer. *PLoS Pathog.* **10**, (2014).
49. Yáñez, A. *et al.* Detection of a TLR2 agonist by hematopoietic stem and progenitor cells impacts the function of the macrophages they produce. *Eur. J. Immunol.* **43**, 2114–2125 (2013).
50. Ng, R. L. X. *et al.* Altered Immunity and Dendritic Cell Activity in the Periphery of Mice after Long-Term Engraftment with Bone Marrow from Ultraviolet-Irradiated Mice. *J. Immunol.* **190**, 5471 LP – 5484 (2013).
51. Kaufmann, E. *et al.* BCG Educates Hematopoietic Stem Cells to Generate Protective Innate Immunity against Tuberculosis. *Cell* **172**, 176-190.e19 (2018).
52. Khosravi, A. *et al.* Gut microbiota promote hematopoiesis to control bacterial infection. *Cell Host Microbe* **15**, 374–381 (2014).
53. Nastasi, C. *et al.* The effect of short-chain fatty acids on human monocyte-derived dendritic cells. *Sci. Rep.* **5**, 16148 (2015).
54. Clarke, T. B. *et al.* Recognition of peptidoglycan from the microbiota by Nod1 enhances systemic innate immunity. *Nat. Med.* **16**, 228–231 (2010).
55. Boraschi, D. & Italiani, P. Innate Immune Memory: Time for Adopting a Correct Terminology. *Front. Immunol.* **9**, 799 (2018).
56. McDonald, D. R. & Levy, O. 3 - Innate Immunity. in (eds. Rich, R. R. et al.) 39-53.e1 (Content Repository Only!, 2019). doi:https://doi.org/10.1016/B978-0-7020-6896-

6.00003-X

57. Chaplin, D. D. Overview of the immune response. *J. Allergy Clin. Immunol.* **125**, S3–S23 (2010).

58. Mogensen, T. H. Pathogen recognition and inflammatory signaling in innate immune defenses. *Clin. Microbiol. Rev.* **22**, 240–273 (2009).

59. Amarante-Mendes, G. P. *et al.* Pattern Recognition Receptors and the Host Cell Death Molecular Machinery. *Front. Immunol.* **9**, 2379 (2018).

60. Takeuchi, O. & Akira, S. Pattern Recognition Receptors and Inflammation. *Cell* **140**, 805–820 (2010).

61. Kawasaki, T. & Kawai, T. Toll-like receptor signaling pathways. *Front. Immunol.* **5**, 461 (2014).

62. Chaturvedi, A. & Pierce, S. K. How location governs toll-like receptor signaling. *Traffic* **10**, 621–628 (2009).

63. Piccinini, A. M. & Midwood, K. S. DAMPening inflammation by modulating TLR signalling. *Mediators Inflamm.* **2010**, 672395 (2010).

64. Kawai, T. & Akira, S. Signaling to NF-κB by Toll-like receptors. *Trends Mol. Med.* **13**, 460–469 (2007).

65. O'Shea, J. J. & Murray, P. J. Cytokine Signaling Modules in Inflammatory Responses. *Immunity* **28**, 477–487 (2008).

66. Wang, X. & Liu, Y. Regulation of innate immune response by MAP kinase phosphatase-1. *Cell. Signal.* **19**, 1372–1382 (2007).

67. Landén, N. X., Li, D. & Ståhle, M. Transition from inflammation to proliferation: a critical step during wound healing. *Cell. Mol. Life Sci.* **73**, 3861–3885 (2016).

68. Fukao, T. & Koyasu, S. PI3K and negative regulation of TLR signaling. *Trends Immunol.* **24**, 358–363 (2003).

69. Butcher, S. K., O'Carroll, C. E., Wells, C. A. & Carmody, R. J. Toll-Like Receptors Drive Specific Patterns of Tolerance and Training on Restimulation of Macrophages. *Front. Immunol.* **9**, 933 (2018).

70. Schröder, M. *et al.* Different Modes of IL-10 and TGF-β to Inhibit Cytokine-Dependent IFN-γ Production: Consequences for Reversal of Lipopolysaccharide Desensitization. *J. Immunol.* **170**, 5260 LP – 5267 (2003).

71. Curtale, G., Renzi, T. A., Drufuca, L., Rubino, M. & Locati, M. Glucocorticoids

downregulate TLR4 signaling activity via its direct targeting by miR-511-5p. *Eur. J. Immunol.* **47**, 2080–2089 (2017).

72. Vergadi, E., Vaporidi, K. & Tsatsanis, C. Regulation of Endotoxin Tolerance and Compensatory Anti-inflammatory Response Syndrome by Non-coding RNAs. *Front. Immunol.* **9**, 2705 (2018).
73. Pena, O. M. *et al.* An Endotoxin Tolerance Signature Predicts Sepsis and Organ Dysfunction at Initial Clinical Presentation. *EBioMedicine* **1**, 64–71 (2014).
74. Zimmermann, H. W., Trautwein, C. & Tacke, F. Functional role of monocytes and macrophages for the inflammatory response in acute liver injury. *Front. Physiol.* **3**, 56 (2012).
75. Pan, H. *et al.* SMAD4 is required for development of maximal endotoxin tolerance. *J. Immunol.* **184**, 5502–5509 (2010).
76. Kim, M. L. *et al.* Repeated lipopolysaccharide exposure leads to placental endotoxin tolerance. *Am. J. Reprod. Immunol.* **81**, e13080 (2019).
77. Mosser, D. M. & Zhang, X. Interleukin-10: new perspectives on an old cytokine. *Immunol. Rev.* **226**, 205–218 (2008).
78. Dinarello, C. A. Interleukin-1 in the pathogenesis and treatment of inflammatory diseases. *Blood* **117**, 3720–32 (2011).
79. Fields, J. K., Günther, S. & Sundberg, E. J. Structural Basis of IL-1 Family Cytokine Signaling . *Frontiers in Immunology* **10**, 1412 (2019).
80. Strauss-Ayali, D., Conrad, S. M. & Mosser, D. M. Monocyte subpopulations and their differentiation patterns during infection. *J. Leukoc. Biol.* **82**, 244–252 (2007).
81. Yona, S. *et al.* Fate mapping reveals origins and dynamics of monocytes and tissue macrophages under homeostasis. *Immunity* **38**, 79–91 (2013).
82. Canè, S. *et al.* The Endless Saga of Monocyte Diversity. *Front. Immunol.* **10**, 1786 (2019).
83. Parihar, A., Eubank, T. D. & Doseff, A. I. Monocytes and macrophages regulate immunity through dynamic networks of survival and cell death. *J. Innate Immun.* **2**, 204–215 (2010).
84. Sieweke, M. H. & Allen, J. E. Beyond Stem Cells: Self-Renewal of Differentiated Macrophages. *Science (80-.).* **342**, 1242974 (2013).
85. Röszer, T. Understanding the Biology of Self-Renewing Macrophages. *Cells* **7**, 103

(2018).

86. Smith, T. D., Tse, M. J., Read, E. L. & Liu, W. F. Regulation of macrophage polarization and plasticity by complex activation signals. *Integr. Biol. (Camb).* **8**, 946–955 (2016).
87. O'Neill, L. A. J., Kishton, R. J. & Rathmell, J. A guide to immunometabolism for immunologists. *Nat. Rev. Immunol.* **16**, 553–565 (2016).
88. Loftus, R. M. & Finlay, D. K. Immunometabolism: Cellular Metabolism Turns Immune Regulator. *J. Biol. Chem.* **291**, 1–10 (2016).
89. Viola, A., Munari, F., Sánchez-Rodríguez, R., Scolaro, T. & Castegna, A. The Metabolic Signature of Macrophage Responses. *Front. Immunol.* **10**, 1462 (2019).
90. Bullon, P., Newman, H. N. & Battino, M. Obesity, diabetes mellitus, atherosclerosis and chronic periodontitis: a shared pathology via oxidative stress and mitochondrial dysfunction? *Periodontol. 2000* **64**, 139–153 (2014).
91. Olive, A. J. & Sassetti, C. M. Metabolic crosstalk between host and pathogen: sensing, adapting and competing. *Nat. Rev. Microbiol.* **14**, 221–234 (2016).
92. Wang, A., Luan, H. H. & Medzhitov, R. An evolutionary perspective on immunometabolism. *Science* **363**, eaar3932 (2019).
93. Lunt, S. Y. & Vander Heiden, M. G. Aerobic Glycolysis: Meeting the Metabolic Requirements of Cell Proliferation. *Annu. Rev. Cell Dev. Biol.* **27**, 441–464 (2011).
94. Marko, A. J., Miller, R. A., Kelman, A. & Frauwirth, K. A. Induction of Glucose Metabolism in Stimulated T Lymphocytes Is Regulated by Mitogen-Activated Protein Kinase Signaling. *PLoS One* **5**, e15425 (2010).
95. Wilson, D. F. Oxidative phosphorylation: regulation and role in cellular and tissue metabolism. *J. Physiol.* **595**, 7023–7038 (2017).
96. Williams, N. C. & O'Neill, L. A. J. A Role for the Krebs Cycle Intermediate Citrate in Metabolic Reprogramming in Innate Immunity and Inflammation. *Front. Immunol.* **9**, 141 (2018).
97. Liu, S., He, L. & Yao, K. The Antioxidative Function of Alpha-Ketoglutarate and Its Applications. *Biomed Res. Int.* **2018**, 3408467 (2018).
98. Zhao, R.-Z., Jiang, S., Zhang, L. & Yu, Z.-B. Mitochondrial electron transport chain, ROS generation and uncoupling (Review). *Int. J. Mol. Med.* **44**, 3–15 (2019).
99. Chen, L. *et al.* Inflammatory responses and inflammation-associated diseases in organs. *Oncotarget* **9**, 7204–7218 (2017).

100. Martinez, J., Verbist, K., Wang, R. & Green, D. R. The Relationship between Metabolism and the Autophagy Machinery during the Innate Immune Response. *Cell Metab.* **17**, 895–900 (2013).

101. Bracho-Valdés, I. *et al.* mTORC1- and mTORC2-interacting proteins keep their multifunctional partners focused. *IUBMB Life* **63**, 896–914 (2011).

102. Zhou, H. & Huang, S. The complexes of mammalian target of rapamycin. *Curr. Protein Pept. Sci.* **11**, 409–424 (2010).

103. Li, J., Kim, S. G. & Blenis, J. Rapamycin: one drug, many effects. *Cell Metab.* **19**, 373–379 (2014).

104. Loewith, R. & Hall, M. N. Target of rapamycin (TOR) in nutrient signaling and growth control. *Genetics* **189**, 1177–1201 (2011).

105. Kim, J. & Guan, K.-L. mTOR as a central hub of nutrient signalling and cell growth. *Nat. Cell Biol.* **21**, 63–71 (2019).

106. Corradetti, M. N. & Guan, K.-L. Upstream of the mammalian target of rapamycin: do all roads pass through mTOR? *Oncogene* **25**, 6347–6360 (2006).

107. Nojima, H. *et al.* The Mammalian Target of Rapamycin (mTOR) Partner, Raptor, Binds the mTOR Substrates p70 S6 Kinase and 4E-BP1 through Their TOR Signaling (TOS) Motif. *J. Biol. Chem.* **278**, 15461–15464 (2003).

108. Oshiro, N. *et al.* The Proline-rich Akt Substrate of 40 kDa (PRAS40) Is a Physiological Substrate of Mammalian Target of Rapamycin Complex 1. *J. Biol. Chem.* **282**, 20329–20339 (2007).

109. Saxton, R. A. & Sabatini, D. M. mTOR Signaling in Growth, Metabolism, and Disease. *Cell* **168**, 960–976 (2017).

110. Hausch, F., Kozany, C., Theodoropoulou, M. & Fabian, A.-K. FKBPs and the Akt/mTOR pathway. *Cell Cycle* **12**, 2366–2370 (2013).

111. Fruman, D. A. *et al.* The PI3K Pathway in Human Disease. *Cell* **170**, 605–635 (2017).

112. Sukhbaatar, N., Hengstschläger, M. & Weichhart, T. mTOR-Mediated Regulation of Dendritic Cell Differentiation and Function. *Trends Immunol.* **37**, 778–789 (2016).

113. Lemmon, M. A. & Schlessinger, J. Cell signaling by receptor tyrosine kinases. *Cell* **141**, 1117–1134 (2010).

114. Pal, I. & Mandal, M. PI3K and Akt as molecular targets for cancer therapy: current clinical outcomes. *Acta Pharmacol. Sin.* **33**, 1441–1458 (2012).

115. Di Blasio, L., Gagliardi, P. A., Puliafito, A. & Primo, L. Serine/Threonine Kinase 3-Phosphoinositide-Dependent Protein Kinase-1 (PDK1) as a Key Regulator of Cell Migration and Cancer Dissemination. *Cancers (Basel).* **9**, 25 (2017).

116. Tee, A. R., Anjum, R. & Blenis, J. Inactivation of the Tuberous Sclerosis Complex-1 and -2 Gene Products Occurs by Phosphoinositide 3-Kinase/Akt-dependent and -independent Phosphorylation of Tuberin. *J. Biol. Chem.* **278**, 37288–37296 (2003).

117. Huang, J. & Manning, B. D. The TSC1-TSC2 complex: a molecular switchboard controlling cell growth. *Biochem. J.* **412**, 179–190 (2008).

118. Mendoza, M. C., Er, E. E. & Blenis, J. The Ras-ERK and PI3K-mTOR pathways: cross-talk and compensation. *Trends Biochem. Sci.* **36**, 320–328 (2011).

119. Roux, P. P. & Topisirovic, I. Signaling Pathways Involved in the Regulation of mRNA Translation. *Mol. Cell. Biol.* **38**, e00070-18 (2018).

120. Magnuson, B., Ekim, B. & Fingar, D. C. Regulation and function of ribosomal protein S6 kinase (S6K) within mTOR signalling networks. *Biochem. J.* **441**, 1–21 (2011).

121. Tanimura, S. *et al.* SH3P2 is a negative regulator of cell motility whose function is inhibited by ribosomal S6 kinase-mediated phosphorylation. *Genes to Cells* **16**, 514–526 (2011).

122. Weichhart, T., Hengstschläger, M. & Linke, M. Regulation of innate immune cell function by mTOR. *Nat. Rev. Immunol.* **15**, 599–614 (2015).

123. Almeida, L., Lochner, M., Berod, L. & Sparwasser, T. Metabolic pathways in T cell activation and lineage differentiation. *Semin. Immunol.* **28**, 514–524 (2016).

124. Delgoffe, G. M. *et al.* The kinase mTOR regulates the differentiation of helper T cells through the selective activation of signaling by mTORC1 and mTORC2. *Nat. Immunol.* **12**, 295–303 (2011).

125. Araki, K. *et al.* mTOR regulates memory CD8 T-cell differentiation. *Nature* **460**, 108–112 (2009).

126. Jones, D. D. *et al.* mTOR has distinct functions in generating versus sustaining humoral immunity. *J. Clin. Invest.* **126**, 4250–4261 (2016).

127. Tsalikis, J., Croitoru, D. O., Philpott, D. J. & Girardin, S. E. Nutrient sensing and metabolic stress pathways in innate immunity. *Cell. Microbiol.* **15**, 1632–1641 (2013).

128. Kumar, R. *et al.* Immunometabolism of Phagocytes During Mycobacterium tuberculosis Infection . *Frontiers in Molecular Biosciences* **6**, 105 (2019).

129. Haidinger, M. *et al.* A Versatile Role of Mammalian Target of Rapamycin in Human Dendritic Cell Function and Differentiation. *J. Immunol.* **185**, 3919 LP – 3931 (2010).
130. Lehman, J. A., Calvo, V. & Gomez-Cambronero, J. Mechanism of Ribosomal p70S6 Kinase Activation by Granulocyte Macrophage Colony-stimulating Factor in Neutrophils: COOPERATION OF A MEK-RELATED, THR421/SER424 KINASE AND A RAPAMYCIN-SENSITIVE, mTOR-RELATED THR389 KINASE. *J. Biol. Chem.* **278**, 28130–28138 (2003).
131. Katholnig, K., Linke, M., Pham, H., Hengstschläger, M. & Weichhart, T. Immune responses of macrophages and dendritic cells regulated by mTOR signalling. *Biochem. Soc. Trans.* **41**, 927–933 (2013).
132. Mao, Y. *et al.* IL-15 activates mTOR and primes stress-activated gene expression leading to prolonged antitumor capacity of NK cells. *Blood* **128**, 1475–1489 (2016).
133. Ganeshan, K. & Chawla, A. Metabolic regulation of immune responses. *Annu. Rev. Immunol.* **32**, 609–634 (2014).
134. Yecies, J. L. & Manning, B. D. Transcriptional control of cellular metabolism by mTOR signaling. *Cancer Res.* **71**, 2815–2820 (2011).
135. Blanchard, P.-G. *et al.* Major involvement of mTOR in the PPARγ-induced stimulation of adipose tissue lipid uptake and fat accretion. *J. Lipid Res.* **53**, 1117–1125 (2012).
136. Ben-Sahra, I. & Manning, B. D. mTORC1 signaling and the metabolic control of cell growth. *Curr. Opin. Cell Biol.* **45**, 72–82 (2017).
137. Barton, G. M. A calculated response: control of inflammation by the innate immune system. *J. Clin. Invest.* **118**, 413–420 (2008).
138. Sokol, C. L. & Luster, A. D. The chemokine system in innate immunity. *Cold Spring Harb. Perspect. Biol.* **7**, a016303 (2015).
139. Krzyszczyk, P., Schloss, R., Palmer, A. & Berthiaume, F. The Role of Macrophages in Acute and Chronic Wound Healing and Interventions to Promote Pro-wound Healing Phenotypes. *Front. Physiol.* **9**, 419 (2018).
140. Oleszycka, E. & Lavelle, E. C. Immunomodulatory properties of the vaccine adjuvant alum. *Curr. Opin. Immunol.* **28**, 1–5 (2014).
141. Oleszycka, E. *et al.* The vaccine adjuvant alum promotes IL-10 production that suppresses Th1 responses. *Eur. J. Immunol.* **48**, 705–715 (2018).
142. de Bree, L. C. J. *et al.* Non-specific effects of vaccines: Current evidence and potential

implications. *Semin. Immunol.* **39**, 35–43 (2018).

143. Aaby, P. *et al.* Randomized Trial of BCG Vaccination at Birth to Low-Birth-Weight Children: Beneficial Nonspecific Effects in the Neonatal Period? *J. Infect. Dis.* **204**, 245–252 (2011).
144. Iyer, S. S. & Cheng, G. Role of interleukin 10 transcriptional regulation in inflammation and autoimmune disease. *Crit. Rev. Immunol.* **32**, 23–63 (2012).
145. Ifrim, D. C. *et al.* Trained Immunity or Tolerance: Opposing Functional Programs Induced in Human Monocytes after Engagement of Various Pattern Recognition Receptors. *Clin. Vaccine Immunol.* **21**, 534 LP – 545 (2014).
146. Normann, E., Lacaze-Masmonteil, T., Winkler-Lowen, B. & Guilbert, L. J. ORIGINAL ARTICLE: Isolation of Non-Activated Monocytes from Human Umbilical Cord Blood. *Am. J. Reprod. Immunol.* **63**, 66–72 (2010).
147. Kooijman, S. *et al.* Novel identified aluminum hydroxide-induced pathways prove monocyte activation and pro-inflammatory preparedness. *J. Proteomics* **175**, 144–155 (2018).
148. Sun, J. C., Ugolini, S. & Vivier, E. Immunological memory within the innate immune system. *EMBO J.* **33**, 1295–1303 (2014).
149. Quintin, J., Cheng, S.-C., van der Meer, J. W. M. & Netea, M. G. Innate immune memory: towards a better understanding of host defense mechanisms. *Curr. Opin. Immunol.* **29**, 1–7 (2014).
150. Melillo, D., Marino, R., Italiani, P. & Boraschi, D. Innate Immune Memory in Invertebrate Metazoans: A Critical Appraisal . *Frontiers in Immunology* **9**, 1915 (2018).
151. Hajj Hussein, I. *et al.* Vaccines Through Centuries: Major Cornerstones of Global Health. *Front. public Heal.* **3**, 269 (2015).
152. Hogenesch, H. Mechanism of immunopotentiation and safety of aluminum adjuvants. *Front. Immunol.* **3**, 406 (2013).
153. Gurcel, L., Abrami, L., Girardin, S., Tschopp, J. & van der Goot, F. G. Caspase-1 Activation of Lipid Metabolic Pathways in Response to Bacterial Pore-Forming Toxins Promotes Cell Survival. *Cell* **126**, 1135–1145 (2006).
154. Prevette, L. E., Mullen, D. G. & Holl, M. M. B. Polycation-induced cell membrane permeability does not enhance cellular uptake or expression efficiency of delivered

DNA. *Mol. Pharm.* **7**, 870–883 (2010).

155. Perry, S. W., Norman, J. P., Barbieri, J., Brown, E. B. & Gelbard, H. A. Mitochondrial membrane potential probes and the proton gradient: a practical usage guide. *Biotechniques* **50**, 98–115 (2011).
156. Balcewicz-Sablinska, M. K., Keane, J., Kornfeld, H. & Remold, H. G. Pathogenic Mycobacterium tuberculosis Evades Apoptosis of Host Macrophages by Release of TNF-R2, Resulting in Inactivation of TNF-α. *J. Immunol.* **161**, 2636 LP – 2641 (1998).
157. Quinn, S. M. *et al.* Anti-inflammatory Trained Immunity Mediated by Helminth Products Attenuates the Induction of T Cell-Mediated Autoimmune Disease. *Front. Immunol.* **10**, 1109 (2019).
158. Jacques, C., Gosset, M., Berenbaum, F. & Gabay, C. B. T.-V. & H. The Role of IL-1 and IL-1Ra in Joint Inflammation and Cartilage Degradation. in *Interleukins* **74**, 371–403 (Academic Press, 2006).
159. Arend, W. P. The balance between IL-1 and IL-1Ra in disease. *Cytokine Growth Factor Rev.* **13**, 323–340 (2002).
160. Jounai, N., Kobiyama, K., Takeshita, F. & Ishii, K. J. Recognition of damage-associated molecular patterns related to nucleic acids during inflammation and vaccination. *Front. Cell. Infect. Microbiol.* **2**, 168 (2013).
161. Lopez-Castejon, G. & Brough, D. Understanding the mechanism of IL-1β secretion. *Cytokine Growth Factor Rev.* **22**, 189–195 (2011).
162. Kool, M. *et al.* Alum adjuvant boosts adaptive immunity by inducing uric acid and activating inflammatory dendritic cells. *J. Exp. Med.* **205**, 869 LP – 882 (2008).
163. McKee, A. S. *et al.* Alum induces innate immune responses through macrophage and mast cell sensors, but these sensors are not required for alum to act as an adjuvant for specific immunity. *J. Immunol.* **183**, 4403–4414 (2009).
164. Sarvothaman, S., Undi, R. B., Pasupuleti, S. R., Gutti, U. & Gutti, R. K. Apoptosis: role in myeloid cell development. *Blood Res.* **50**, 73–79 (2015).
165. Zhang, Y., Morgan, M. J., Chen, K., Choksi, S. & Liu, Z. Induction of autophagy is essential for monocyte-macrophage differentiation. *Blood* **119**, 2895–2905 (2012).
166. Stanley, E. R. & Chitu, V. CSF-1 receptor signaling in myeloid cells. *Cold Spring Harb. Perspect. Biol.* **6**, a021857 (2014).

167. Novak, U. *et al.* Colony-stimulating factor 1-induced STAT1 and STAT3 activation is accompanied by phosphorylation of Tyk2 in macrophages and Tyk2 and JAK1 in fibroblasts. *Blood* **86**, 2948 LP – 2956 (1995).

168. Guidez, F., Li, A. C., Horvai, A., Welch, J. S. & Glass, C. K. Differential Utilization of Ras Signaling Pathways by Macrophage Colony-Stimulating Factor (CSF) and Granulocyte-Macrophage CSF Receptors during Macrophage Differentiation. *Mol. Cell. Biol.* **18**, 3851 LP – 3861 (1998).

169. Katsuoka, F. & Yamamoto, M. Small Maf proteins (MafF, MafG, MafK): History, structure and function. *Gene* **586**, 197–205 (2016).

170. Vomund, S., Schäfer, A., Parnham, M. J., Brüne, B. & von Knethen, A. Nrf2, the Master Regulator of Anti-Oxidative Responses. *Int. J. Mol. Sci.* **18**, 2772 (2017).

171. Mills, E. L. *et al.* Succinate Dehydrogenase Supports Metabolic Repurposing of Mitochondria to Drive Inflammatory Macrophages. *Cell* **167**, 457-470.e13 (2016).

172. Groß, O. *et al.* Inflammasome Activators Induce Interleukin-1α Secretion via Distinct Pathways with Differential Requirement for the Protease Function of Caspase-1. *Immunity* **36**, 388–400 (2012).

173. Franchi, L. & Núñez, G. The Nlrp3 inflammasome is critical for aluminium hydroxide-mediated IL-1beta secretion but dispensable for adjuvant activity. *Eur. J. Immunol.* **38**, 2085–2089 (2008).

174. Rőszer, T. *et al.* Understanding the Mysterious M2 Macrophage through Activation Markers and Effector Mechanisms. *Mediators Inflamm.* **2015**, 816460 (2015).

175. Thapa, B. & Lee, K. Metabolic influence on macrophage polarization and pathogenesis. *BMB Rep.* **52**, 360–372 (2019).

176. Vazquez, A., Liu, J., Zhou, Y. & Oltvai, Z. N. Catabolic efficiency of aerobic glycolysis: The Warburg effect revisited. *BMC Syst. Biol.* **4**, 58 (2010).

177. Hill, B. G. *et al.* Integration of cellular bioenergetics with mitochondrial quality control and autophagy. *Biol. Chem.* **393**, 1485–1512 (2012).

178. Weinstein, S. L. *et al.* Phosphatidylinositol 3-kinase and mTOR mediate lipopolysaccharide-stimulated nitric oxide production in macrophages via interferon-β. *J. Leukoc. Biol.* **67**, 405–414 (2000).

179. Dan, H. C. *et al.* Akt-dependent regulation of NF-{kappa}B is controlled by mTOR and Raptor in association with IKK. *Genes Dev.* **22**, 1490–1500 (2008).

180. Fingar, D. C. & Blenis, J. Target of rapamycin (TOR): an integrator of nutrient and growth factor signals and coordinator of cell growth and cell cycle progression. *Oncogene* **23**, 3151–3171 (2004).

181. Dibble, C. C. & Cantley, L. C. Regulation of mTORC1 by PI3K signaling. *Trends Cell Biol.* **25**, 545–555 (2015).

182. Kim, S. G., Buel, G. R. & Blenis, J. Nutrient regulation of the mTOR complex 1 signaling pathway. *Mol. Cells* **35**, 463–473 (2013).

183. Edinger, A. L. & Thompson, C. B. Akt maintains cell size and survival by increasing mTOR-dependent nutrient uptake. *Mol. Biol. Cell* **13**, 2276–2288 (2002).

184. Sawicka, K., Pyronneau, A., Chao, M., Bennett, M. V. L. & Zukin, R. S. Elevated ERK/p90 ribosomal S6 kinase activity underlies audiogenic seizure susceptibility in fragile X mice. *Proc. Natl. Acad. Sci.* **113**, E6290 LP-E6297 (2016).

185. Salmond, R. J., Emery, J., Okkenhaug, K. & Zamoyska, R. MAPK, Phosphatidylinositol 3-Kinase, and Mammalian Target of Rapamycin Pathways Converge at the Level of Ribosomal Protein S6 Phosphorylation to Control Metabolic Signaling in CD8 T Cells. *J. Immunol.* **183**, 7388 LP – 7397 (2009).

186. Aziz, A. U. R., Farid, S., Qin, K., Wang, H. & Liu, B. PIM Kinases and Their Relevance to the PI3K/AKT/mTOR Pathway in the Regulation of Ovarian Cancer. *Biomolecules* **8**, 7 (2018).

187. Kalimuthu, S. & Se-Kwon, K. Cell survival and apoptosis signaling as therapeutic target for cancer: marine bioactive compounds. *Int. J. Mol. Sci.* **14**, 2334–2354 (2013).

188. Smith, R. L., Soeters, M. R., Wüst, R. C. I. & Houtkooper, R. H. Metabolic Flexibility as an Adaptation to Energy Resources and Requirements in Health and Disease. *Endocr. Rev.* **39**, 489–517 (2018).

189. Goetzman, E. S. & Prochownik, E. V. The Role for Myc in Coordinating Glycolysis, Oxidative Phosphorylation, Glutaminolysis, and Fatty Acid Metabolism in Normal and Neoplastic Tissues. *Front. Endocrinol. (Lausanne).* **9**, 129 (2018).

190. Ehninger, A. *et al.* Posttranscriptional regulation of c-Myc expression in adult murine HSCs during homeostasis and interferon-α-induced stress response. *Blood* **123**, 3909–3913 (2014).

191. Cui, J. & Placzek, W. J. Post-Transcriptional Regulation of Anti-Apoptotic BCL2 Family Members. *Int. J. Mol. Sci.* **19**, 308 (2018).

192. Kwak, M.-K., Itoh, K., Yamamoto, M. & Kensler, T. W. Enhanced Expression of the Transcription Factor Nrf2 by Cancer Chemopreventive Agents: Role of Antioxidant Response Element-Like Sequences in the nrf2 Promoter. *Mol. Cell. Biol.* **22**, 2883 LP – 2892 (2002).

193. Schieber, M. & Chandel, N. S. ROS function in redox signaling and oxidative stress. *Curr. Biol.* **24**, R453–R462 (2014).

194. Li, W. *et al.* Activation of Nrf2-antioxidant signaling attenuates NFκB-inflammatory response and elicits apoptosis. *Biochem. Pharmacol.* **76**, 1485–1489 (2008).

195. Piantadosi, C. A. *et al.* Heme Oxygenase-1 Couples Activation of Mitochondrial Biogenesis to Anti-inflammatory Cytokine Expression. *J. Biol. Chem.* **286**, 16374–16385 (2011).

196. Rappuoli, R., Pizza, M., Del Giudice, G. & De Gregorio, E. Vaccines, new opportunities for a new society. *Proc. Natl. Acad. Sci. U. S. A.* **111**, 12288–12293 (2014).

197. Netea, M. G., Latz, E., Mills, K. H. G. & O'Neill, L. A. J. Innate immune memory: a paradigm shift in understanding host defense. *Nat. Immunol.* **16**, 675–679 (2015).

198. Arts, R. J. W. *et al.* Immunometabolic Pathways in BCG-Induced Trained Immunity. *Cell Rep.* **17**, 2562–2571 (2016).

199. Weichhart, T. *et al.* The TSC-mTOR Signaling Pathway Regulates the Innate Inflammatory Response. *Immunity* **29**, 565–577 (2008).

200. Macedo, C. *et al.* Rapamycin augments human DC IL-12p70 and IL-27 secretion to promote allogeneic Type 1 polarization modulated by NK cells. *Am. J. Transplant* **13**, 2322–2333 (2013).

201. Godbout, J. P. & Glaser, R. Stress-Induced Immune Dysregulation: Implications for Wound Healing, Infectious Disease and Cancer. *J. Neuroimmune Pharmacol.* **1**, 421–427 (2006).

202. WERNER, S. & GROSE, R. Regulation of Wound Healing by Growth Factors and Cytokines. *Physiol. Rev.* **83**, 835–870 (2003).

203. Mittal, M., Siddiqui, M. R., Tran, K., Reddy, S. P. & Malik, A. B. Reactive oxygen species in inflammation and tissue injury. *Antioxid. Redox Signal.* **20**, 1126–1167 (2014).

204. Xing, W. *et al.* Acemannan accelerates cell proliferation and skin wound healing through AKT/mTOR signaling pathway. *J. Dermatol. Sci.* **79**, 101–109 (2015).

205. Squarize, C. H., Castilho, R. M., Bugge, T. H. & Gutkind, J. S. Accelerated wound healing by mTOR activation in genetically defined mouse models. *PLoS One* **5**, e10643–e10643 (2010).

206. Italiani, P. & Boraschi, D. From Monocytes to M1/M2 Macrophages: Phenotypical vs. Functional Differentiation. *Front. Immunol.* **5**, 514 (2014).

207. Chamberlain, C. S. *et al.* Interleukin Expression after Injury and the Effects of Interleukin-1 Receptor Antagonist. *PLoS One* **8**, e71631 (2013).

208. Hung, C.-M., Garcia-Haro, L., Sparks, C. A. & Guertin, D. A. mTOR-dependent cell survival mechanisms. *Cold Spring Harb. Perspect. Biol.* **4**, a008771 (2012).

Graphical figures created using BioRender
https://biorender.com/

(A)

	Fold Change Compared to Un-trained		
Gene Name	**Mouse 1**	**Mouse 2**	**Mouse 3**
Ccl2	6.85	6.18	6.97
Cxcl2	4.92	4.57	5.12
Cxcl1	4.55	3.51	3.13
Ccl3	3.92	4.08	4.33
Csf2	3.82	1.59	1.34
Ccl22	3.7	1.6	2.22
Il1rn	3.64	3.35	3.63
Ccl4	3.42	3.2	3.66
Ccl7	3.28	1.84	2.46
Cxcl3	2.99	2.78	2.67
Cxcl5	2.88	3.61	-1.98
Tnfsf14	2.72	2.74	2.6
Tnf	2.68	2.76	3.15
Cd40lg	2.36	1.48	2.8
Pla2g4a	2.18	1.84	2.01
Chi3l3	2.17	1.02	-1.95
Maff	2.15	2.52	2.62
Csf1	2.08	1.45	1.42
Bcl2l1	2.03	2.06	2.24
Tnfaip3	2.03	1.85	1.95
Mafk	1.94	2.06	2.02
Ptgir	1.9	1.87	2.04
Ptgs2	1.85	1.24	-1.15
C1s	1.81	-1.32	1.43
Nlrp3	1.67	1.4	1.48
Nfe2l2	1.62	1.46	1.65
Ptgfr	1.6	-2	-1.08
C1ra	1.44	-1.15	1.17
Tlr2	1.4	1.39	1.52
C8a	1.38	1.08	2
Gapdh	1.38	1.32	1.43
Il5	1.37	-1.95	-1.16
Ccl20	1.35	1.27	1.3
Ripk2	1.35	1.23	1.28
Cxcr2	1.34	1.89	-1.89
Fasl	1.33	-3.15	1.05
Myc	1.31	1.45	1.34
Areg	1.3	-1.09	1.11
Jun	1.28	1.39	1.38
Tollip	1.24	1.36	1.39

Hc	1.18	-1.81	1.39
Il9	1.18	1.93	1.86
Ptger1	1.18	1.38	1.86
Ccl5	1.18	-1.16	1.06
Itgb2	1.17	1.14	1.24
Mapkapk5	1.15	1.19	1.36
Il7	1.15	-1.86	-1.32
Gnas	1.15	1.24	1.16
Cxcl10	1.13	-1.12	1.07
Defa-rs1	1.12	-1.66	-1.32
Pik3c2g	1.11	-1.44	-1.71
Cd40	1.1	-1.22	-1.11
Lta	1.08	-2.46	1.2
Tslp	1.08	-1.48	-1.32
Cebpb	1.07	1.09	1.14
Relb	1.05	1.03	1.08
Nod2	1.03	1.2	1.12
Ddit3	1.01	-1.07	1.03
Cd55	-1.01	-1.07	-1.13
Nfkb1	-1.02	-1.07	-1.02
Cfl1	-1.05	-1.02	-1.02
Il23a	-1.05	-1.43	-1.71
Mapkapk2	-1.06	-1.11	-1.03
Gnb1	-1.06	-1.08	-1.02
Hdac4	-1.08	-1.16	-1.16
Il22ra2	-1.08	-1.44	-1.14
Map2k4	-1.08	-1.05	-1.03
Ptk2	-1.09	-1.16	-1.19
Mmp3	-1.09	-1.16	1.3
Hmgn1	-1.11	-1.21	-1.21
C8b	-1.13	-2.89	-1.43
Flt1	-1.13	-2.01	-1.43
Irf5	-1.15	-1.05	1.02
Map3k7	-1.17	-1.22	-1.23
Ptger4	-1.17	-1.11	-1.2
Prkca	-1.18	-2.67	-1.59
Csf3	-1.19	-2.11	-1.88
Il3	-1.19	-1.52	1.54
Limk1	-1.19	-1.17	-1.12
Gngt1	-1.2	-2.23	-1.52
Mapk1	-1.2	-1.07	-1.04
Fos	-1.21	-1.1	-1.37

Cdc42	-1.21	-1.2	-1.16
Rhoa	-1.22	-1.22	-1.19
Max	-1.22	-1.17	-1.09
Ccl21a	-1.22	-1.3	-1.29
Nos2	-1.23	-1.96	-2.33
Tgfb1	-1.23	-1.26	-1.15
Ppp1r12b	-1.24	-1.06	-1.23
Il12b	-1.25	2.01	-1.35
Myl2	-1.25	-1.02	1.31
Tgfb2	-1.28	-1.77	-2.34
Rapgef2	-1.28	-1.42	-1.42
Il1r1	-1.28	-1.15	-2.32
C9	-1.28	-1.7	1.23
Retnla	-1.3	-4.07	-1.64
Tlr3	-1.31	-2.58	-1.2
Il13	-1.31	-2.1	-8.24
Rela	-1.31	-1.37	-1.28
C7	-1.34	-2.15	-1.02
Oas1a	-1.34	-1.62	-1.5
Map2k1	-1.34	-1.34	-1.36
Masp1	-1.35	-2.64	-2.36
Trem2	-1.38	-1.36	-1.33
Ltb4r1	-1.39	-1.85	1.36
Raf1	-1.39	-1.41	-1.22
Tyrobp	-1.39	-1.41	-1.26
Ltb	-1.4	-1.28	1.41
Prkcb	-1.4	-1.58	-1.37
Grb2	-1.42	-1.42	-1.33
Tlr4	-1.42	-1.39	-1.27
Elk1	-1.43	-1.29	-1.4
Alox15	-1.43	-2.04	-1.45
Rac1	-1.44	-1.46	-1.43
Ptger2	-1.45	-1.46	-1.2
Tlr1	-1.45	-1.73	-1.45
Traf2	-1.46	-1.55	-1.22
H2-Ea-ps	-1.46	-3.51	-2.39
Tlr6	-1.47	-1.41	-1.37
Myd88	-1.47	-1.74	-1.55
Nfatc3	-1.48	-1.47	-1.52
Ifnb1	-1.48	-1.09	-1.12
Shc1	-1.48	-1.64	-1.59
Ripk1	-1.49	-1.6	-1.42

Cd163	-1.49	-3.44	-2.38
Hmgb2	-1.5	-1.6	-1.32
C6	-1.53	1.07	-1.55
Cxcr1	-1.53	1.07	-1.55
Keap1	-1.53	-1.52	-1.31
Map2k6	-1.54	-1.55	-1.53
Irf1	-1.54	-1.87	-1.37
Il12a	-1.54	-2.3	-2.28
Cd4	-1.55	-1.81	-1.01
Mapk8	-1.56	-1.39	-1.23
Il21	-1.56	1.2	1.77
Map3k1	-1.57	-1.59	-1.42
C3	-1.57	-1.96	-1.57
Il1rap	-1.58	-1.41	-1.4
Pdgfa	-1.59	-1.4	-1.36
Gnaq	-1.62	-1.66	-1.61
Atf2	-1.62	-1.58	-1.53
Nox1	-1.63	-1.31	-1.11
Kng1	-1.64	-1.53	-1.82
Mapk3	-1.68	-1.64	-1.52
Nr3c1	-1.69	-1.67	-1.6
Il22	-1.69	-2.7	-1.61
Masp2	-1.71	-2.28	-5.43
Tradd	-1.72	-1.71	-1.65
Hmgb1	-1.72	-1.8	-1.6
Il10rb	-1.73	-1.71	-1.6
Ly96	-1.75	-1.71	-1.56
Ifit1	-1.76	-4.35	-2.26
Twist2	-1.76	-1.87	-1.34
Cfb	-1.76	-1.69	1.1
C3ar1	-1.77	-1.84	-1.82
Ltb4r2	-1.78	-1.36	1.24
Rock2	-1.78	-1.61	-1.8
Ccr1	-1.81	-1.39	-1.5
Hras1	-1.82	-1.36	-1.79
Ccr3	-1.84	-1.96	-2.13
Hif1a	-1.86	-2.21	-2.04
Il17a	-1.86	-1.49	-1.77
Mbl2	-1.87	-1.99	1.27
Mapk14	-1.87	-1.91	-1.84
Ifi27l2a	-1.88	-1.77	-2.05
Mmp9	-1.9	-1.55	-2.18

Bcl6	-1.9	-1.83	-1.94
Oasl1	-1.92	-7.3	-3.92
Nod1	-1.93	-2.02	-1.88
Mknk1	-1.93	-1.89	-1.74
Mef2c_Mm	-1.96	-2.03	-1.77
Mafg	-1.96	-2.15	-2.19
Il18	-1.99	-1.66	-1.47
Tlr7	-1.99	-2.2	-1.81
Birc2	-2.01	-2.26	-2.13
Stat3	-2.01	-2.12	-1.98
Arg1	-2.06	1.06	-1.12
Mef2d	-2.06	-1.72	-1.81
Daxx	-2.06	-2.05	-1.9
C1qb	-2.07	-2.24	-1.94
Il1a	-2.09	-1.12	1.22
Stat1	-2.1	-2.54	-2.38
Tgfbr1	-2.13	-2.01	-1.92
Hspb2	-2.18	-1.85	-2.21
Il1b	-2.25	-3.04	-3.68
Ccl17	-2.25	-1.92	-5.71
Cxcr4	-2.26	-2.23	-2.03
Hspb1	-2.3	-2.85	-15.29
Plcb1	-2.3	-1.96	-1.67
Il10	-2.32	-1.58	-1.29
Mx2	-2.34	-2.77	-3.3
Il6	-2.38	-1.69	-4.02
Ccr4	-2.39	-5	-5
Cysltr2	-2.39	-2.74	-1.32
Cysltr1	-2.39	-3.11	-2.81
Ifit2	-2.43	-4.12	-2.71
Ccl8	-2.43	-1.55	-1.42
Irf7	-2.44	-4.78	-3.92
Stat2	-2.46	-2.74	-2.61
Il11	-2.47	-2.63	-2.08
Alox5	-2.49	-3.5	-2.67
Mrc1	-2.77	-3.01	-2.83
Ifna1	-2.79	-1.28	1.13
Il2	-2.82	-1.34	-2.04
Il6ra	-2.86	-2.55	-2.68
Smad7	-2.87	-2.6	-2.39
Il15	-2.88	-3.14	-2.98
C1qa	-2.89	-3.45	-2.8

Irf3	-2.89	-2.77	-2.06
Tcf4	-2.9	-3.03	-2.85
Creb1	-2.93	-2.55	-3.93
Tlr9	-2.94	-3.48	-3.07
Oas2	-2.95	-3.54	-3.37
C4a	-2.96	-1.58	-2.05
Mx1	-2.97	-4.86	-2.79
Iigp1	-3.01	-6.42	-2.86
Tlr8	-3.05	-3.37	-3.37
Gpr44	-3.14	-5.02	-2.39
Map3k5	-3.15	-3.22	-3.09
Il18rap	-3.23	-2.67	-3.1
Mef2b	-3.29	-1.75	-1.79
Il23r	-3.37	-1.34	-4.27
Ccr7	-3.37	-3.59	-1.42
Cd86	-3.38	-3.46	-2.96
Alox12	-3.4	-3.55	1.16
Cxcl9	-3.46	-3.07	-1.99
Ifit3	-3.69	-6.57	-4.78
Hsh2d	-3.74	-1.33	1.05
Ifng	-3.74	-1.99	1.48
Mef2a	-3.76	-3.41	-3.23
Rps6ka5	-3.83	-4.46	-3.53
Map3k9	-3.91	-1.85	-3.96
Tbxa2r	-4.12	-1.46	-1.3
Tgfb3	-4.16	-5.62	-5.82
C2	-4.2	-2.24	-1.64
Tlr5	-4.3	-7.72	-6.12
Ccl11	-4.9	-5.13	-1.04
Ccl19	-4.9	-1.04	-1.55
Il4	-5.08	-5.31	-2.14
Ager	-5.18	-3.22	-2.55
Ptger3	-5.85	-8.72	-7.98
Ifi44	-7.01	-12.14	-12.16
Ptgs1	-7.02	-6.43	-6.71
Cfd	-7.04	-1.25	-2.23
Ccl24	-8.49	-11.76	-4.67
Crp	-9.15	-1.95	-1.45
Fxyd2	-9.64	-16.44	-8.22
Ccr2	-13.03	-19.52	-12.82
H2-Eb1	-39.19	-54.48	-37.17

(B)

Gene	Class	Analyte Type	Avg Count	Min Count	Max Count	% Samples	%CV
Tubb5	Housekeeping	mRNA	1,798.50	1,464	2,168	100	18.078
Pgk1	Housekeeping	mRNA	1,163.33	978	1,343	100	13.744
Cltc	Housekeeping	mRNA	16,013.36	13,406	19,273	100	17.167
Gusb	Housekeeping	mRNA	8,745.56	8,240	9,317	100	4.329
Hprt	Housekeeping	mRNA	532.29	419	640	100	17.039

Supplementary Table 1. NanoString gene list with fold changes. Alum-trained BMDMs were compared to un-trained control cells using nSolver software. Fold changes for 249 genes are shown in (A). Internal reference genes are shown in (B).

(A)

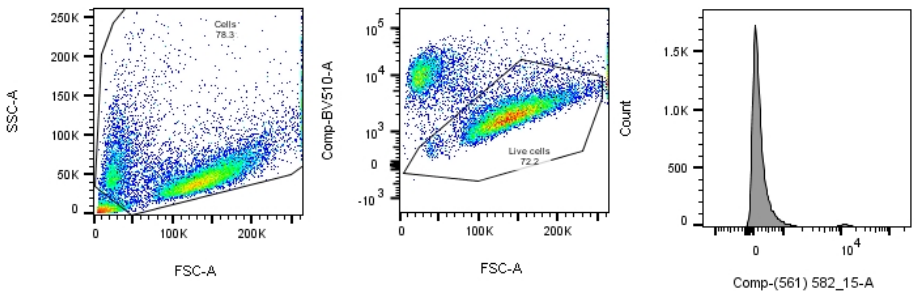

(B)

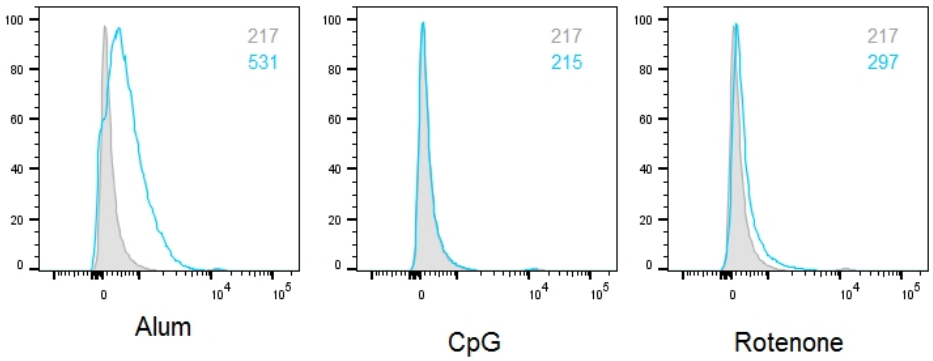

(C)

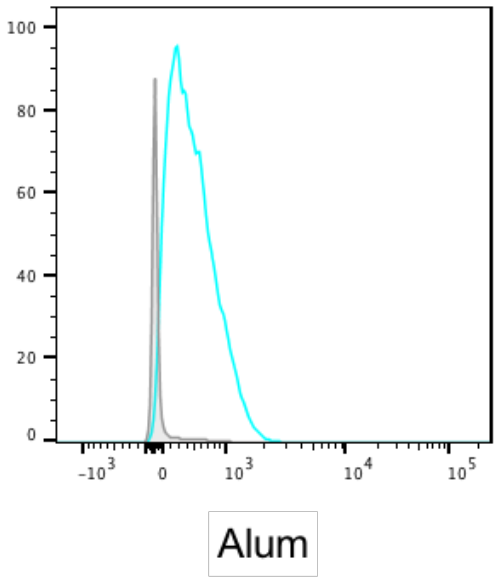

Supplementary Figure 1: Alum induces mitochondrial ROS production in BMDMs BMDMs were incubated with alum (10μg/ml) CpG (4μg/ml) and Rotenone (5μM) for 1 hour. Live cells were analysed for expression of MitoSOX by flow cytometry*. (A) Gating strategy (B) Immunofluorescence is shown for alum, CpG or rotenone (blue line) compared to untreated cells (shaded histograms). Results are representative of two independent experiments. (C) Immunofluorescence is shown for alum (blue line) compared to DMEM treated cells (shaded histograms). *Flow cytometry performed by Joanna Turley (B.A.)